MODEL PREDICTIVE CONTROL TECHNIQUES FOR WIND TURBINES

BY

MOJEED OPEYEMI OYEDEJI

A Thesis Presented to the
DEANSHIP OF GRADUATE STUDIES

KING FAHD UNIVERSITY OF PETROLEUM & MINERALS

DHAHRAN, SAUDI ARABIA

In Partial Fulfillment of the
Requirements for the Degree of

MASTER OF SCIENCE

In

SYSTEMS AND CONTROL ENGINEERING

MAY 2017

KING FAHD UNIVERSITY OF PETROLEUM & MINERALS
DHAHRAN 31261, SAUDI ARABIA

DEANSHIP OF GRADUATE STUDIES

This thesis, written by **MOJEED OPEYEMI OYEDEJI** under the direction of his thesis adviser and approved by his thesis committee, has been presented to and accepted by the Dean of Graduate Studies, in partial fulfillment of the requirements for the degree of **MASTER OF SCIENCE IN SYSTEMS AND CONTROL ENGINEERING**.

Thesis Committee

Dr. Magdi S. Mahmoud (Adviser)

Dr. Sami El-Ferik (Member)

Dr. Samir Al-Amer (Member)

for

Dr. Hesham K. Al-Fares
Department Chairman

Dr. Salam A. Zummo
Dean of Graduate Studies

17/5/12
Date

To those who care about me and whom I equally care about

ACKNOWLEDGMENTS

All Glory to Almighty God, The Entirely Merciful, The Especially Merciful. My heartfelt gratitude goes to the government of the Kingdom of Saudi Arabia and the management of King Fahd University of Petroleum and Minerals, Saudi Arabia for giving me the opportunity to complete my Masters Studies in the Kingdom of Saudi Arabia. My sincere gratitude to my adviser, Dr. Madgi S. Mahmoud for his patience, dedication and strict policy towards deadlines. I will also like to thank my thesis committee members, Dr. Sami El-ferik and Dr. Samir Al-Amer for their contributions to the research work. Also, I would like to thank the Department Chairman, Dr. Hesham Al-Fares and entire staff of the Department of Systems Engineering for making my learning experience a conducive one. A very warm thanks to members of the Nigerian Community in KFUPM for their kind reception on my arrival and continual assistance over my entire stay period in the Kingdom. Many thanks to my friends and colleagues for being there in my time of need. Also to my friends back home in Nigeria, many thanks for your continual support and understanding. Finally, sincere appreciations to my parents for their many sacrifices over the years without which I may not have been able to reach this present position.

TABLE OF CONTENTS

LIST OF TABLES

LIST OF FIGURES

LIST OF ABBREVIATIONS

DFIG	Doubly-fed Induction Generator
FSWT	Fixed Speed Wind Turbine
GSA	Gravitational Search Algorithm
HAWT	Horizontal Axis Wind Turbine
HOSM	High-Order Sliding Mode
LiDAR	Light Detection and Ranging
LMI	Linear Matrix Inequalities
MRAC	Model Reference Adaptive Control
MPC	Model Predictive Control
MPPT	Maximum Power Point Tracking
PI	Proportional Integral
PMSG	Permanent Magnet Synchronous Generator
P&O	Perturb and Observe
PSF	Power Signal Feedback
RBF	Radial Basis Function
SCIG	Squirrel Cage Induction Generator
SMC	Sliding Mode Control
STR	Self Tuning Regulator
TSR	Tip Speed Ratio
WECS	Wind Energy Conversion System
WT	Wind Turbine
WTS	Wind Turbine System
VAWT	Vertical Axis Wind Turbine
VSWT	Variable Speed Wind Turbine
VSWT-DDG	Variable Speed Wind Turbine with Direct Driven Generators

THESIS ABSTRACT

NAME: Mojeed Opeyemi Oyedeji

TITLE OF STUDY: Model Predictive Control Techniques for Wind Turbines

MAJOR FIELD: Systems and Control Engineering

DATE OF DEGREE: May 2017

Renewable energy systems are receiving more attention around the globe due to increasing environmental concerns stemming from over-dependence on fossil energy sources. Wind energy is the fastest growing renewable energy source with an estimated annual growth rate of 16.8 % in 2015. A wind turbine is an electromechanical device used for conversion of kinetic energy present in the wind to mechanical energy to drive generators to produce power of kilowatt to multi-megawatt scale. Control systems are designed for wind turbines to alleviate mechanical loads, maximize and limit power production at below and above rated wind speeds respectively. The operation and control of a wind turbine is a function of wind speed which is intermittent in nature. Also, the operation of the turbine over a wide range of wind speeds must satisfy some safety constraints on the system. Model predictive control refers to a class of control algorithms that performs on-line opti-

mization using predictions based on the dynamic model of the plant to optimize the control action to be applied at the current time instant. Model predictive control algorithms are favored in process industries due to their ability to represent the control problem as optimization problems with constraints on the plant's inputs and outputs. In this study, adaptive and multi-model predictive controllers were designed using orthonormal functions. In the former case, a linearized model obtained from the non-linear plant was parameterized as a function of the measured wind speed. A linear model predictive controller that updates its parameters based on the measured wind speed was designed using the parametrized linear model. In the multi-model case, four controllers were designed using linearized models at operating wind speeds of $4ms^{-1}$, $8ms^{-1}$, $11ms^{-1}$, *and* $18ms^{-1}$ *which denote low, mid, high and top operating regions. A continuous-time Bayesian probability function was used to make transition between these controllers using the errors between the nonlinear system output and output at each operating point. Simulation studies were conducted using a benchmark 5MW wind turbine model to test the performance of the proposed controllers.*

أطروحة ملخص

الاسم: مجيد أوبيمي أويديجي

عنوان الدراسة: نموذج تقنيات التحكم التنبؤية لتوربينات الرياح

المجال الرئيسي: نظم وهندسة التحكم

تاريخ الشهادة: مايو ٧١٠٢

وتتلقى نظم الطاقة المتجددة مزيدا من الاهتمام في جميع أنحاء العالم بسبب تزايد المخاوف البيئية الناجمة عن الاعتماد المفرط على مصادر الطاقة الأحفورية. طاقة الرياح هي أسرع مصدر للطاقة المتجددة نموا بمعدل نمو سنوي يقدر ب ٨.٦١٪ في عام ٥١٠٢. توربينات الرياح هي جهاز كهروميكانيكي يستخدم لتحويل الطاقة الحركية الموجودة في مهب الريح إلى طاقة ميكانيكية لدفع المولدات لإنتاج طاقة كيلووات إلى مقياس متعدد ميجاوات. تم تصميم أنظمة التحكم لتوربينات الرياح لتخفيف الأحمال الميكانيكية، وتعظيم والحد من إنتاج الطاقة في أدناه وأعلى تصنيف سرعة الرياح على التوالي. تشغيل والسيطرة على توربينات الرياح هي وظيفة من سرعة الرياح التي هي متقطعة في الطبيعة. كما أن تشغيل التوربين على نطاق واسع من سرعات الرياح يجب أن يفي ببعض قيود السلامة على النظام. ويشير عنصر التحكم التنبئي النموذجي إلى فئة من خوارزميات التحكم التي تؤدي إلى التحسين على الخط باستخدام التنبؤات القائمة على النموذج الديناميكي للنبات لتحسين إجراءات التحكم التي يتعين تطبيقها في الوقت الحالي. خوارزميات التحكم التنبؤية النموذجية مفضلة في الصناعات العملية نظرا لقدرتها على تمثيل مشكلة السيطرة كمشاكل تحسينية مع قيود على مدخلات المصنع ومخرجاته. في هذه الدراسة، تم تصميم وحدات التحكم التنبؤية التكيفية ومتعددة النماذج باستخدام وظائف أورثونورمال. وفي الحالة الأولى، تم وضع نموذج

خطي تم الحصول عليه من المحطة غير الخطية كدالة لسرعة الرياح المقاسة. تم تصميم وحدة تحكم تنبؤية نموذجية خطية تقوم بتحديث معلماتها على أساس سرعة الرياح المقاسة باستخدام نموذج خطي بارامتريزد. في حالة متعددة النماذج، تم تصميم أربعة وحدات تحكم باستخدام نماذج خطية عند تشغيل سرعات الرياح من ٤ مللي ثانية ms^{-1}٨ ms^{-1}١١ ms^{-1}٨١ والتي تشير إلى مناطق التشغيل المنخفضة والمتوسطة والعالية والراقية. واستخدمت دالة الاحتمال البيزي المستمر للوقت للانتقال بين وحدات التحكم هذه باستخدام الأخطاء بين مخرجات النظام غير الخطية والإخراج عند كل نقطة تشغيل. أجريت دراسات المحاكاة باستخدام نموذج توربينات الرياح القياسية ٥ش‌ط لاختبار أداء وحدات التحكم المقترحة. وتتلقَ

CHAPTER 1

INTRODUCTION

1.1 Background

Wind energy is one of the primitive sources of energy. The kinetic energy from the wind can be converted to mechanical energy using wind energy conversion systems. Wind energy conversion systems include: wind mill, wind pump and the modern-day wind turbine. The first practical windmill, called Sistan mill was developed in the 7th century in Iran. According to [1], windmills were used in the USA in the 1930's for electricity production and pumping of water and the first utility grid connected wind turbine was built by John Brown and Co. in 1951. The advantages of wind energy include;

- It is a clean energy source, thereby not contributing to CO_2 emissions
- It is abundant in availability and renewable on a natural timescale.
- It is accessible in remote areas.

Some disadvantages may include:

- Wind turbines causes noise pollution
- Wind supply is intermittent.
- The initial investment in commissioning a wind power plant is huge.

Although there are some disadvantages, more attention is being shifted to clean energy sources due to increasing environmental concerns, nations are contributing more to clean energy research and increasing the amount of power generated from the wind. The total capacity of wind power in the world at the end of 2014 was estimated around some 370 GW and is estimated to reach 670 GW by the end of 2019 [1].

1.2 Wind Energy Conversion Systems

A wind energy conversion system (WECS) is an energy conversion system that transforms the kinetic energy from the wind into mechanical energy and subsequently into electrical energy. The components of a WECS includes; wind turbine, generators, storage and grid (for grid connected systems). The primary component of a WECS is the wind turbine and it is the main subject of research in most studies. Depending on the axis of rotation, wind turbines can be differentiated into two categories: Horizontal axis wind turbine (HAWT) and vertical axis wind turbine (VAWT) (see Figure 1). Compared with the VAWT, the HAWT has a higher wind energy conversion efficiency due to its blade design but it requires stronger

tower support due to heavy weight of the nacelle and the cost of installation is higher compared with the VAWT. The operation of the VAWT is independent of the wind direction but has lower wind energy conversion efficiency and it is more susceptible to higher torque fluctuations and mechanical vibrations. It is commonly found in domestic/private installations where the energy demand is not so high. Wind turbine systems can be classified into three basic system configurations typically used on wind farms depending on the type of generators used [1–3]: fixed-speed wind turbine (FSWT), variable-speed wind turbine (VSWT) [4] and variable-speed wind turbine with direct driven generators (VSWT-DDG).

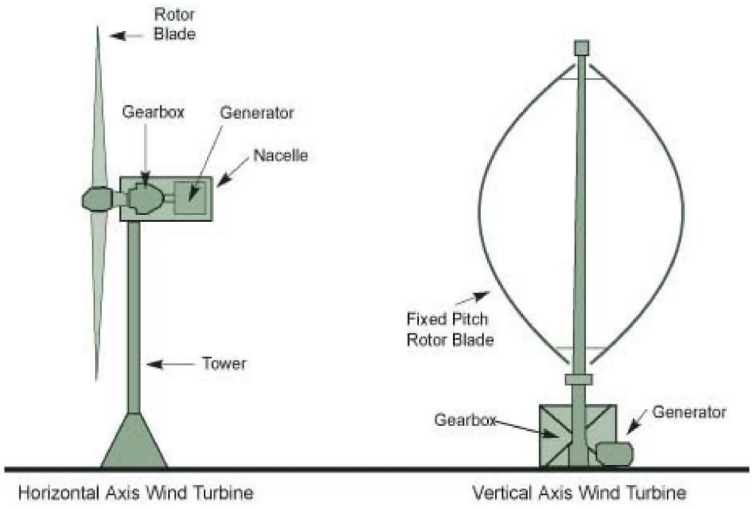

Figure 1.1: Wind Turbine: Vertical and Horizontal Axis

In the case of the FSWT, the squirrel-cage induction generator (SCIG) is connected directly to the grid using a multistage gearing system to match the rotor speed with the turbine. The doubly-fed induction generator (DFIG) is used in the VSWT, its stator windings are connected directly to the grid, while its rotor windings are connected to the grid using an electronic converter that utilizes

thirty percents of the total generator capacity. In the VWST-DDG, a synchronous generator and a full-scale power electronic converter are used. Compared with other configurations, it does not need a multi-stage gearbox system because a low-speed high torque synchronous generator is used. The FSWT configurations have the advantage of simplicity, low cost and low maintenance but they have low energy conversion efficiency because they cannot take advantage of the increasing wind speed to improve their efficiency. The VSWT configurations have higher energy conversion efficiency but are characterized by large installations.

1.3 Operating Regions of Wind Turbines

Based on the wind speed, four operating regimes can be defined for the wind turbine, namely: low, mid, top and high region. As shown in Figure 1.2, the low region represent the turbine operation when the incoming speed is less than the rated wind speed. In this region, the control objective is to maintain the rotor speed at its rated value. In the mid-region, the rotor speed and the generated power are at between the specified upper and lower limits. In the high region, the rotor speed is at its rated value while the generated power is slightly below its nominal value. This region is very narrow and is considered as a transition region between the top and mid region. In the top region, both rotor speed and generated power are at the rated value.

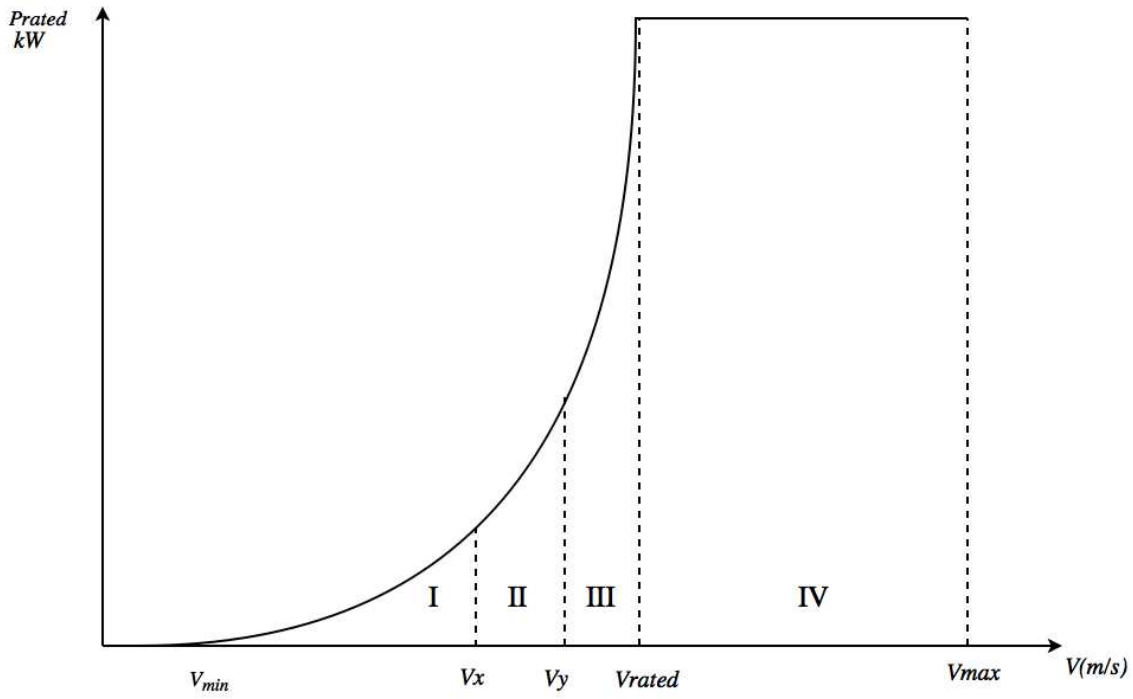

Figure 1.2: Operating Regions of the Wind Turbine

1.4 Objectives in Wind Turbine Control

The control strategies in wind turbine literature depends on the objective in the current operating region of the turbine. Although the wind turbine has four operating regions, it is operational in only Region II and III. The control objectives for wind turbines include; maximum power extraction, power regulation, minimization of mechanical loads, and enhancement of fault-ride through capabilities (for grid connected systems).

1.4.1 Maximum Power Point Tracking Control and Power Regulation

Maximum power point tracking (MPPT) is a phenomenon in wind turbine control that refers to the ability of the controller to track the optimum rotor speed for maximum power extraction in the low wind speed region. Common MPPT strategies in wind turbine control literature include: tip-speed ratio (TSR) [5–8], power signal feedback [9–12], perturb and observe (P & O) [5, 9, 13–26].The TSR method relies on the wind and rotor speed measurements to track the optimal tip speed ratio where maximum power can be extracted.

The P & O technique is a gradient-based search technique where the rotor speed ω_r is perturbed in small increments and the ratio $\Delta P_r/\Delta\omega_r$ is measured. ω_r is increased in small increments until $\Delta P_r/\Delta\omega_r = 0$ and decreased if $\Delta P_r/\Delta\omega_r < 0$. The P & O algorithm does not rely on a priori knowledge about the wind turbine power characteristics. However, the P & O technique is only suitable for systems with small inertial response, for large wind turbines the turbine speed is unable to follow the changes in wind velocity, therefore the P & O strategy will be unsuitable. The power signal feedback technique uses the turbine power characteristics.

In power signal feedback (PSF), the knowledge of the wind turbine power characteristics to track the optimum power point. The maximum power curves at different wind speeds are obtained through offline experiments and stored in a lookup table. The power reference is then computed using the mechanical power

equation of the wind turbine. The primary control objective in Region III (above rated speed) is to regulate the generator power within the specified operating limit even when the wind speed fluctuation is high.

1.4.2 Mitigation of Mechanical Loads

There are two types of mechanical loads acting on the turbine namely; static and dynamic loads. Static loads are developed as a result of interaction of the turbine with average wind velocity [27] while dynamic loads are as a result of net aerodynamic torque that transmits down the drive train and the variation of aerodynamic loads that affect the mechanical structure of the turbine. Dynamic loads can be further classified into two categories: transient loads and cyclic loads. Transient loads are induced by turbulence and gust from the wind and are predominantly classified as low frequency loads. According to [27], the transition between Region II and Region III have significant effect on transient loads. Hence control design must ensure a smooth transition between Region II and Region III operation. The focus of most control designs [28–37] is centered about minimization of mechanical loads.

1.4.3 Enhancement of Fault Ride Through Capability

Fault ride through is a measure of the ability of a generator to stay connected during short periods of voltage dips. Grid codes require that wind turbines ride through grid faults. In DFIG-based WTS, This is mostly achieved by limiting the

stator and rotor currents. A discussion on Low voltage ride through capabilities of wind turbines can be found in [38–82].

1.5 Survey of Existing Literature

1.5.1 Optimal and Robust Control

Maximum power point tracking (MPPT) algorithm of a small VSWT system based on $\mathcal{L}_1$ adaptive control was presented in [83]. A simplified model of the system using a transfer function model with generator torque as control input and generator speed as measured output was considered. It was reported that the $\mathcal{L}_1$ adaptive controller showed good tracking performance with fast adaptation to disturbances. A gain scheduled $\mathcal{L}_1$ optimal control of a VSVP WT was presented in [84]. The control synthesis problem was considered non-convex, an optimal output feedback controller was designed for a linear model of the WT at different operating points using genetic algorithm. A nonlinear robust control for maximization of output power of VSWT was presented in [85] to maximize energy capture from the wind. In [86], robust linear matrix inequalities (LMI)-based controller was designed for a VSWT along all operating points. A robust predictive controller was discussed in [87] to address the problem of parameter variations in controller design for WT generator system due to stochastic wind behavior. An auto-regressive model was used to represent the win speed signal and a two-mass drive train model was considered. A self tuning-regulator (STR) was developed using local generator

speed to generate suitable control signals for handling parametric uncertainties. The STR parameters are updated on-line for smoothing the output power of the generator under fluctuating wind speeds. A robust controller was designed for damping the tower oscillations in a WT consisting with a hydrostatic drive train and a permanent magnet synchronous generator in [88]. For proper consideration of parametric uncertainties, the proposed controller was derived using LMIs. The rotor angular velocity is controlled by adjusting the hydrostatic transmission and the tower bending oscillations were controlled using the pitch angle as control input. A disturbance observer was used to approximate the aerodynamic rotor torque and leakage effects in the hydrostatic transmission.6

1.5.2 Sliding Mode Control

Integral SMC without reaching phase was designed for a VSWT in [89] to maximize energy capture at below rated power. An exponential function was used to minimize the output error in order to eliminate the reaching phase. Fuzzy-PI and SMC were analyzed in [90]. It was concluded that with Fuzzy-PI controllers, settling time was reduced, maximum overshoot are reduced and oscillations are canceled out faster. Overall, the transient response of the Fuzzy-PI is better in comparison to classical PI and SMC controllers. Quasi sliding mode control was applied to the control of direct-driven permanent magnet synchronous generator WT to eliminate chattering problems attributed to conventional sliding mode controllers. Second-order sliding mode control was applied to the control of grid-side

and rotor side converters in [91], single control loops instead of usual cascaded current and power loops was used. Although, the closed loop system showed good steady state performance, the closed loop response of the system still showed some chattering. Back-stepping sliding mode control was applied to control a VSWT in [92], it was demonstrated that the performance of the back-stepping sliding mode control was better and robust than conventional SMC. Adaptive sliding mode back-stepping control of a pitch regulated VSWT controlled by a variable-displacement pump was proposed in [93]. It was demonstrated that the generator output power fluctuations and flap-wise mechanical load on the turbine were better mitigated when compared to a pitch system equipped with a valve.

1.5.3 Adaptive Control

In this section, a summary of recent works that has been carried out in the design of adaptive controllers for wind turbine systems is discussed. Model Reference Adaptive Control (MRAC) of a PMSG-based small wind turbine turbine was discussed in [94]. The parameter variations considered were related to the drive-train inertia and damping, electrical resistance and inductance of the generator. The controller was implemented in the Region II regime of the turbine. The stability of the adaptive control system was guaranteed using Lyapunov equations. The performance of the developed controller was compared against the conventional PI controller. In [95], adaptive sliding mode control using high-order sliding mode (HOSM) theory of a DFIG-based wind energy system was studied. A robust con-

trol scheme was designed incorporating an HOSM torque observer. The designed torque observer was used for calculating turbine reference speed for maximum wind power capture. The stability analysis of the HOSM observer was proven using Lyapunov analysis. It was demonstrated that maximum power extraction goal was achieved under strong wind speed variations and system uncertainties.

Nonlinear adaptive power control for DFIG-based wind turbine during unbalanced network conditions was proposed in [96]. A feedback linearization scheme was applied to linearize the system and design a feedback law. Two perturbation terms were defined to include system nonlinearities, uncertainties and external disturbances. The nonlinear adaptive control was designed by considering the perturbation terms as extended states. Three test scenarios were evaluated for the designed control scheme, the decoupled control of stator active and reactive power , robustness against parameter variations and operation under unbalanced conditions. It was demonstrated that the adaptive controller has smaller tracking error as compared to conventional vector control. Overall, the author suggests that the adaptive controller provides better dynamic performance than conventional vector control.

Extreme learning machine and adaptive particle swarm optimization was applied to optimal control of a variable speed wind turbine in [97]. The desired control objectives were maximization of energy capture below rated wind speed and minimization of stress on the drive train shaft. Extreme learning machine was used to approximate the unmodeled nonlinear dynamics of the system, sliding

mode control was used to compensate against external disturbances and adaptive PSO was used to optimize the gain of the SMC controller. The stability and robustness of the proposed controller was demonstrated using simulation plots. A speed control strategy based on adaptive neuro-fuzzy control for a switched reluctance generator driven by a variable speed wind turbine was designed in [98]. The proposed control scheme is compared with the conventional PI controller. The authors report excellent dynamic performance compared with conventional PI control.

Receding horizon adaptive second-order SMC for DFIG-based wind turbine was presented in [99]. Two control objectives were considered. The first was to ensure maximum power extraction in Zone II and III region of operation. The strategy in the Zone II region was to track the time-varying optimum torque reference towards attaining optimum energy conversion. In the Zone III region where the wind speed is quite high, the limitation of rated power is achieved by also tracking a time varying torque reference. The second control objective was to track reactive power reference towards controlling the system power factor. An adaptive voltage control strategy for a voltage control strategy for a VSWT connected to a weak grid was discussed in [100]. The control objective was minimization of significant voltage oscillations and improvement of power quality for wind generation systems connected to a weak network. Adaptive voltage control was proposed to maintain constant voltage and smoothness at point of common coupling.

An adaptive disturbance rejection scheme for DFIG-based wind turbine was discussed in [101]. A novel observer was designed using discrete-time higher-order sliding mode controller to construct reference value for power extraction based on operating conditions. It was reported that the performance of the closed loop system subject to abrupt wind variations was improved. A wind turbine control scheme based on adaptive sliding mode controller and observer was discussed in [102]. The chattering problem was handled by smoothing out the control within a thin boundary layer neighboring the switching surface. A 20% uncertainty in process parameters was assumed and it was demonstrated that the closed loop system was able to achieve maximum power extraction under system uncertainties.

A pitch angle controller based on $\mathcal{L}_1$ adaptive control was presented in [103]. An affine model was used to represent the nonlinear dynamics of the system using wind speed and aerodynamic torque as uncertain parameters. It was demonstrated that the $\mathcal{L}_1$ controller can keep the generator speed withing a specified bound of rated speed which is an indication of steady operation of the turbine. The nonlinear adaptive backstepping control of a wind turbine with lightweight tower was investigated in [33]. The full load region of operation of the turbine was studied. The reference trajectory for the adaptive pitch controller was generated using a fourth-order low pass filter. From the results presented, it was demonstrated that the controller stabilizes the tower deflection around its reference trajectory without overloading the pitch actuator.

An adaptive nonsingular terminal sliding mode control was developed in [104]

for variable speed wind turbine. The performance of controller was proven to be robust to input disturbances and parametric uncertainties. Adaptive H_∞ control of large wind turbines was discussed in [34]. The designed controller was presented using LMIs and linear parameter varying theory was used to design a multi-variable adaptive controller with the control objective being improving rotational speed control and reduction of tower vibrations. Increased pitch variations was reported as the main downside in the implementation of the controller. An adaptive H_∞ controller with wind estimator was proposed in [35]. The designed estimator use the plant dynamics to track the average change of the wind profile. According to the authors, the proposed scheme allows robust rejection of $\mathcal{L}_2$ bounded perturbations.

Fault ride through capability of a wind turbine system describes the ability of the system to remain connected to the power grid during and after grid faults, or when the system is experiencing voltage dips due to load disturbances. The enhancement of fault ride-through capability for a full rated converter wind turbine using nonlinear adaptive control was studied in [105]. The proposed non linear adaptive control is based on output feedback control and was proven to be adaptive to parameter uncertainties, unknown nonlinearities, time dependent external disturbances such as grid faults, voltage dips and intermittent wind speeds. The proposed control scheme was compared with conventional vector control and feedback linearizing control and it was demonstrated that better fault ride through control was achieved with the proposed control scheme.

Adaptive control of a WTS based on neural networks was studied in [106]. The nonlinear system was identified using a nonlinear autoregressive network with exogenous inputs. Consequently an indirect model reference adaptive neuro controller was developed based on the NARX model. Based on simulation results, the proposed system showed good robustness, load disturbance attenuation and better tracking in the presence of parameter variations due to variation in hydraulic pressure in hydraulic pitch system. A novel adaptive radial-basis function neural network was proposed in [107] for non-affine variable-speed variable-pitch wind turbines with unmodeled dynamics. The adaptive radial basis function was used to approximate the non-parametric uncertainties present in the system. The radial basis neural networks was used to estimated the unmodeled dynamics in the system. The control law was implemented in two phases; in the first phase, the generator torque was used to control the rotor speed while the pitch angle was kept at a constant value. The parameter uncertainties considered with respect to the dynamics of the system include the rotor and generator inertia. Adaptive control laws were formulated based on the tracking error of the rotor speed, estimation error of the damping coefficient, the neural network weight parameters, the disturbance bounds and error resulting from the neural network estimation. In the second phase, the generator torque was assumed constant while the pitch angle was used as control input. Due to the non-affine nature of the pitch angle, the properties of Nussbaum-type functions were used to address the problem of the unknown direction of the control input. The stability of the control scheme

was proven used Lyapunov analysis. Adaptive maximum power tracking control of a DFIG-based wind generation system was discussed in [108]. According to the authors, the proposed adaptive scheme does not rely on the precise parameters of the turbine system or wind speed measurements. Although, the proposed scheme does not use real-time wind measurements, the wind speed was assumed to be bounded by a certain value.

An adaptive pitch control scheme based on recursive least squares estimation was proposed in [109] for reduction of fatigue loads in small wind turbines. A self-tuning regulator (STR) is designed for pitch angle control. The proposed STR consists of a recursive least squares estimator and a PID controller with adjustable gains. In [110], an adaptive system was designed for MPPT control of wind turbine using PI controller, RBF neural network and Gravitational Search Algorithm (GSA). The GSA algorithm was used to obtain the optimal values of the PI controller at different wind speeds. The optimal values were then used to train the RBF neural network. Adaptive fuzzy sliding-mode control for a variable speed wind turbine was discussed in [36]. The chattering caused by sliding mode controllers was minimized by the implementation of adaptation in the fuzzy sliding mode controller. The weights used in the fuzzy controller output was tuned using an adaptation mechanism based on gradient descent algorithm. Also, in [37], adaptive control of VSVP wind turbine was studied for different operation modes. The RBF-NN weight updating rules were obtained using Lyapunov stability analysis.

1.5.4 Model Predictive Control

In [28], a fuzzy model based multivariable predictive control was proposed for a wind turbine system. The control law was obtained by solving a convex optimization problem subject to LMI conditions. Takagi-Sugeno fuzzy inference system was used to represent the nonlinear system by using linear models obtained by linearizing the system at different operating wind speeds. The predictive control problem was cast into LMI form using Schur complement. The control objective was to obtain the best tracking of rated power while regulating rotor speed. The reported error between desired and actual power was 6.5% of desired value.

A robust nonlinear model predictive control (MPC) strategy for a permanent magnet synchronous magnet generator based WTS was discussed in [111]. The control objective was to track the desired reference in the presence of disturbances. The manipulated variable was the d-axis current and the control input used were the d- and q- axis voltage components. The prediction of the outputs was done using Taylor's series expansion using Lie' derivatives. It is possible to formulate the MPC control problem of WT systems as a multi-objective optimization problem with two conflicting objectives namely generated power and structural loads. In [112], the tuning of a linear multi-objective controller for wind turbines using Pareto-optimality was discussed. The objective of this paper was to achieve a suitable trade-off between damping tower fore-aft vibrations and mean generated power.

The model predictive direct power control of DFIG generators under unbal-

anced grid voltage was studied in [113]. Power regulation (Active and Reactive) and cancellation of torque oscillations were the desired control objective . Two objective functions were formulated. The first objective function was formulated for minimization of error between desired and actual active and reactive powers. In [114], a semi-definite programming approach was applied to the regulation of output power in a wind energy conversion system. The controller was designed to operate in the full load region of operation of the turbine. A cost function was formulated to minimize the deviation of the generator angular velocity and output power from their rated values using generator torque and blade pitch angle as control inputs.

Robust MPC for variable speed wind turbines was discussed in [29]. The control objective was minimization of tower damping oscillations. The model used for designing the controller were obtained by performing system identification using step response and regression identification. The robust MPC and nominal MPC controllers were compared. It was demonstrated that the robust MPC outperforms the nominal MPC controller. Nonlinear Model Predictive Control was applied to a DFIG-based wind generation system in [115]. The nonlinear model of the DFIG-based turbine takes into account unbalanced grid conditions. The prediction was done based on input-output feedback linearization scheme. The objective function used was formulated to take into consideration economic and reference tracking under specific constraints.

The rotation effect of wind turbine blades generate mechanical loads on the

blades and the hub that are sampled with harmonics of the rotor speed. These frequency components are denoted as 1P, 2P, 3P and so on. These fluctuating loads lead to fatigues on the turbine blades. A frequency-weighted model predictive controller of trailing edge flaps towards minimization of mechanical loads on the turbine blades was discussed in [30]. An average load reduction of about 13.8 % was recorded. State-constrained MPC incorporating both feedback and feedforward control of wind turbines was studied in [116]. The collective pitch and torque control under full load condition was examined. The MPC control problem was formulated to enforce some constraints on the state of the system. It was deduced that the inclusion of state constraints can be used to avoid unnecessary shutdowns that may result due to any of the state violating their rated values. Three different scenarios were examined in the simulation for the controller; normal operation, grid-loss and wind gust scenarios.

Classical feedback based control systems are late in responding to wind changes because they control action is implemented to a wind variation that has already passed. In [31], the subject of LiDAR(Light Detection and Ranging) enabled model predictive control of wind turbines was discussed. LiDAR is a sensory devices for estimating the spatial distribution of wind flow at a distance of tens of meters from the turbine. Constrained MPC controller was developed for a wind turbine model for maximum power extraction and load minimization in [32]. Four different MPC controllers were implemented for different operating regions. In the first three operating regions, the control objective is optimal power capture while

in the fourth region, the control objective is power regulation. The generator speed is low, variable and at nominal levels in Region I, II and III respectively.

1.6 Statement of Research Problem

The intermittent and unsteady nature of the wind is an important problem in control design for wind turbines due to the presence of numerous operating conditions. An ideal wind turbine controller should guarantee stable operation across these operating regions and also fulfill the control objectives in a given operating region. Therefore, it is imperative to design a controller that adjusts its parameters based on the wind speed. In this thesis, the design of model predictive controllers using continuous-time models is considered.

1.7 Objectives of the Research

The objectives of this research are:

- Obtain a detailed nonlinear model of the wind turbine system from existing literature and linearize around specific operating wind speeds.
- Design an adaptive model predictive controller for the wind turbine system using linearized models.
- Design a multi-model predictive controller for the wind turbine system using linearized models.

- Perform simulation studies on the developed controllers under wind variations.

1.8 Limitations of the Research

The scope of this study is limited to the control of variable-speed, variable-pitch horizontal axis wind turbines. The dynamics considered include; the drive-train, pitch actuator and generator torque actuator. The tower and electrical dynamics of the system are neglected in the model description.

1.9 Thesis Structure

The thesis is composed of four main sections. In Chapter Two, some important modeling concepts for wind turbine systems are reviewed. A detailed wind turbine for control design is defined and some simplifying assumptions are established. Chapter Three describes the mathematical formulation for continuous model predictive control using Laguerre functions. The continuous-time model predictive controller was designed for the wind turbine at each operating condition. In Chapter Four, an adaptive model predictive controller that adjusts its parameters based on measured wind speed is presented. In Chapter Five, a continuous-time multi-model predictive controller is designed to control the wind turbine system over multiple operating conditions using linearized model describing the behavior of the turbine at each operating point. Chapter Six presents the

conclusion and future outlook of the research.

CHAPTER 2

MODELING AND SYSTEM ANALYSIS

2.1 Introduction

Wind turbines systems (WTS) are electromechanical systems comprising of multiple interconnected subsystems. In modeling WTS, some important components are considered such as the aerodynamics, drive-train, generator and the grid (for grid-connected systems). In this chapter, some important modeling equations are reviewed based on [27, 117–122]. The following subsections describe each of the subsystems. Finally, the linearization of the system model was also carried out as well as eigenvalue analysis at different operating wind speed.

2.2 Aerodynamics

The mechanical power, aerodynamic torque and thrust force of the turbine are given in Equation 2.1. The thrust force, F_t, is responsible for tower displacements and blade flapping and bending. T_r defines the torque produced as a result of wind flowing through the turbine and P_r is the resulting mechanical power.

$$\begin{aligned} F_t &= \frac{1}{2}\rho\pi R_b^2 V_w^2 C_t(\lambda,\beta) \\ T_r &= \frac{1}{2}\rho\pi R_b^3 V_w^2 C_q(\lambda,\beta) \\ P_r &= \frac{1}{2}\rho\pi R_b^2 V_w^3 C_p(\lambda,\beta) \end{aligned} \tag{2.1}$$

ρ represents the air density; R_b is the blade radius; V_w is the wind velocity; β is the blade pitch angle. C_p, C_q, C_t, are the power, torque and thrust coefficient respectively. λ and β are tip-speed ratio and blade pitch angle respectively. The tip speed ratio, blade radius, rotor speed and wind velocity are related by

$$\lambda = \frac{\omega_r R_b}{V_w} \tag{2.2}$$

The torque and power coefficient are related by the expression:

$$C_Q(\lambda,\beta) = \frac{C_p(\lambda,\beta)}{\lambda} \tag{2.3}$$

The power coefficient is a highly nonlinear function of λ and β and may have different mathematical definitions. In [117–120], the power coefficient is expressed as:

$$C_p(\lambda, \beta) = c_1(\frac{c_2}{\lambda_i} - c_3\beta - c_4\beta^{c_5} - c_6)e^{-\frac{c_7}{\lambda_i}} \tag{2.4}$$

where

$$\lambda_i = \frac{1}{\frac{1}{\lambda - c_8\beta} - \frac{c_9}{\lambda - \beta^3}}$$

Another mathematical definition of C_p is given by [117, 121, 122]:

$$C_p(\lambda, \beta) = (c_1 - c_2\beta)\sin(\frac{\pi(\lambda + c_3)}{c_4 + c_5\beta}) - c_6(\lambda - 3)\beta \tag{2.5}$$

For fixed-pitch wind turbine system, the torque coefficient can be expressed as [123]:

$$C_Q(\lambda) = a_0 + a_1\lambda + a_2\lambda^2 + a_3\lambda^3 + a_4\lambda^4 + a_5\lambda^5 + a_6\lambda^6$$

2.3 Mechanical System

The mechanical subsystem can be represented by the general second-order model (2.6)

$$M\ddot{q} + C\dot{q} + Kq = Q(\dot{q}, q, t, u) \tag{2.6}$$

where M, C, K represent mass, damping and stiffness matrices respectively. The dynamics of the system can be derived using the Lagrangian equation (2.7):

$$\frac{d}{dt}\left(\frac{\partial E_k}{\partial \dot{q}}\right) - \frac{\partial E_k}{\partial q} + \frac{\partial E_d}{\partial \dot{q}} + \frac{\partial E_p}{\partial q} = Q \tag{2.7}$$

where E_k, E_d, E_p represent the kinetic, potential and dissipated energy in the system, q and Q denote vector of system states and force respectively. In defining the states of the mechanical subsystem of the wind turbines, the system states are defined as $q = [y_t\ \zeta\ \theta_r\ \theta_g]^T$ where y_t is the axial displacement of the tower head, ζ is the angular displacement of the out of plane rotation, θ_r and θ_g are angular displacement of rotor and generator respectively.The driving forces $Q = [NF_T\ NF_TR_b\ T_r\ -T_g]$. F_T, R_b, T_r and T_g are thrust force, blade radius, rotor torque and generator torque respectively. N is the number of blades of the turbine. The kinetic, potential and dissipated energy are defined as:

$$
\begin{aligned}
E_k &= \frac{1}{2}m_t\dot{y}_t^2 + \frac{1}{2}Nm_b(\dot{y}_t + R_b\dot{\zeta})^2 + \frac{1}{2}J_r\Omega_r^2 + \frac{1}{2}J_g\Omega_g^2 \\
E_d &= \frac{1}{2}B_t\dot{y}_t^2 + \frac{1}{2}NB_b(R_b\dot{\zeta})^2 + \frac{1}{2}B_s(\Omega_r - \Omega_g)^2 \\
E_p &= \frac{1}{2}K_t y_t^2 + \frac{1}{2}NK_b(R_b\zeta)^2 + \frac{1}{2}B_s(\theta_r - \theta_g)^2
\end{aligned} \tag{2.8}
$$

Taking the derivative of each of the terms in (2.8) , according to (2.7)

$$
\frac{d}{dt}\left(\frac{\partial E_k}{\partial \dot{q}}\right) = \begin{bmatrix} \ddot{y}_t(M_t + NM_b) \\ NM_b(\ddot{y}_t + R_b\ddot{\zeta})R_b \\ J_r\dot{\Omega}_r \\ J_g\dot{\Omega}_g \end{bmatrix}, \quad \frac{\partial E_d}{\partial \dot{q}} = \begin{bmatrix} B_t\dot{y}_t \\ NB_bR_b\dot{\zeta} \\ B_s(\Omega_r - \Omega_g) \\ -B_s(\Omega_r - \Omega_g) \end{bmatrix}
$$

$$
\frac{\partial E_p}{\partial q} = \begin{bmatrix} K_t y_t \\ NK_b r_b\zeta \\ K_s(\theta_r - \theta_g) \\ -K_s(\theta_r - \theta_g) \end{bmatrix}, \quad \frac{\partial E_k}{\partial q} = 0
$$

It is now possible to write (2.7) in terms of (2.6) with the matrices M, C and K defined as:

$$M = \begin{bmatrix} (M_t + NM_b) & NM_bR_b & 0 & 0 \\ NM_br_b & NM_bR_b^2 & 0 & 0 \\ 0 & 0 & J_r & 0 \\ 0 & 0 & 0 & J_g \end{bmatrix} \quad C = \begin{bmatrix} B_t & 0 & 0 & 0 \\ 0 & B_bR_b^2 & 0 & 0 \\ 0 & 0 & B_s & -B_s \\ 0 & 0 & -B_s & B_s \end{bmatrix}$$

$$K = \begin{bmatrix} K_t & 0 & 0 & 0 \\ 0 & K_bR_b^2 & 0 & 0 \\ 0 & 0 & K_s & -K_s \\ 0 & 0 & -K_s & K_s \end{bmatrix}$$

In this study, the tower bending dynamics are neglected to arrive at the following two-mass state-space representation for the drive train

$$\begin{aligned} \dot{\Omega}_r &= -\frac{B_s}{J_r}\Omega_r + \frac{B_s}{J_rN_g}\Omega_g - \frac{K_s}{J_r}\Omega_t + \frac{P_r}{J_r\Omega_r} \\ \dot{\Omega}_g &= -\frac{B_s}{J_gN_g^2}\Omega_g + \frac{B_s}{J_gN_g}\Omega_r + \frac{K_s}{J_gN_g}\Omega_t - \frac{T_g}{J_g} \\ \dot{\Omega}_t &= \Omega_r - \frac{1}{N_g}\Omega_g \end{aligned}$$

An extra state Ω_t, which represent the torsional displacement has been included in the drive-train dynamics.

2.4 Pitch Actuator

The pitch actuation system is represented by a second-order dynamical system with the following dynamics:

$$\ddot{\beta} = -\omega_n^2 \beta + 2\zeta\omega_n \dot{\beta} + \omega_n^2 \beta_{ref} \tag{2.9}$$

ω_n is the natural frequency of blade pitch actuator, ζ is the pitch actuator damping constant.

2.5 Generator

Also, the dynamics of the generator is represented by a first-order system as follows;

$$\dot{T}_g = -\frac{1}{\tau_g} T_g + \frac{1}{\tau_g} T_{g,ref} \tag{2.10}$$

τ_g is the generator actuator time constant. The generator power P_g is defined as

$$P_g = T_g \Omega_g \tag{2.11}$$

2.6 Aggregated System Model

The entire nonlinear system is described by the following dynamics:

$$\begin{aligned} \dot{x} &= Ax + Bu + g(x, w) \\ y &= f(x) \end{aligned} \tag{2.12}$$

where $x(t) \in \mathcal{R}^n$, $u(t) \in \mathcal{R}^m$, $y(t) \in \mathcal{R}^p$ are system state, input and output matrices respectively. The states are defined as $x = [\Omega_r\ \Omega_g\ \Omega_t\ \beta\ \dot{\beta}\ T_g]^T$, the control inputs are defined as $u = [\beta_{ref}\ T_{g,ref}]^T$, the disturbance inputs are $w = V_w$ and the measured outputs are $y = [P_g\ \Omega_r]^T$.

$$A = \begin{bmatrix} -\frac{B_s}{J_r} & \frac{B_s}{J_r N_g} & -\frac{K_s}{J_r} & 0 & 0 & 0 \\ \frac{B_s}{J_g N_g} & -\frac{B_s}{J_g N_g^2} & \frac{K_s}{J_g} & 0 & 0 & -\frac{1}{J_g} \\ 1 & -\frac{1}{N_g} & 0 & 0 & 0 & 0 \\ 0 & 0 & 0 & 0 & 1 & 0 \\ 0 & 0 & 0 & -\omega_n^2 & -2\zeta\omega_n & 0 \\ 0 & 0 & 0 & 0 & 0 & -\frac{1}{\tau} \end{bmatrix}$$

$$B^T = \begin{bmatrix} 0 & 0 & 0 & 0 & \omega_n^2 & 0 \\ 0 & 0 & 0 & 0 & 0 & \frac{1}{\tau} \end{bmatrix}$$

$$g^T(x, w) = \begin{bmatrix} \frac{P_r}{\Omega_r J_r} & 0 & 0 & 0 & 0 & 0 \end{bmatrix}$$

The system parameters are defined in Table 2.1:

Table 2.1: NREL offshore 5-MW baseline wind turbine

Parameter	Symbol/Unit	Value
Rated Power	$P_g(kW)$	5000
Rated Rotor Speed	$\Omega_{r,max}$	12.1
Cut-in Rotor Speed	$\Omega_{r,min}$	6.9
Drive train Spring Constant	$K_s(Nm/rad)$	867.637×10^6
Drive train Damping Constant	$D_s(Nm/rad/s)$	6.215×10^6
Generator inertia	$J_g(Kgm^2)$	534.116
Rotor inertia	$J_r(Kgm^2)$	3.8768×10^7
Blade Radius	R_b	63
Gear Ratio	N_g	97
Max blade pitch	$\beta_{max}(deg)$	90
Min blade pitch	$\beta_{min}(deg)$	-1
Max generator torque	$T_{g,max}(Nm)$	47402.97
Generator time constant	τ_g	0.1
Natural frequency of blade pitch actuator	ω_n	0.88
Damping constant of blade pitch actuator	ζ	0.9

2.7 Linearized Model

Consider the nonlinear system model in (2.12), a linear approximation of the system can be obtained about an operating point $(\bar{x}, \bar{w})$ described by:

$$\begin{aligned} \dot{x} &= \left(A + \left.\frac{\partial g(x,w)}{\partial x}\right|_{\bar{x},\bar{w}} \right) x + Bu + \left(\left.\frac{\partial g(x,w)}{\partial w}\right|_{\bar{x},\bar{w}} \right) w \\ y &= \left.\frac{\partial f(x)}{\partial x}\right|_{\bar{x}} x \end{aligned} \tag{2.13}$$

where $\left.\frac{\partial g(x,w)}{\partial x}\right|_{\bar{x},\bar{w}}$ and $\left.\frac{\partial g(x,w)}{\partial w}\right|_{\bar{x},\bar{w}}$ are Jacobian matrices of appropriate dimensions.

Since $g(x,w)$ is a function of only Ω_r, β and V_w, $\frac{\partial g(x,w)}{\partial x}$ with respect to the other system states will be zero. Hence, we proceed to obtain $\frac{\partial g(x,w)}{\partial \Omega_r}$, $\frac{\partial g(x,w)}{\partial \beta}$ and $\frac{\partial g(x,w)}{\partial V_w}$.

$$g(\Omega_r, \beta, V_w) = \frac{P_r}{\Omega_r J_r}, \text{and } P_r = \frac{1}{2}\rho\pi R_b^2 V_w^3 C_p(\lambda, \beta)$$

Therefore,

$$g(\Omega_r, \beta, V_w) = \frac{1}{2}\frac{\rho\pi R_b^2}{\Omega_r J_r} V_w^3 C_p(\lambda, \beta)$$

The C_p surface used is given by:

$$\begin{aligned} C_p(\lambda,\beta) &= 0.5176\left(\frac{116}{\lambda_i} - 0.4\beta - 5\right)e^{-\frac{21}{\lambda_i}} + 0.068\lambda \\ \frac{1}{\lambda_i} &= \frac{1}{\lambda + 0.08\beta} - \frac{0.035}{\beta^3 + 1} \end{aligned}$$

Since $\lambda = \frac{\Omega_r R_b}{V_w}$,

$$C_p(\Omega_r, \beta, V_w) = 0.5176\left(\frac{116}{\frac{\Omega_r R_b}{V_w} + 0.08\beta} - \frac{4.06}{\beta^3 + 1} - 0.4\beta - 5\right)e^{-\left(\frac{21}{\frac{\Omega_r R_b}{V_w} + 0.08\beta} - \frac{0.735}{\beta^3 + 1}\right)} + 0.068\frac{\Omega_r R_b}{V_w}$$

.

Let $h(\Omega_r, V_w) = \frac{1}{2}\frac{\rho\pi R_b^2}{\Omega_r J_r}V_w^3$, therefore we can re-write $g(\Omega_r, \beta, V_w) = h(\Omega_r, V_w)C_p(\Omega_r, \beta, V_w)$.

Hence,

$$\frac{\partial g(\Omega_r, \beta, V_w)}{\partial \Omega_r} = \frac{\partial h(\Omega_r, V_w)}{\partial \Omega_r}C_p(\Omega_r, \beta, V_w) + h(\Omega_r, V_w)\frac{\partial C_p(\Omega_r, \beta, V_w)}{\partial \Omega_r}$$
$$\frac{\partial g(\Omega_r, \beta, V_w)}{\partial \beta} = \frac{\partial h(\Omega_r, V_w)}{\partial \beta}C_p(\Omega_r, \beta, V_w) + h(\Omega_r, V_w)\frac{\partial C_p(\Omega_r, \beta, V_w)}{\partial \beta}$$
$$\frac{\partial g(\Omega_r, \beta, V_w)}{\partial V_w} = \frac{\partial h(\Omega_r, V_w)}{\partial V_w}C_p(\Omega_r, \beta, V_w) + h(\Omega_r, V_w)\frac{\partial C_p(\Omega_r, \beta, V_w)}{\partial V_w}$$

.

$$\frac{\partial h(\Omega_r, V_w)}{\partial \Omega_r} = -\frac{1}{2}\frac{\rho\pi R_b^2}{\Omega_r^2 J_r}V_w^3, \qquad \frac{\partial h(\Omega_r, V_w)}{\partial V_w} = \frac{3}{2}\frac{\rho\pi R_b^2}{\Omega_r J_r}V_w^2, \qquad \frac{\partial h(\Omega_r, V_w)}{\partial \beta} = 0$$

$$\frac{\partial C_p(\Omega_r,\beta,V_w)}{\partial \Omega_r} = 0.5176\left[\frac{-116R_b}{V_w\Big(\frac{\Omega_r R_b}{V_w}+0.08\beta\Big)^2}\right]e^{-\left(\frac{21}{\frac{\Omega_r R_b}{V_w}+0.08\beta}-\frac{0.735}{\beta^3+1}\right)} +$$

$$0.5176\left[\frac{116}{\frac{\Omega_r R_b}{V_w}+0.08\beta}-\frac{4.06}{\beta^3+1}-0.4\beta-5\right]\times$$

$$\frac{21R}{V_w\Big(\frac{\Omega_r R_b}{V_w}+0.08\beta\Big)^2}e^{-\left(\frac{21}{\frac{\Omega_r R_b}{V_w}+0.08\beta}-\frac{0.735}{\beta^3+1}\right)} + \frac{0.068R_b}{V_w}$$

$$\frac{\partial C_p(\Omega_r,\beta,V_w)}{\partial V_w} = 0.5176\frac{116\Omega_r R_b}{V_w^2\Big(\frac{\Omega_r R_b}{V_w}+0.08\beta\Big)^2}e^{-\left(\frac{21}{\frac{\Omega_r R_b}{V_w}+0.08\beta}-\frac{0.735}{\beta^3+1}\right)} +$$

$$0.5176\left[\frac{116}{\frac{\Omega_r R_b}{V_w}+0.08\beta}-\frac{4.06}{\beta^3+1}-0.4\beta-5\right]\times$$

$$\frac{-21\Omega_r R_b}{V_w^2\Big(\frac{\Omega_r R_b}{V_w}+0.08\beta\Big)^2}e^{-\left(\frac{21}{\frac{\Omega_r R_b}{V_w}+0.08\beta}-\frac{0.735}{\beta^3+1}\right)} - \frac{0.068\Omega_r R_b}{V_w^2}$$

$$\frac{\partial C_p(\Omega_r,\beta,V_w)}{\partial\beta} = 0.5176\left[\frac{-9.28}{\left(\frac{\Omega_r R_b}{V_w}+0.08\beta\right)^2}+\frac{12.18\beta^2}{(\beta^3+1)^2}-0.4\right]\times$$
$$e^{-\left(\frac{21}{\frac{\Omega_r R_b}{V_w}+0.08\beta}-\frac{0.735}{\beta^3+1}\right)} - 0.5176\left[\frac{116}{\frac{\Omega_r R_b}{V_w}+0.08\beta}-\frac{4.06}{\beta^3+1}-0.4\beta-5\right]\times$$
$$\left[\frac{-1.68}{\left(\frac{\Omega_r R_b}{V_w}+0.08\beta\right)^2}+\frac{0.735\beta^2}{(\beta^3+1)^2}\right]e^{-\left(\frac{21}{\frac{\Omega_r R_b}{V_w}+0.08\beta}-\frac{0.735}{\beta^3+1}\right)}$$

2.8 Model Analysis

The linearized system in (2.13) can be written as:

$$\begin{aligned}\dot{x}_c(t) &= A_c x(t) + B_c u(t) + \Gamma_c d_c(t)\\ y_c(t) &= C_c x(t)\end{aligned} \tag{2.14}$$

where $x_c(t) \in \mathcal{R}^n$, $u_c(t) \in \mathcal{R}^m$, $d_c(t) \in \mathcal{R}^l$ and $y_c(t) \in \mathcal{R}^p$ represent states, inputs, disturbances and outputs respectively. Also, $A_c \in \mathcal{R}^{n\times n}$, $B_c \in \mathcal{R}^{n\times m}$, $\Gamma_c \in \mathcal{R}^{n\times l}$, and $C_c \in \mathcal{R}^{p\times n}$ are state, input, disturbance and output matrices respectively.

2.8.1 System Matrices

The system matrices A_c, B_c, C_c are given below for wind speeds at $4ms^{-1}$, $8ms^{-1}$, $11ms^{-1}$ and $18ms^{-1}$.

Linearized model at $4ms^{-1}$

$$A_c = \begin{bmatrix} -0.1880 & 0.0016528 & -22.381 & -0.0009162 & 0 & 0 \\ 119.96 & -1.2367 & 16747 & 0 & 0 & -0.0018723 \\ 1 & -0.010309 & 0 & 0 & 0 & 0 \\ 0 & 0 & 0 & 0 & 1 & 0 \\ 0 & 0 & 0 & -0.7740 & -1.5840 & 0 \\ 0 & 0 & 0 & 0 & 0 & -10 \end{bmatrix}$$

$$B_c^T = \begin{bmatrix} 0 & 0 & 0 & 0 & 0.7740 & 0 \\ 0 & 0 & 0 & 0 & 0 & 10 \end{bmatrix}$$

$$\Gamma_c^T = \begin{bmatrix} 0.0061 & 0 & 0 & 0 & 0 & 0 \end{bmatrix}$$

$$C_c = \begin{bmatrix} 0 & 3.3477 & 0 & 0 & 0 & 0.070082 \\ 9.549 & 0 & 0 & 0 & 0 & 0 \end{bmatrix}$$

Linearized model at $8ms^{-1}$

$$
\begin{aligned}
A_c &= \begin{bmatrix}
-0.2387 & 0.0016528 & -22.381 & -0.0028 & 0 & 0 \\
119.96 & -1.2367 & 16747 & 0 & 0 & -0.0018723 \\
1 & -0.010309 & 0 & 0 & 0 & 0 \\
0 & 0 & 0 & 0 & 1 & 0 \\
0 & 0 & 0 & -0.7740 & -1.5840 & 0 \\
0 & 0 & 0 & 0 & 0 & -10
\end{bmatrix} \\
B_c^T &= \begin{bmatrix}
0 & 0 & 0 & 0 & 0.7740 & 0 \\
0 & 0 & 0 & 0 & 0 & 10
\end{bmatrix} \\
\Gamma_c^T &= \begin{bmatrix}
0.0208 & 0 & 0 & 0 & 0 & 0
\end{bmatrix} \\
C_c &= \begin{bmatrix}
0 & 18.812 & 0 & 0 & 0 & 0.0997714 \\
9.549 & 0 & 0 & 0 & 0 & 0
\end{bmatrix}
\end{aligned}
$$

Linearized model at $11ms^{-1}$

$$
\begin{aligned}
A_c &= \begin{bmatrix}
-0.2680 & 0.0016528 & -22.381 & -0.0054 & 0 & 0 \\
119.96 & -1.2367 & 16747 & 0 & 0 & -0.0018723 \\
1 & -0.010309 & 0 & 0 & 0 & 0 \\
0 & 0 & 0 & 0 & 1 & 0 \\
0 & 0 & 0 & -0.7740 & -1.5840 & 0 \\
0 & 0 & 0 & 0 & 0 & -10
\end{bmatrix} \\
B_c^T &= \begin{bmatrix}
0 & 0 & 0 & 0 & 0.7740 & 0 \\
0 & 0 & 0 & 0 & 0 & 10
\end{bmatrix} \\
\Gamma_c^T &= \begin{bmatrix} 0.0286 & 0 & 0 & 0 & 0 & 0 \end{bmatrix} \\
C_c &= \begin{bmatrix}
0 & 39.701 & 0 & 0 & 0 & 0.12290 \\
9.549 & 0 & 0 & 0 & 0 & 0
\end{bmatrix}
\end{aligned}
$$

Linearized model at $18ms^{-1}$

$$
A_c = \begin{bmatrix}
-0.4219 & 0.0016528 & -22.381 & -0.0256 & 0 & 0 \\
119.96 & -1.2367 & 16747 & 0 & 0 & -0.0018723 \\
1 & -0.010309 & 0 & 0 & 0 & 0 \\
0 & 0 & 0 & 0 & 1 & 0 \\
0 & 0 & 0 & -0.7740 & -1.5840 & 0 \\
0 & 0 & 0 & 0 & 0 & -10
\end{bmatrix}
$$

$$
B_c^T = \begin{bmatrix}
0 & 0 & 0 & 0 & 0.7740 & 0 \\
0 & 0 & 0 & 0 & 0 & 10
\end{bmatrix}
$$

$$
\Gamma_c^T = \begin{bmatrix}
-0.0066 & 0 & 0 & 0 & 0 & 0
\end{bmatrix}
$$

$$
C_c = \begin{bmatrix}
0 & 40.683 & 0 & 0 & 0 & 0.12290 \\
9.549 & 0 & 0 & 0 & 0 & 0
\end{bmatrix}
$$

2.8.2 System Eigenvalues

Table 2.2 presents the eigenvalues of the system at wind speeds of $4ms^{-1}$, $8ms^{-1}$, $11ms^{-1}$ and $18ms^{-1}$ characterizing different operating regions of the wind turbine. From Table 2.2, it can be inferred that at these different wind speeds, the system is stable. Also, the effect of changing wind speeds can be observed significantly in the first eigenvalue, λ_1 of the system.

Table 2.2: Eigenvalues at Different Wind Speeds

λ	$4ms^{-1}$	$8ms^{-1}$	$11ms^{-1}$	$18ms^{-1}$
λ_1	-0.0245	-0.0694	-0.0953	-0.2316
λ_2	$-0.7001 + 13.9476i$	$-0.7030 + 13.9474i$	$-0.7047 + 13.9473i$	$-0.7135 + 13.9467i$
λ_3	$-0.7001 - 13.9476i$	$-0.7030 - 13.9474i$	$-0.7047 - 13.9473i$	$-0.7135 - 13.9467i$
λ_4	$-0.7920 + 0.3836i$	$-0.7920 + 0.3836i$	$-0.7920 + 0.3836i$	$-0.7920 + 0.3836i$
λ_5	$-0.7920 - 0.3836i$	$-0.7920 - 0.3836i$	$-0.7920 - 0.3836i$	$-0.7920 - 0.3836i$
λ_6	-10.000	-10.000	-10.000	-10.000

CHAPTER 3

CONTINUOUS-TIME MODEL PREDICTIVE CONTROL

3.1 Introduction

In this chapter, the mathematical definitions that form the basis for continuous model predictive control design including orthonormal set and Laguerre functions are reviewed based on the work by [17]. Subsequently, continuous-time model predictive controller was designed for the wind turbine system at different wind speeds using the linearized models obtained in the preceding chapter. Finally, the performance of these controllers were evaluated by simulations using constant wind speeds.

3.2 Orthonormal Set and Laguerre Functions

An orthonormal set can be formed over the interval $[0,\ \infty)$ from a sequence of real valued functions, $l_i(t)$, $i = 1, 2, ...$, if they satisfy the orthonormal property

$$\begin{aligned} \int_0^\infty l_i^2(t)dt &= 1 \\ \int_0^\infty l_i(t)l_j(t)dt &= 0,\ i \neq j \end{aligned} \tag{3.1}$$

A function $f(t)$ can be approximated by an orthonormal set as:

$$f(t) = \sum_{i=1}^{\infty} \alpha_i l_i(t) \tag{3.2}$$

$\alpha_i(t)$ are appropriate weighting coefficients computed as:

$$\alpha_i = \int_0^\infty l_i(t)f(t)dt \tag{3.3}$$

In theory, infinite number of coefficients are required for approximating the function $f(t)$. The orthonormal set is complete if for any piecewise continuous function $f(t)$ with

$$\int_0^\infty f^2(t)dt < \infty \tag{3.4}$$

there exists an integer N such that

$$\int_0^\infty (f(t) - \sum_{i=1}^{N} \alpha_i l_i(t))^2 dt < \epsilon \tag{3.5}$$

for any $\epsilon > 0$

Consider a transfer function $G(s) = \dfrac{0.5}{s^2 + 3s + 2}$, its impulse response $g(t)$ can be modeled using a set of orthonormal functions as shown in Figure 3.1

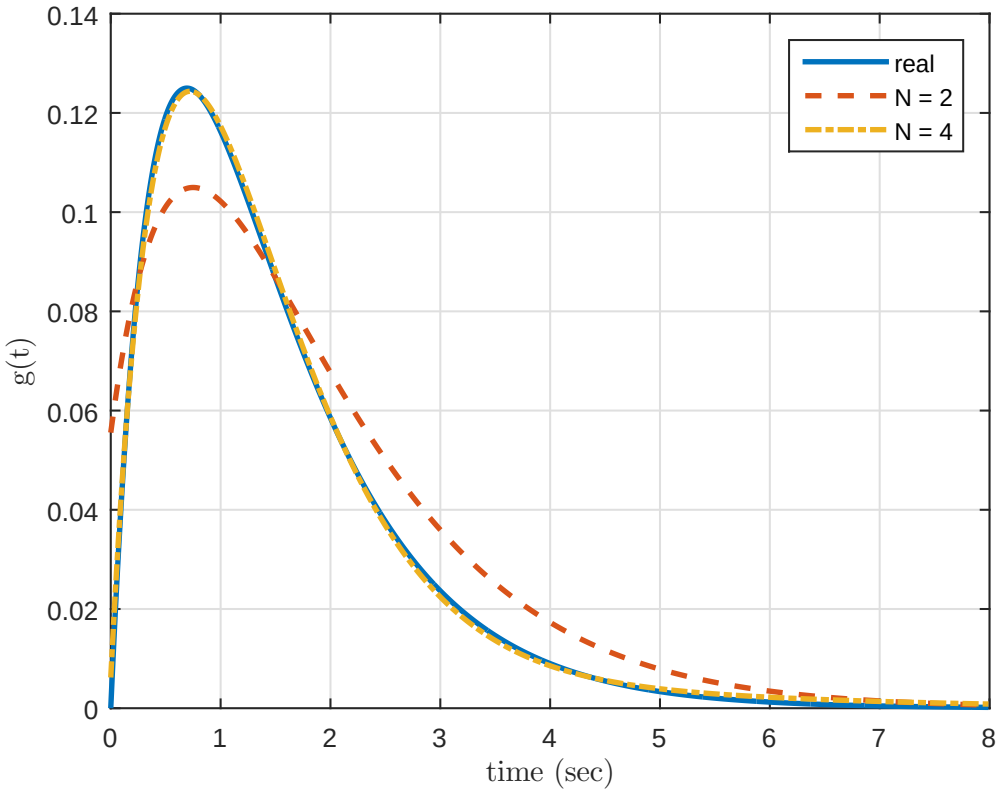

Figure 3.1: Impulse response $g(t)$ using orthonormal functions

Laguerre functions belong to a class of orthonormal functions that satisfy the property (3.1). The set of Laguerre functions are defined as follows for any $p > 0$

$$
\begin{aligned}
l_1(t) &= (\sqrt{2p})e^{-pt} \\
l_2(t) &= \sqrt{2p}(-2pt+1)e^{-pt} \\
\vdots &= \vdots \\
l_i(t) &= \sqrt{2p}\frac{e^{pt}}{(i-1)!}\frac{d^{i-1}}{dt^{i-1}}[t^{i-1}e^{-2pt}]
\end{aligned} \tag{3.6}
$$

p is a time scaling factor that determines the exponential decay rate. p and N are design parameters that are specified in the application of Laguerre functions. The Laplace transform of the Laguerre functions forms the Laguerre networks $L_i(s), i = 1, 2, ...$

$$
\begin{aligned}
L_1(s) &= \int_0^\infty l_1(t)e^{-st}dt = \frac{\sqrt{2p}}{s+p} \\
L_2(s) &= \int_0^\infty l_2(t)e^{-st}dt = \frac{\sqrt{2p}(s-p)}{(s+p)^2} \\
\vdots &= \vdots \\
L_i(s) &= \int_0^\infty l_i(t)e^{-st}dt = \frac{\sqrt{2p}(s-p)^{i-1}}{(s+p)^i}
\end{aligned} \tag{3.7}
$$

A state representation of the Laguerre functions is given by

$$
L(t) = e^{A_p t}L(0) \tag{3.8}
$$

where the initial condition state vector, $L(0) = \sqrt{2p}[1\ 1\ \ldots\ 1]^T$ and

$$A_p = \begin{bmatrix} -p & 0 & \ldots & 0 \\ -2p & -p & \ldots & 0 \\ \vdots & \vdots & \ddots & 0 \\ -2p & \ldots & -2p & -p \end{bmatrix} \tag{3.9}$$

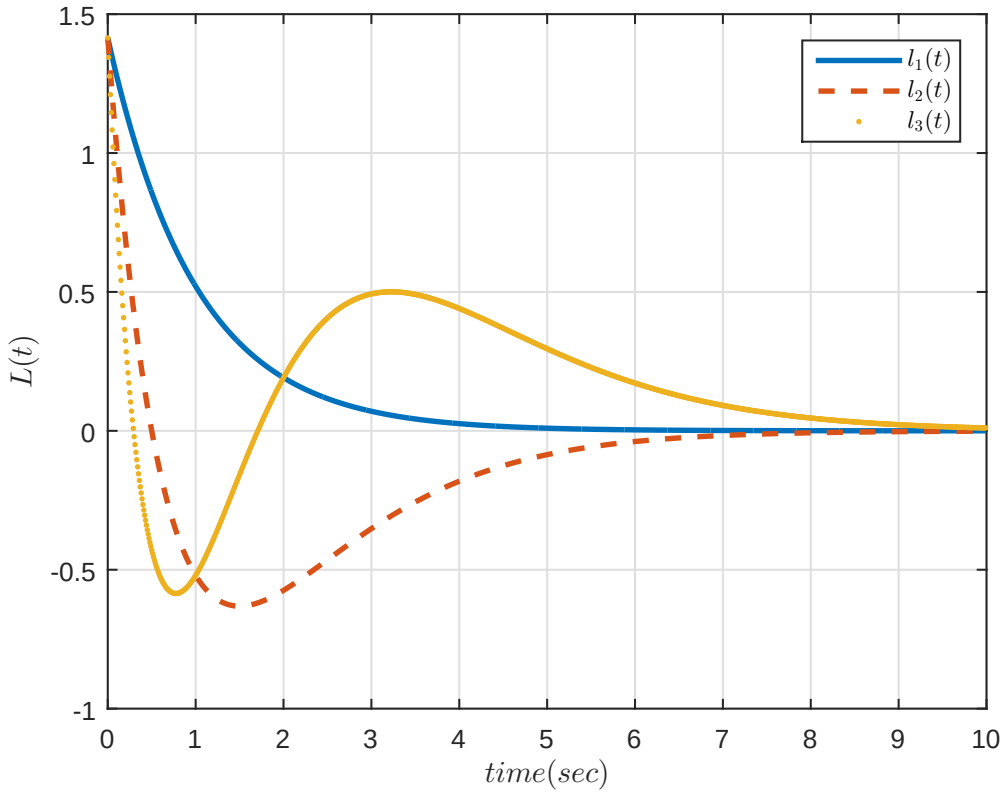

Figure 3.2: Graphical representation of Laguerre functions with $p = 1$ and $N = 3$

3.3 Continuous-time Model Predictive Control

Consider a continuous time linear state-space representation of the non-linear plant (2.12) described by :

$$\begin{aligned} \dot{x}_c(t) &= A_c x_c(t) + B_c u(t) + \Gamma_c d(t) \\ y_c(t) &= C_c x_c(t) \end{aligned} \tag{3.10}$$

where $x_c(t) \in \mathcal{R}^n$, $u(t) \in \mathcal{R}^m$, $d(t) \in \mathcal{R}^w$ $y_c(t) \in \mathcal{R}^p$ are system state, input, disturbance and output vectors respectively. In the design of predictive control law for a continuous time system, the control trajectory is represented by a set of orthonormal functions [17]. Hence the control signal $u(t)$, must satisfy the property (3.4), that is $\int_0^\infty u^2(t)dt < \infty$. However, if the input signal is a constant reference signal, the $u(t)$ does not satisfy (3.4). According to [17], this is because for the control signal to track the set point, it needs to converge to a non-zero constant related to the steady state gain of the plant and the magnitude of the set-point change. Consequently, the derivative of the set-point signal will be modeled to satisfy,

$$\int_0^\infty \dot{u}^2(t)dt < \infty$$

By taking the derivative of (3.10), a new state vector $x(t) = [\dot{x}_c(t)^T \; y_c(t)^T]^T$ can be derived based on (3.10) to arrive at the augmented state-space representation

given by:

$$\begin{aligned} \dot{x}(t) &= Ax(t) + B\dot{u}(t) \\ y(t) &= Cx(t) \end{aligned} \tag{3.11}$$

It is assumed that the disturbance is constant and thus $\dot{d}(t) = 0$, the system matrices A, B and C are defined as follows:

$$A \triangleq \begin{bmatrix} A_c & O_{n\times p} \\ C_c & O_{p\times p} \end{bmatrix} \; B \triangleq \begin{bmatrix} B_c \\ O_{p\times m} \end{bmatrix} \; C \triangleq \begin{bmatrix} O_{p\times n} & I_{p\times p} \end{bmatrix}$$

It is required to find an optimal control trajectory such that the system output $y(t)$ tracks a given reference $r_s(t)$ as $t \to \infty$. As MPC relies on prediction obtained from the dynamic model of the system, the prediction of the system states $x(t+\tau|t)$ at time t is computed as:

$$x(t+\tau|t) = e^{A\tau}x(t) + \int_0^\tau e^{A(\tau-\gamma)}B\dot{u}(\gamma)d\gamma$$

If the system is comprised of m control inputs and the input matrix B can be written in the form

$$B = [B_1 \;\; B_2 \;\; \ldots \;\; B_m]$$

Then the ith ($i = 1 \ldots m$) control signal is expressed in terms of the using Laguerre functions [17] as,

$$\dot{u}_i(\tau) = L_i(\tau)^T \eta_i$$

$L_i(\tau)^T = [l_1^i(\tau)\ l_2^i(\tau)\ \ldots\ l_{N_i}^i(\tau)]$ represent a vector of Laguerre functions for describing the control signals and η_i is a vector of coefficients defined as:

$$\eta_i = [c_1^i(\tau)\ c_2^i(\tau)\ \ldots\ c_{N_i}^i(\tau)]^T$$

The representation of the estimated system over the prediction horizon in (3.12) becomes:

$$x(t+\tau|t) \quad = \quad e^{A\tau}x(t) + \int_0^\tau e^{A(\tau-\gamma)}[B_1 L_1(\tau)^T \ldots \quad B_m L_m(\tau)^T]d\tau\ \eta$$

In compact form,

$$x(t+\tau|t) \quad = \quad e^{A\tau}x(t) + \Psi(\tau)^T \eta$$

$\Psi(\tau)$ is the convolution integral defined as:

$$\begin{aligned} \Psi(\tau)^T &= \int_0^\tau e^{A(\tau-\gamma)}[B_1 L_1(\tau)^T \ \ldots \ B_m L_m(\tau)^T]d\tau \\ \text{and} \ \ \eta^T &= [\eta_1^T \ \eta_2^T \ \ldots \ \eta_m^T] \end{aligned}$$

The predicted output at time T is:

$$y(t+\tau|t) = Ce^{A\tau}x(t) + C\Psi(\tau)^T\eta \tag{3.12}$$

Keeping in mind that the control objective is to track a desired reference, the cost function for the optimization of the control trajectory of the estimated system in (3.11) is:

$$J = \int_0^{T_p} ([r_s(t) - y(t+\tau|t)]^T[r_s(t) - y(t+\tau|t)] + \dot{u}(\tau)^T R\dot{u}(\tau))d\tau \tag{3.13}$$

With the assumption that the set point signal $r_s(t)$ is constant within the optimization window (i.e $\dot{r}_s(t) = 0$), (3.13) can be written in terms of the augmented state in (3.11), we get

$$J = \int_0^{T_p} (x(t+\tau|t)^T Q x(t+\tau|t) + \dot{u}(\tau)^T R\dot{u}(\tau))d\tau$$

where $x = [x_c \ y - r]^T$ and $Q = C^T C$

But $u_i(\tau) = L_i(\tau)^T \eta_i$,

$$J = \int_0^{T_p} (x(t+\tau|t)^T Q x(t+\tau|t) + \sum_{k=1}^{m} \eta_k^T L_k(\tau) L_k(\tau)^T \eta_k) d\tau \tag{3.14}$$

If $T_p \to \infty$, according to the orthonormal property of the Laguerre functions $\int_0^\infty L_k(\tau) L_k(\tau)^T d\tau$ is an identity matrix with an dimension equal to the number of Laguerre coefficients for the kth input

An alternative representation of the cost is;

$$J = \int_0^{T_p} (x(t+\tau|t)^T Q x(t+\tau|t)) d\tau + \eta^T R_y \eta$$

R_y is a block diagonal matrix with kth block being R_k and $R_k = r_k I_{N_k \times N_k}$

$$J = \int_0^{T_p} \left((e^{A\tau} x(t) + \Psi(\tau)^T \eta)^T Q (e^{A\tau} x(t) + \Psi(\tau)^T \eta) \right) d\tau + \eta^T R_y \eta$$

$$J = \eta^T \left[\int_0^{T_p} \Psi(\tau) Q \Psi(\tau)^T d\tau + R_y \right] \eta + 2\eta^T \int_0^{T_p} \Psi(\tau) Q e^{A\tau} x(t) d\tau + x(t)^T \int_0^{T_p} e^{A^T \tau} Q e^{A\tau} d\tau x(t) \tag{3.15}$$

For simplicity,

$$\Pi = \int_0^{T_p} \Psi(\tau) Q \Psi(\tau)^T d\tau + R_y, \qquad \Lambda = \int_0^{T_p} \Psi(\tau) Q e^{A\tau} d\tau$$

$$\begin{aligned} J &= [\eta + \Pi^{-1}\Lambda x(t)]^T \Pi(t) [\eta + \Pi^{-1}\Lambda x(t)] \\ &+ x(t)^T \int_0^{T_p} e^{A^T\tau} Q e^{A\tau} d\tau - x(t)^T \Lambda^T \Pi^{-1} \Lambda x(t) \end{aligned} \tag{3.16}$$

Since, the last two terms in the above expression does not depend on η, the simplified form of the cost function becomes,

$$J = [\eta + \Pi^{-1}\Lambda x(t)]^T \Pi [\eta + \Pi^{-1}\Lambda x(t)] \tag{3.17}$$

In an unconstrained case, taking $\dfrac{\partial J}{\partial \eta} = 0$, yields the optimal η is given as:

$$\eta^*(t) = -\Pi^{-1}\Lambda x(t) \tag{3.18}$$

The trajectory of $\dot{u}(\tau)$ over the prediction horizon is constructed as:

$$\dot{u}(\tau) = \begin{bmatrix} L_1(\tau)^T & 0 & \dots & 0 \\ 0 & L_2(\tau)^T & \dots & 0 \\ \vdots & \vdots & \ddots & \vdots \\ 0 & \dots & 0 & L_m(\tau)^T \end{bmatrix} \begin{bmatrix} \eta_1(t) \\ \eta_2(t) \\ \vdots \\ \eta_m(t) \end{bmatrix} \tag{3.19}$$

By applying the receding horizon strategy and expressing $\dot{u}(t)$ as a function of the state

$$\dot{u}(t) = - \begin{bmatrix} L_1(0)^T & 0 & \dots & 0 \\ 0 & L_2(0)^T & \dots & 0 \\ \vdots & \vdots & \ddots & \vdots \\ 0 & \dots & 0 & L_m(0)^T \end{bmatrix} \Pi^{-1}\Lambda x(t)$$

It is possible to write $\dot{u}(t) = Kx(t)$ where K is the

$$K = \begin{bmatrix} L_1(0)^T & 0 & \dots & 0 \\ 0 & L_2(0)^T & \dots & 0 \\ \vdots & \vdots & \ddots & \vdots \\ 0 & \dots & 0 & L_m(0)^T \end{bmatrix} \Pi^{-1}\Lambda$$

The control signal $u(t)$ at time t is obtained by integrating $\dot{u}(t)$,

$$u(t) = \int_0^t \dot{u}(\tau) d\tau \tag{3.20}$$

Constraints on the derivative of the control signal can be expressed as:

$$\dot{u}_{min} \leq \dot{u}(t) \leq \dot{u}_{max} \tag{3.21}$$

Since $\dot{u}(\tau) = L(\tau)^T \eta$ then, the constraints can be written in the form $M\eta \leq N$ as

$$\begin{bmatrix} -L(\tau) \\ L(\tau) \end{bmatrix} \eta \leq \begin{bmatrix} -\dot{u}_{min} \\ \dot{u}_{max} \end{bmatrix} \tag{3.22}$$

Using a sampling interval of Δt, the control signal $u(t)$ within the optimization window can be written as:

$$u(t) = u(t - \Delta t) + L(0)^T \eta \Delta t \tag{3.23}$$

where $L(0)^T \eta$ represent the derivative of the control signal at the beginning of the optimization window [17]. The constraints on the control signal is thus

written as:

$$u_{min} - u(t - \Delta t) \leq L(0)^T \eta \Delta t \leq u_{max} - u(t - \Delta t) \tag{3.24}$$

The control action $\dot{u}(t)$ is then obtained in terms of the variable η by optimizing (3.17) with respect to (3.22) and (3.24) using quadratic programming.

3.4 Simulation Studies

In this section, the results from closed-loop simulation with the continuous time MPC controller presented in the previous section using linearized models obtained at $4ms^{-1}$ and $8ms^{-1}$ are presented.

3.4.1 Simulation with Constant Wind Speed of $4ms^{-1}$

A constant wind speed of $4ms^{-1}$ (Figure 3.3) was applied to the system (2.12). The main control input in this region is the generator torque $T_{g,ref}$, the blade pitch angle command, β_{ref} is kept at its optimal position $\beta_{opt} = 0$. This is achieved by setting the diagonal element in the control weighting matrix, R corresponding to the β_{ref} very high relative to $T_{g,ref}$. Also, the most important objective in the low wind speed regime is the ensuring that Ω_r does not fall below $\Omega_{r,min}$, for this reason, the diagonal element in the weighting matrix Q corresponding to Ω_r was set higher relative to the P_g. The reference power $P_{g,ref}$ was computed using (3.25). The expression in (3.25) represents the maximum power that could be extracted from the wind at V_w.

$$P_{g,ref} = 0.5\rho\pi R_b^2 C_{p,max} V_w^3 \tag{3.25}$$

The system outputs P_g and Ω_r are shown in Figure 3.4. Ω_r was regulated at its minimum value $\Omega_{r,min}$, but P_g was unable to reach its maximum value because

the controller weights Q and R were tuned to give more priority to regulating Ω_r.

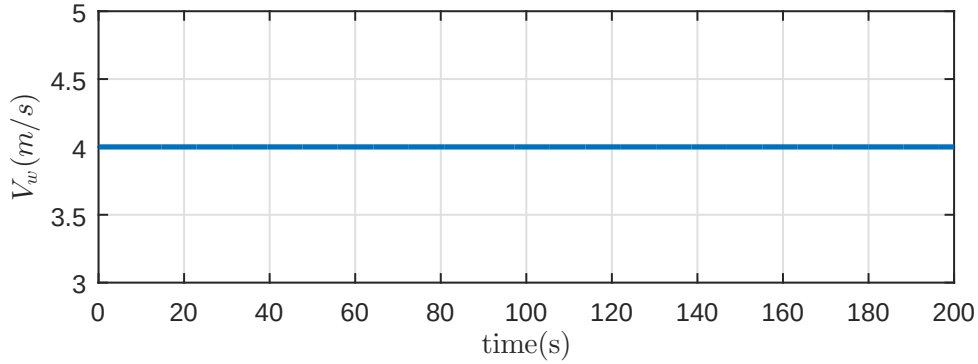

Figure 3.3: Constant wind speed, $V_w = 4ms^{-1}$

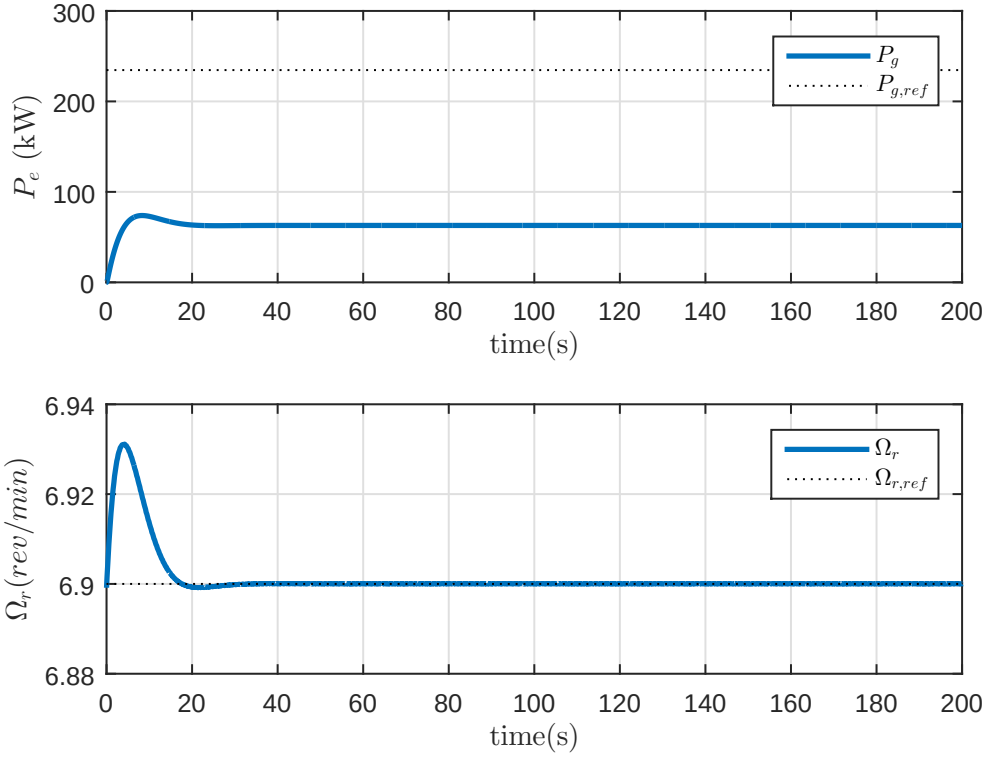

Figure 3.4: Simulation with constant wind speed $V_w = 4ms^{-1}$; generator power (top), rotor speed (bottom).

The main control input in this region is the generator toque as demonstrated by 3.5.

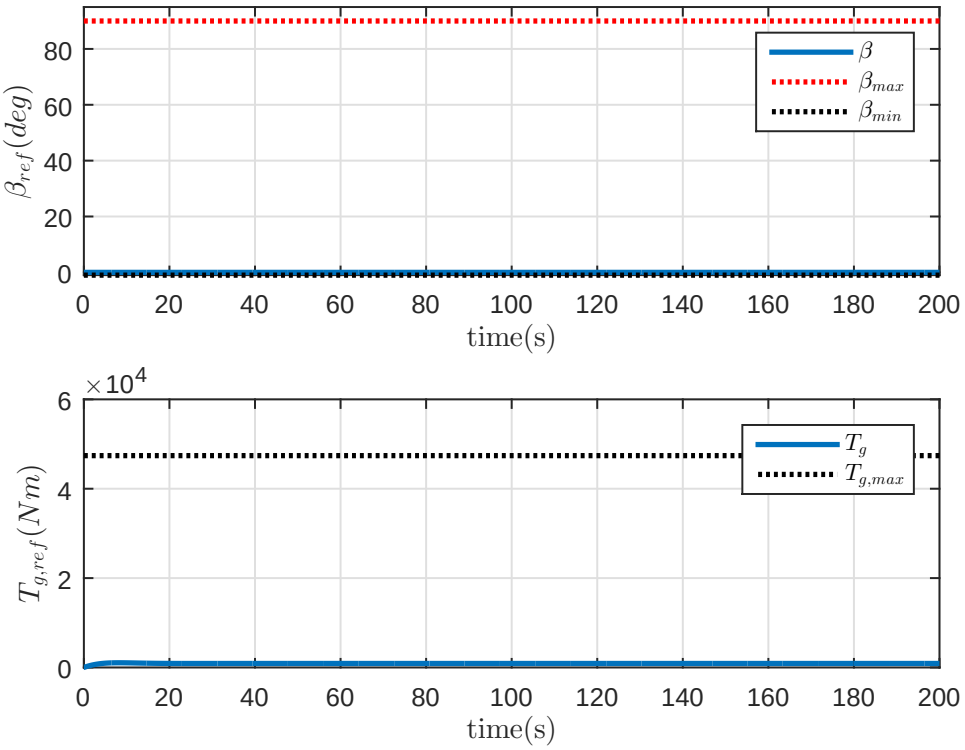

Figure 3.5: Simulation with constant wind speed $V_w = 4ms^{-1}$; pitch angle command (top), generator torque command (bottom).

3.4.2 Simulation with Constant Wind Speed of $8ms^{-1}$

The wind profile used in this simulation is shown in Figure 3.6. In this region, the generator power reference $P_{g,ref}$ was computed using the same relation as in (3.25). The rotor speed reference was computed using Equation (3.26).

$$\Omega_{r,opt} = \frac{\lambda_{opt} V_w}{R_b} \tag{3.26}$$

As shown in Figure 3.7, both Ω_r and P_g were able to track their reference values. The control inputs are shown in Figure 3.8.

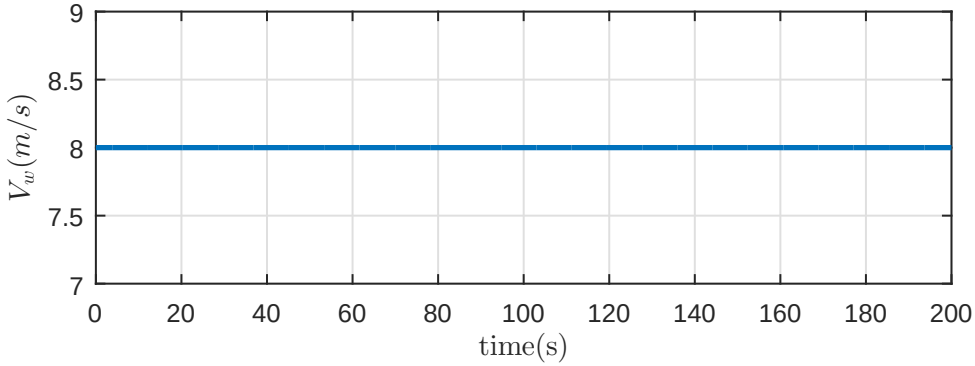

Figure 3.6: Constant wind speed, $V_w = 8ms^{-1}$

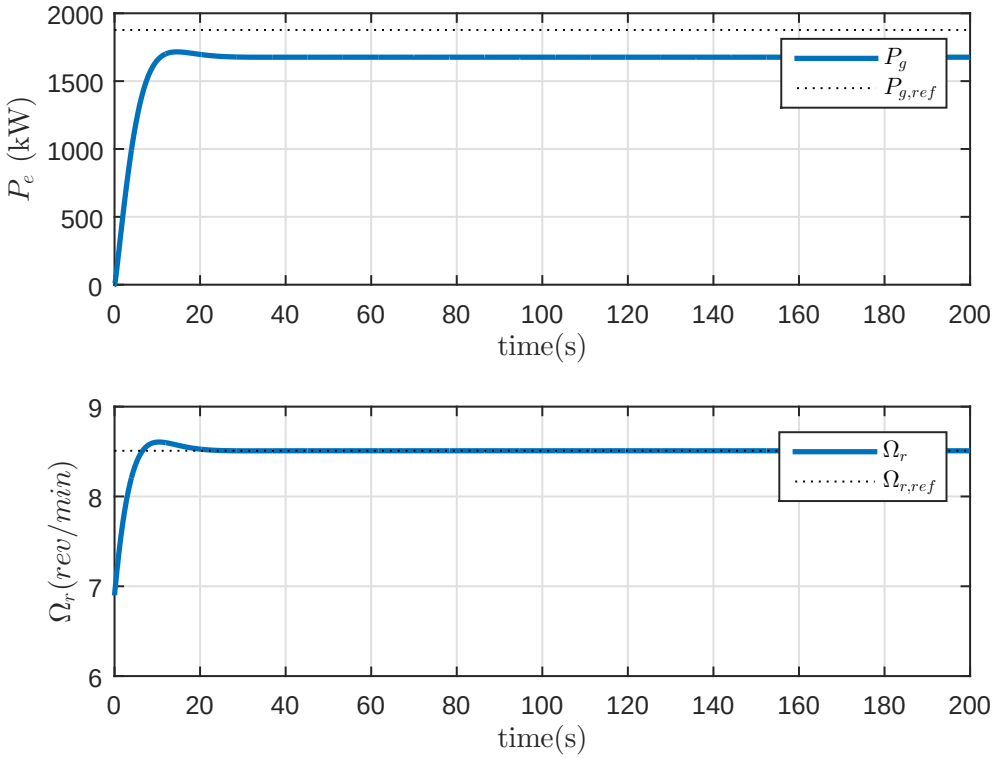

Figure 3.7: Simulation with constant wind speed $V_w = 8ms^{-1}$; generator power (top), rotor speed (bottom).

==

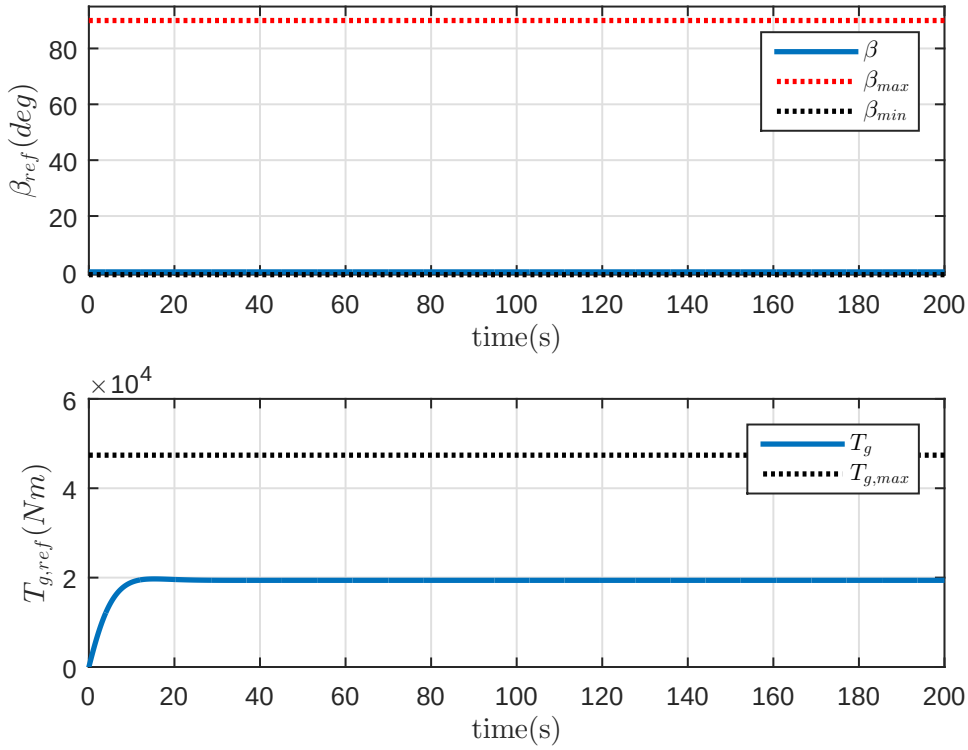

Figure 3.8: Simulation with constant wind speed $V_w = 8ms^{-1}$; blade pitch angle (top), generator torque (bottom) command.

3.5 Summary

In this section, the equations for model predictive controller design using orthonormal functions are presented. Also, controllers are designed to control the nonlinear wind turbine system about single operating conditions. Simulation studies were conducted using a 5MW wind turbine.

CHAPTER 4

CONTINUOUS-TIME ADAPTIVE MODEL PREDICTIVE CONTROL

4.1 Introduction

The operation of the turbine is highly dependent on the current wind speed, therefore, the controller design presented in the previous chapter can only guarantee satisfactory performance at only one operating speed. In this chapter, an adaptive gain-scheduled controller that updates its parameters based on the measured wind speed is presented. The performance of the controller was evaluated at different wind speeds using step and turbulent changes in wind speed. Simulation studies were carried out in the low, mid, high and top regions.

4.2 Adaptive Model Predictive Control

Consider the wind turbine system described by the following nonlinear dynamics:

$$\begin{aligned} \dot{x}_c(t) &= A_c x_c(t) + B_c u(t) + g(x_c(t), w(t)) \\ y_c(t) &= f(x_c(t)) \end{aligned} \tag{4.1}$$

where $x_c(t) \in \mathcal{R}^n$, $u_c(t) \in \mathcal{R}^m$, $y_c(t) \in \mathcal{R}^p$ are system state, input and output matrices respectively. A linear approximation of (4.1) can be obtained by linearizing the nonlinear term $g(x_c(t), w(t))$ to obtain the following linear system

$$\begin{aligned} \dot{x}_c(t) &= A_c(\bar{w}) x_c(t) + B_c u(t) + G(\bar{w}) w(t) \\ y_c(t) &= C_c(\bar{w}) x_c(t) \end{aligned} \tag{4.2}$$

$\bar{w}$ is an operating wind speed, $A_c(\bar{w}) = A_c + H(\bar{w})$, $C_c(\bar{w}) = \left.\dfrac{\partial f(x_c(t))}{\partial x_c(t)}\right|_{w(t)=\bar{w}}$

$H(\bar{w}) = \left.\dfrac{\partial g(x_c(t), w(t))}{\partial x_c(t)}\right|_{w(t)=\bar{w}}$ and $G(\bar{w}) = \left.\dfrac{\partial g(x_c(t), w(t))}{\partial w(t)}\right|_{w(t)=\bar{w}}$

In the design of predictive control law for a continuous time system, the control trajectory is represented by a set of orthonormal functions [17]. Hence the control signal $u(t)$, must satisfy the property (3.4), that is $\int_0^\infty u(t)dt < \infty$. However, if the input signal is a constant reference signal, the $u(t)$ does not satisfy (3.4). According to [17], this is because for the control signal to track the set point, it needs to converge to a non-zero constant related to the steady state gain of the

plant and the magnitude of the set-point change. Consequently, the derivative of the set-point signal will be modeled to satisfy,

$$\int_0^\infty \dot{u}^2(t)dt < \infty$$

With reference to the property in (3.4), the control design will be derived in terms of $\dot{u}(t)$, therefore we take the derivative of (4.2) and define the state variable $x(t) = [\dot{x_c}(t)^T \; y(t)^T]^T$. We now proceed to examine two distinct cases,

Case A: Constant disturbance $\dot{w}(t) = 0$

If $w(t)$ is assumed to be a constant, that is $\dot{w}(t) = 0$, the derivative of (4.2) reduces

$$\begin{aligned} \dot{x}(t) &= A(\bar{w})x(t) + Bu(t) \\ y(t) &= Cx(t) \end{aligned} \tag{4.3}$$

The system matrices A, B, C are defined as follows

$$A(\bar{w}) \triangleq \begin{bmatrix} A_c(\bar{w}) & O_{n\times p} \\ C_c(\bar{w}) & O_{p\times p} \end{bmatrix} \; B \triangleq \begin{bmatrix} B_c \\ O_{p\times m} \end{bmatrix}$$

$$C \triangleq \begin{bmatrix} O_{p\times n} & I_{p\times p} \end{bmatrix}$$

The predicted state information $x(t+\tau|t)$ is given by:

$$x(t+\tau|t) \;=\; e^{A(\bar{w})\tau}x(t) + \int_0^{\tau} e^{A(\bar{w})(\tau-\gamma)}B\dot{u}(\gamma)d\gamma$$

If the system is comprised of m control inputs, the input matrix B can be written in the form

$$B = [B_1 \;\; B_2 \;\; \ldots \;\; B_m]$$

Then the ith ($i = 1 \ldots m$) control signal is expressed in terms of Laguerre functions [17] as,

$$\dot{u}_i(\tau) = L_i(\tau)^T \eta_i$$

$L_i(\tau)^T = [l_1^i(\tau) \;\; l_2^i(\tau) \;\; \ldots \;\; l_{N_i}^i(\tau)]$ represent a vector of Laguerre functions for describing the control signals and η is a vector of coefficients defined as:

$$\eta_i = [c_1^i(\tau) \;\; c_2^i(\tau) \;\; \ldots \;\; c_{N_i}^i(\tau)]^T$$

The predicted state $x(t+\tau|t)$ at time τ is computed as:

$$x(t+\tau|t) \;=\; e^{A(\bar{w})\tau}x(t) + \int_0^{\tau} e^{A(\bar{w})(\tau-\gamma)}[B_1L_1(\tau)^T \ldots \;\; B_mL_m(\tau)^T]d\tau \;\; \eta$$

In compact form,

$$x(t+\tau|t) \;=\; e^{A(\bar{w})\tau}x(t) + \Psi(\bar{w},\tau)^T\eta$$

$\Psi(\bar{w},\tau)$ is the convolution integral defined as:

$$\begin{aligned}\Psi(\bar{w},\tau)^T &= \int_0^\tau e^{A(\bar{w})(\tau-\gamma)}[B_1L_1(\tau)^T \;\ldots\; B_mL_m(\tau)^T]d\tau \\ \text{and}\;\; \eta^T &= [\eta_1^T\;\eta_2^T\;\ldots\;\eta_m^T]\end{aligned}$$

The predicted output at time τ is:

$$y(t+\tau|t) \;=\; Ce^{A(\bar{w})\tau}x(t) + C\Psi(\bar{w},\tau)^T\eta \tag{4.4}$$

Keeping in mind that the control objective is to track a desired reference, the cost function for the optimization of the control trajectory of the system in (4.3) is:

$$J = \int_0^{T_p}([r_s(t) - y(t+\tau|t)]^T[r_s(t) - y(t+\tau|t)] + \dot{u}(\tau)^TR\dot{u}(\tau))d\tau \tag{4.5}$$

With the assumption that the set point signal $r_s(t)$ is constant within the optimization window (i.e $\dot{r}_s(t) = 0$), (4.5) can be written in terms of the augmented

state in (4.3), we get

$$J = \int_0^{T_p} (x(t+\tau|t)^T Q x(t+\tau|t) + \dot{u}(\tau)^T R \dot{u}(\tau)) d\tau \tag{4.6}$$

But $u_i(\tau) = L_i(\tau)^T \eta_i$,

$$J = \int_0^{T_p} (x(t+\tau|t)^T Q x(t+\tau|t) + \sum_{k=1}^{m} \eta_k^T L_k(\tau) L_k(\tau)^T \eta_k) d\tau$$

If $T_p \to \infty$, according to the orthonormal property of the Laguerre functions $\int_0^\infty L_k(\tau) L_k(\tau)^T d\tau$ is an identity matrix with an dimension equal to the number of Laguerre coefficients for the kth input

An alternative representation of the cost is;

$$J = \int_0^{T_p} (x(t+\tau|t)^T Q x(t+\tau|t) + \eta^T R_y \eta) d\tau$$

R_y is a block diagonal matrix with kth block being R_k and $R_k = r_k I_{N_k \times N_k}$

$$J = \int_0^{T_p} \left((e^{A(\bar{w})\tau} x(t) + \Psi(\bar{w}, \tau)^T \eta)^T Q (e^{A(\bar{w})\tau} x(t) + \Psi(\bar{w}, \tau)^T \eta) \right) d\tau + \eta^T R_y \eta$$

$$J = \eta^T \left[\int_0^{T_p} \Psi(\bar{w},\tau) Q \Psi(\bar{w},\tau)^T d\tau + R_y \right] \eta + 2\eta^T \int_0^{T_p} \Psi(\bar{w},\tau) Q e^{A(\bar{w})\tau} x(t) d\tau + x(t)^T \int_0^{T_p} e^{A(\bar{w})^T \tau} Q e^{A(\bar{w})\tau} d\tau x(t) \quad (4.7)$$

For simplicity,

$$\Pi(\bar{w}) = \int_0^{T_p} \Psi(\bar{w},\tau) Q \bar{w}, \Psi(\tau)^T d\tau + R_y, \qquad \Lambda(\bar{w}) = \int_0^{T_p} \Psi(\tau) Q e^{A(\bar{w})\tau} d\tau$$

$$J = [\eta + \Pi^{-1}(\bar{w})\Lambda(\bar{w})x(t)]^T \Pi(t) [\eta + \Pi^{-1}(\bar{w})\Lambda(\bar{w})x(t)]$$
$$+ x(t)^T \int_0^{T_p} e^{A(\bar{w})^T \tau} Q e^{A(\bar{w})\tau} d\tau - x(t)^T \Lambda(\bar{w})^T \Pi^{-1}(\bar{w}) \Lambda(\bar{w}) x(t) \quad (4.8)$$

Since, the last two terms in the above expression does not depend on η, the simplified form of the cost function becomes,

$$J = [\eta + \Pi^{-1}(\bar{w})\Lambda(\bar{w})x(t)]^T \Pi [\eta + \Pi^{-1}(\bar{w})\Lambda(\bar{w})x(t)] \quad (4.9)$$

In an unconstrained case, taking $\dfrac{\partial J}{\partial \eta} = 0$, yields the optimal η is given as:

$$\eta^*(t) = -\Pi^{-1}(\bar{w})\Lambda(\bar{w})x(t) \quad (4.10)$$

The trajectory of $\dot{u}(\tau)$ over the prediction horizon is constructed as:

$$\dot{u}(\tau) = \begin{bmatrix} L_1(\tau)^T & 0 & \dots & 0 \\ 0 & L_2(\tau)^T & \dots & 0 \\ \vdots & \vdots & \ddots & \vdots \\ 0 & \dots & 0 & L_m(\tau)^T \end{bmatrix} \begin{bmatrix} \eta_1(t) \\ \eta_2(t) \\ \vdots \\ \eta_m(t) \end{bmatrix} \tag{4.11}$$

By applying the receding horizon strategy and expressing $\dot{u}(t)$ as a function of the state $x(t)$,

$$\dot{u}(t) = - \begin{bmatrix} L_1(0)^T & 0 & \dots & 0 \\ 0 & L_2(0)^T & \dots & 0 \\ \vdots & \vdots & \ddots & \vdots \\ 0 & \dots & 0 & L_m(0)^T \end{bmatrix} \Pi^{-1}(\bar{w})\Lambda(\bar{w})x(t)$$

It is possible to write $\dot{u}(t) = K(\bar{w})x(t)$ where $K(\bar{w})$ is an adaptive feedback gain.

$$K(\bar{w}) = \begin{bmatrix} L_1(0)^T & 0 & \dots & 0 \\ 0 & L_2(0)^T & \dots & 0 \\ \vdots & \vdots & \ddots & \vdots \\ 0 & \dots & 0 & L_m(0)^T \end{bmatrix} \Pi^{-1}(\bar{w})\Lambda(\bar{w})$$

The control signal $u(t)$ at time t is obtained by integrating $\dot{u}(t)$,

$$u(t) = \int_0^t \dot{u}(\tau) d\tau \tag{4.12}$$

Constraints on the derivative of the control signal can be expressed as:

$$\dot{u}_{min} \leq \dot{u}(t) \leq \dot{u}_{max} \tag{4.13}$$

Since $\dot{u}(\tau) = L(\tau)^T \eta$ then, the constraints can be written in the form $M\eta \leq N$ as

$$\begin{bmatrix} -L(\tau) \\ L(\tau) \end{bmatrix} \eta \leq \begin{bmatrix} -\dot{u}_{min} \\ \dot{u}_{max} \end{bmatrix} \tag{4.14}$$

Using a sampling interval of Δt, the control signal $u(t)$ within the optimization window can be written as:

$$u(t) = u(t - \Delta t) + L(0)^T \eta \Delta t \tag{4.15}$$

where $L(0)^T \eta$ represent the derivative of the control signal at the beginning of the optimization window [17]. The constraints on the control signal is thus written as:

$$u_{min} - u(t - \Delta t) \leq L(0)^T \eta \Delta t \leq u_{max} - u(t - \Delta t) \tag{4.16}$$

The control action $\dot{u}(t)$ is then obtained in terms of the variable η by optimizing

(4.5) with respect to (4.14) and (4.16) using quadratic programming.

Case B: Stochastic disturbance $\dot{w}(t) \neq 0$

If $w(t)$ is represented as continuous-time integrated white-noise, $\epsilon(t)$, that is:

$$w(t) = \int_0^t \epsilon(\tau) d\tau \tag{4.17}$$

Thus (4.3) is re-written as:

$$\begin{aligned} \dot{x}(t) &= A(\bar{w})x(t) + B\dot{u}(t) + \Gamma(\bar{w})\epsilon(t) \\ y(t) &= Cx(t) \end{aligned} \tag{4.18}$$

where $\Gamma(\bar{w}) = [G(\bar{w}) \;\; 0]^T$ The predicted states $x(t+\tau|t)$ are computed using the relation:

$$x(t+\tau|t) = e^{A(\bar{w})\tau}x(t) + \Psi(\bar{w},\tau)^T\eta + \Xi(\bar{w},\tau)$$

where $\Psi(\bar{w},\tau)^T = \int_0^\tau e^{A(\bar{w})(\tau-\gamma)}BL^T(\tau)(\gamma)d\gamma$ and

$\Xi(\bar{w},\tau) = \int_0^\tau e^{A(\bar{w})(\tau-\gamma)}\Gamma(\bar{w})\epsilon(\gamma)d\gamma$. Using the same cost function as (4.6)

$$J = \int_0^{T_p} (x(t+\tau|t)^T Q x(t+\tau|t) + \dot{u}(\tau)^T R\dot{u}(\tau))d\tau \tag{4.19}$$

$$J = \int_0^{T_p} ([e^{A(\bar{w})\tau}x(t) + \Psi(\bar{w},\tau)^T\eta + \Xi(\bar{w},\tau)]^T Q[e^{A(\bar{w})\tau}x(t) + \Psi(\bar{w},\tau)^T\eta + \Xi(\bar{w},\tau)] + \dot{u}(\tau)^T R\dot{u}(\tau))d\tau$$

$$\begin{aligned} J &= \int_0^{T_p} [x(t)^T e^{A^T(\bar{w})\tau} Q e^{A(\bar{w})\tau}x(t) + 2\eta^T\Psi(\bar{w},\tau)Qe^{A(\bar{w})\tau}x(t) + 2\Xi(\bar{w},\tau)^T Q e^{A(\bar{w})\tau}x(t) \\ &+ 2\eta^T\Psi(\bar{w},\tau)Q\Xi(\bar{w},\tau) + \eta^T\Psi(\bar{w},\tau)Q\Psi(\bar{w},\tau)^T\eta + \Xi(\bar{w},\tau)^T Q\Xi(\bar{w},\tau)]d\tau + \eta^T R_l\eta \end{aligned}$$

$$\begin{aligned} J &= \eta^T\Omega(\bar{w})\eta + 2\eta^T\Phi(\bar{w})x(t) + 2\int_0^{T_p} \Xi(\bar{w},\tau)^T Q e^{A(\bar{w})\tau}d\tau x(t) \\ &+ 2\eta^T\Lambda(\bar{w}) + \int_0^{T_p} \Xi(\bar{w},\tau)^T Q\Xi(\bar{w},\tau)d\tau \end{aligned} \tag{4.20}$$

where $\Omega(\bar{w}) = \int_0^{T_p} \Psi(\bar{w},\tau)Q\Psi(\bar{w},\tau)^T d\tau + R_l$, $\Phi(\bar{w}) = \int_0^{T_p} \Psi(\bar{w},\tau)Qe^{A(\bar{w})\tau}d\tau$ and $\Lambda(\bar{w}) = \int_0^{T_p} \Psi(\bar{w},\tau)Q\Xi(\bar{w},\tau)d\tau$. In the unconstrained case, we directly take the derivative of (4.20) with respect to η to obtain

$$\eta^* = -\Omega^{-1}(\bar{w})(\Phi(\bar{w})x(t) + \Lambda(\bar{w})) \tag{4.21}$$

4.3 Simulation Studies

In this section, the behavior of the closed loop system with the controller is evaluated using step and turbulent changes in wind speed. The following subsections present the simulation plots. The simulations were carried out in the low, mid, high and top regions.

4.3.1 Step Changes in The Low Region

Figure 4.1 shows the wind profile used for evaluating the performance of the closed-loop system. The main control objective in the low region is to regulate the rotor speed Ω_r to its lower limit $\Omega_{r,min}$. Normally, intensity of wind present in the low region is barely able to keep the rotor speed at $\Omega_{r,min}$. Below $\Omega_{r,min}$, the turbine is shut-down, hence the controller must ensure this constraint on the output is satisfied. The reference value for the measured output, Ω_r is $\Omega_{r,min}$. Based on the design parameters of the turbine used in the simulation, $\Omega_{r,min} = 6.9 rad/s$. The reference for P_g is computed using relation (3.25). The maximum power coefficient C_p used was $C_{p,max} = 0.48$. Also, it is worthy to mention here that, since the main objective is to regulate the rotor speed, the diagonal element in the weighting matrices Q corresponding to the measured output, Ω_r must be set higher relative to P_g. The effect of this weighting can be observed in Figures (4.2), Ω_r was able to track $\Omega_{r,min}$. However, although P_g was able to track $P_{g,ref}$, a deficit exists between P_g and $P_{g,ref}$. The main control input in the low region is the generator torque command $T_{g,ref}$ and the pitch angle should be kept at its

optimal value $\beta_{opt} = 0$. The generator torque and pitch angle response are shown in Figures (4.3).

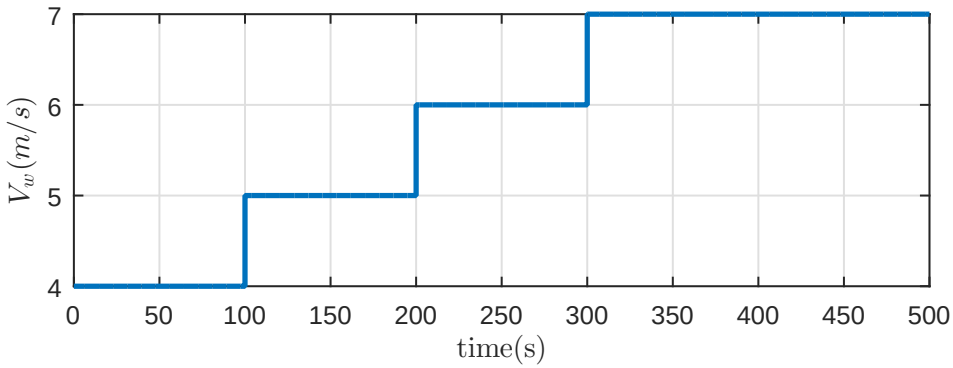

Figure 4.1: Step changes in wind speed from $4ms^{-1}$ to $7ms^{-1}$

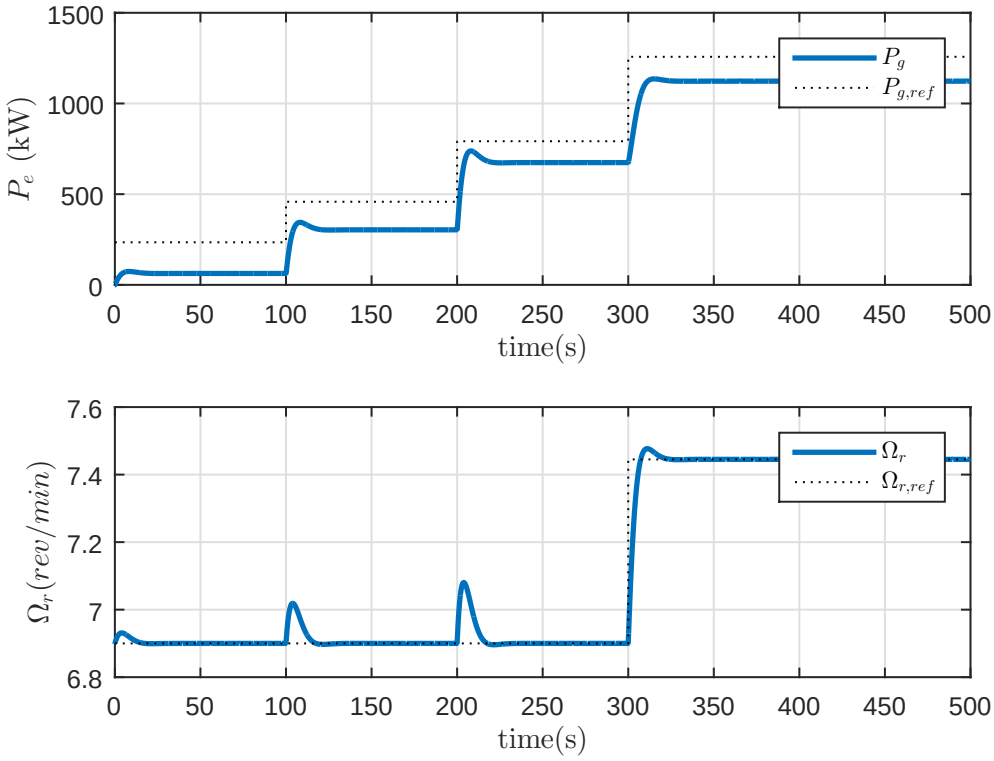

Figure 4.2: Simulation with step changes in wind speed from $4ms^{-1}$ to $7ms^{-1}$; generator power (top), rotor speed (bottom) response

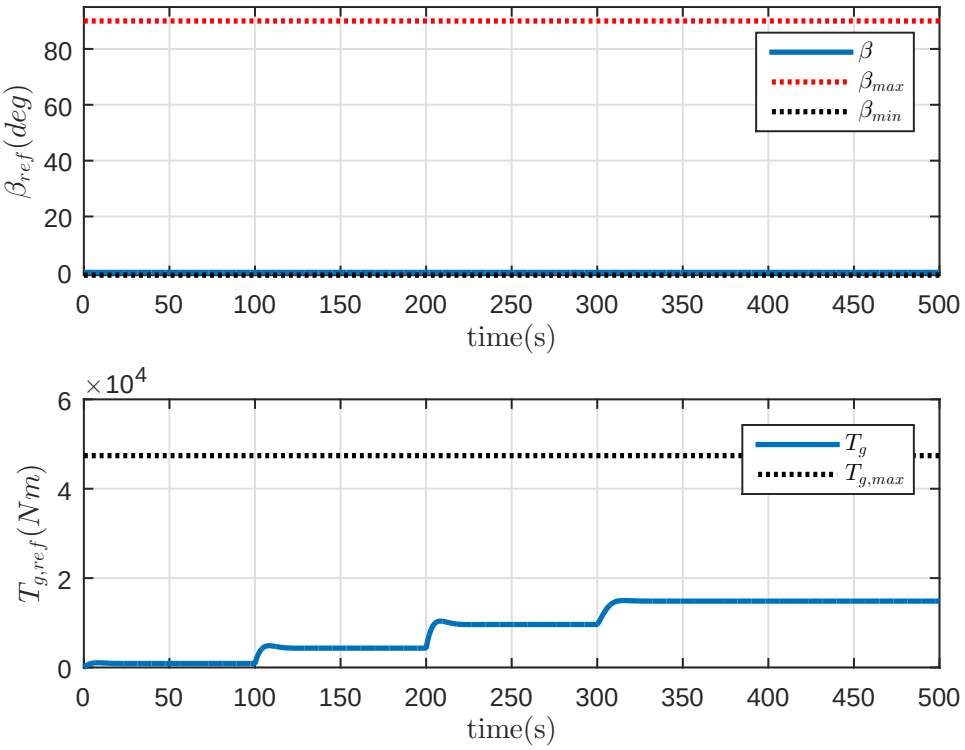

Figure 4.3: Simulation with step changes in wind speed from $4ms^{-1}$ to $7ms^{-1}$; blade pitch angle (top), generator torque (bottom) command

4.3.2 Step Changes in the Mid/High Region

The wind profile used in this simulation is shown in Figure 4.4. The control objective in mid/high region is speed and power reference tracking. The reference value for Ω_r is the optimal rotor speed $\Omega_{r,opt}$ obtained at the optimal tip-speed ratio λ_{opt} as defined in (3.26). The optimal tip-speed ratio used is 7.071. The reference power $P_{g,ref}$ used is the same as in (3.25).

The elements of the objective weighting matrix Q was set to balance the difference in magnitude between P_g and Ω_r. The system outputs Ω_r and P_g were able to track their reference values $\Omega_{r,ref}$ and $P_{g,ref}$ as shown in Figure 4.5, although

better tracking can be observed in the case of Ω_r compared to P_g. Also, in this region, the main control input is $T_{g,ref}$ while β_{ref} is kept at the optimal value $\beta_{opt} = 0$ as demonstrated in Figure 4.6.

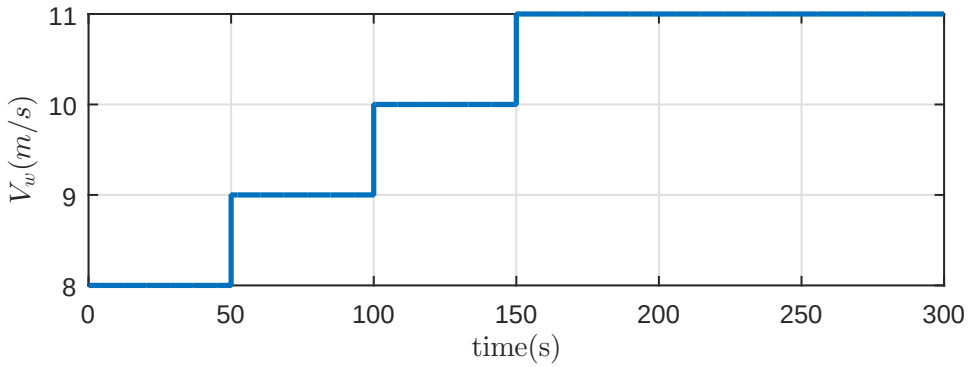

Figure 4.4: Step changes in wind speed from $8ms^{-1}$ to $11ms^{-1}$

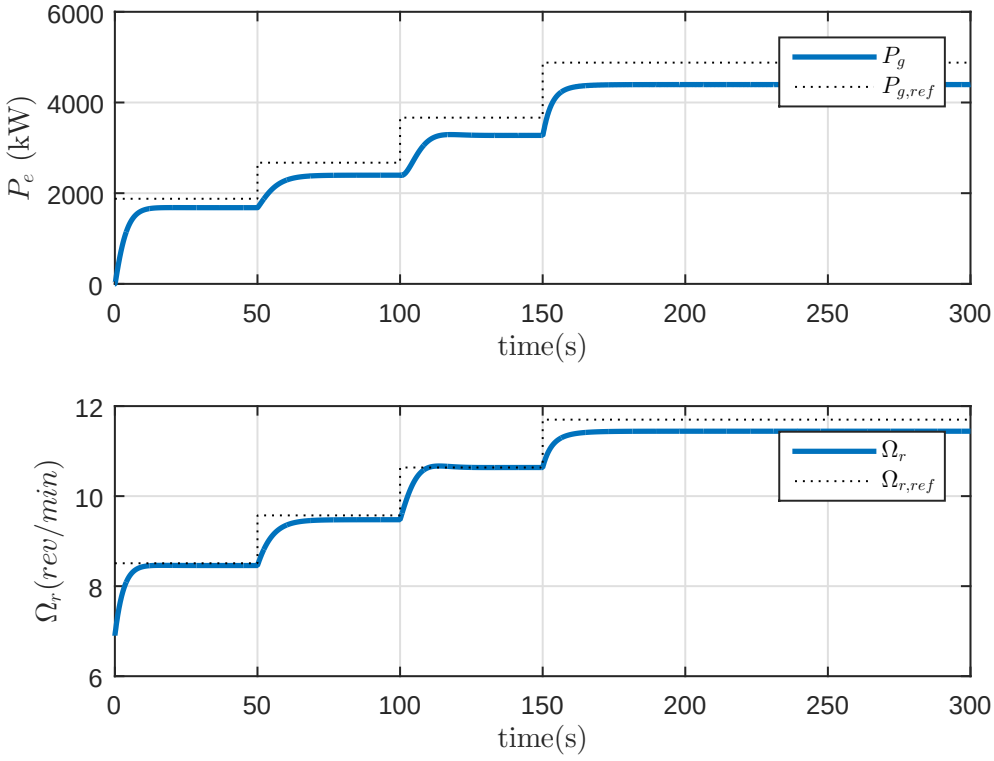

Figure 4.5: Simulation with step changes in wind speed from $8ms^{-1}$ to $11ms^{-1}$; generator power (top), rotor speed (bottom) response

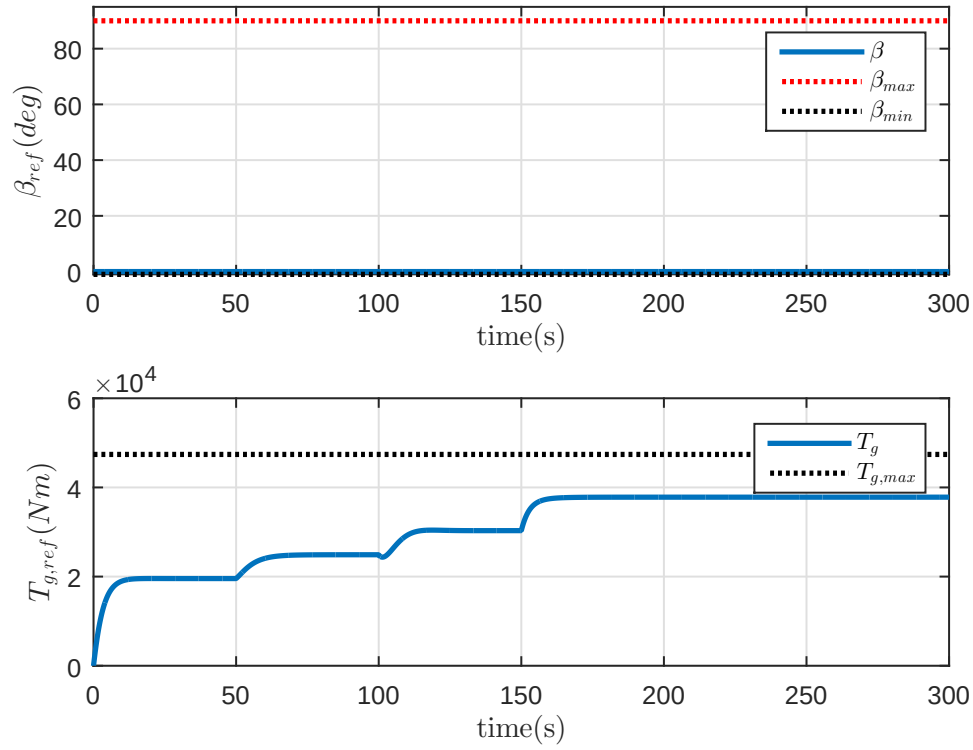

Figure 4.6: Simulation with step changes in wind speed from $8ms^{-1}$ to $11ms^{-1}$; blade pitch angle (top), generator torque (bottom) command

4.3.3 Turbulent Wind Simulation for a Mean Speed of $8ms^{-1}$

A turbulent wind profile (Figure 4.7) was generated using the TurbSim software from NREL using a mean speed of $8ms^{-1}$. The purpose of this simulation is to evaluate the behavior of the closed loop system in response to fast changing wind speeds. The rotor speed and generator power reference values were computed as in 3.26 and 3.25 respectively. As shown in Figure 4.8, Ω_r and P_g were able to track their fast changing reference values $\Omega_{r,ref}$ and $P_{g,ref}$.

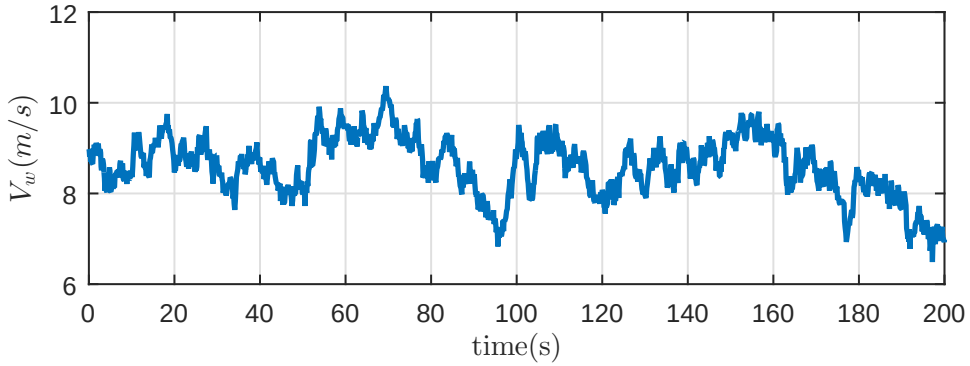

Figure 4.7: Turbulent wind with mean speed of $8ms^{-1}$

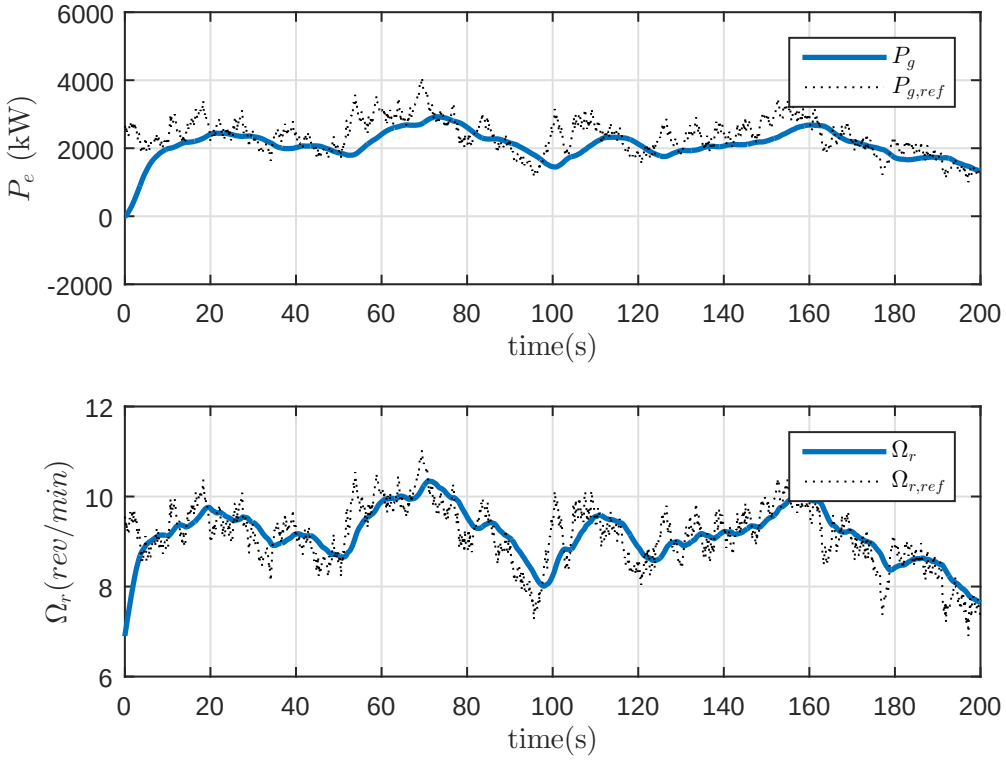

Figure 4.8: Simulation with turbulent wind with mean speed of $8ms^{-1}$; generator power (top), rotor speed (bottom) response.

4.3.4 Step Changes in the Top Region

Finally, the response of the system was evaluated in the top region using step changes in wind speed from $12ms^{-1}$ to $22ms^{-1}$ (see Figure 4.10). In this region,

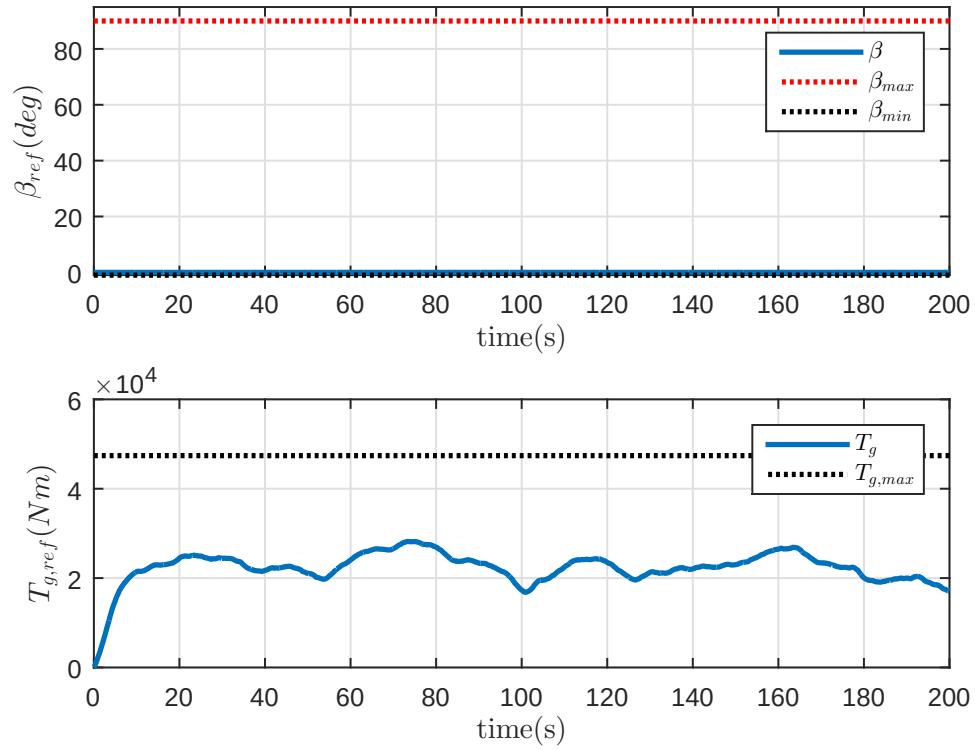

Figure 4.9: Simulation with turbulent wind with mean speed of $8ms^{-1}$; blade pitch angle (top), generator torque (bottom) command.

the control objective is to keep both P_g and Ω_r at their rated values. The is mostly done by pitching the turbine blades while keeping the generator torque around its rated value. As shown in Figure 4.11, both Ω_r and P_g were kept at their rated values. The pitch angle command control input, β_{ref} is active in this region as demonstrated in 4.12. The pitch angle β is constrained to lie between $\beta_{min} = -1$ and $\beta_{max} = 90$ according to the turbine specifications. Also, the generator torque was kept below its rated value.

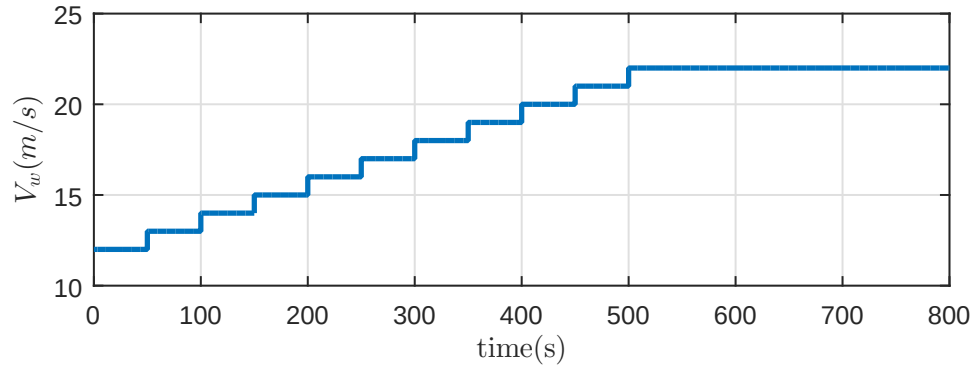

Figure 4.10: Step changes in wind speed from $12ms^{-1}$ to $22ms^{-1}$

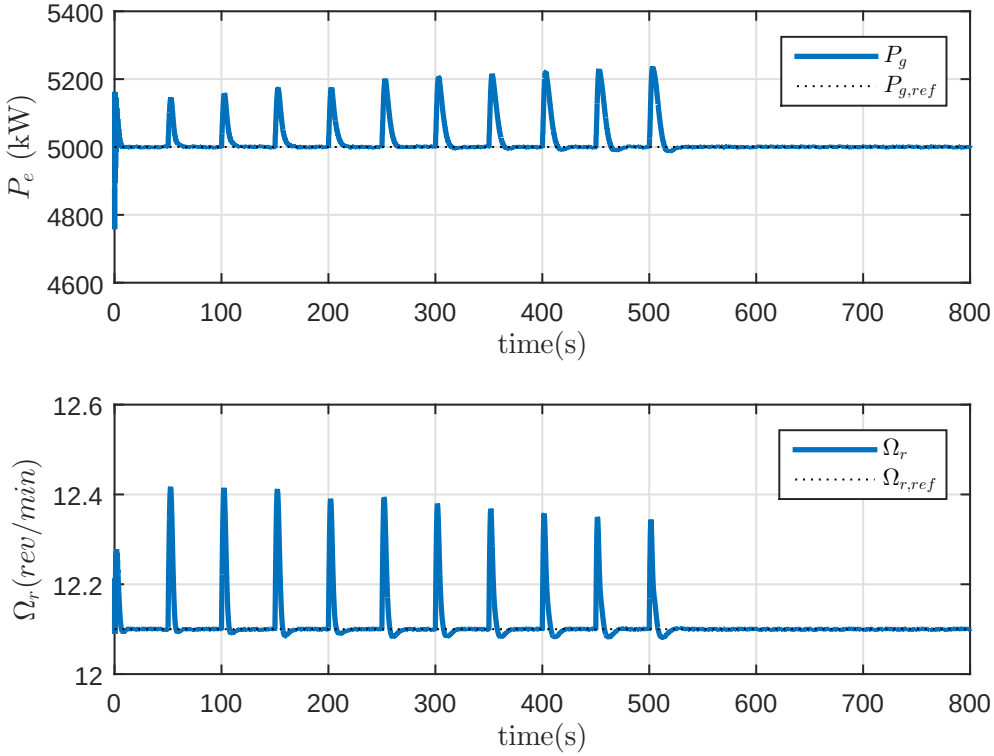

Figure 4.11: Simulation with step changes in wind speed from $12ms^{-1}$ to $22ms^{-1}$; generator power (top), rotor speed (bottom) response.

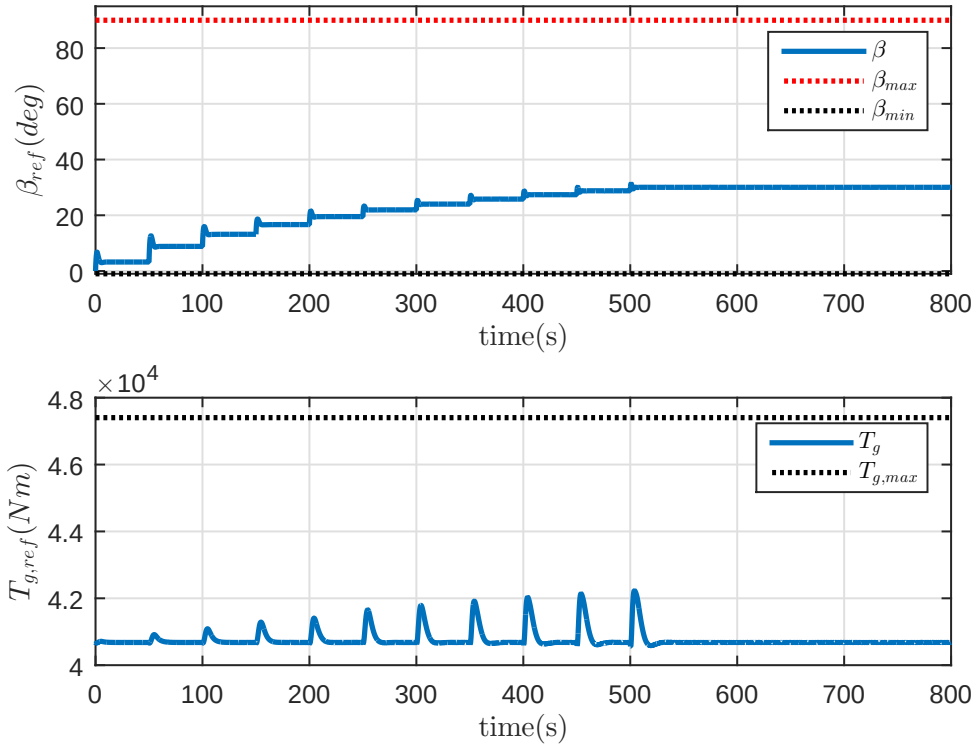

Figure 4.12: Simulation with step changes in wind speed from $12ms^{-1}$ to $22ms^{-1}$; blade pitch angle (top), generator torque (bottom) command.

4.4 Summary

In this chapter, a continuous-time adaptive gain-scheduled predictive controller was designed for a wind turbine system. The linearized model of the turbine was parameterized as a function of wind speed. Based on the wind speed, the state feedback gain matrix of the controller is updated. From simulation studies, it was observed that the closed loop system demonstrated excellent reference tracking performance.

CHAPTER 5

CONTINUOUS-TIME MULTI-MODEL PREDICTIVE CONTROL

5.1 Introduction

In this chapter, a multi-model approach is used for the design of a continuous-time predictive control law based on Laguerre functions considering multiple operating conditions of the turbine. Four operating regions were considered denoted as low, mid, top and high regions representing the behavior of the turbine at $4ms^{-1}$, $8ms^{-1}$, $11ms^{-1}$ and $18ms^{-1}$ respectively. Controllers were designed using linearized models at each operating point and a continuous-time Bayesian probability function was used to switch between the controllers based on the errors between the system output and the output at each operating point. Simulation

studies were used to demonstrate the performance of the proposed controller.

5.2 Multi-Model Control Design

Consider the nonlinear plant with the dynamics in Equation (2.12), linear approximations of the system behavior can be obtained around multiple operating conditions described by:

$$\begin{aligned} \dot{x}_j^c(t) &= A_j^c x_j^c(t) + B_j^c u^c(t) + \Gamma_j^c d(t) \\ y_j^c(t) &= C_j^c x_j^c(t) \end{aligned} \tag{5.1}$$

The jth subscript is used to denote the linear model at operating condition j. As indicated in the previous section, the control design using orthonormal functions requires that condition (3.4) be satisfied, hence as in the previous section we take the derivative of (5.1) and define a state variable $x_j(t) = [x_j^c(t)\ y_j^c(t)]^T$ to arrive at the following state-space formulation.

$$\begin{aligned} \dot{x}_j(t) &= A_j x_j(t) + B_j \dot{u}(t) \\ y_j(t) &= C_j x_j(t) \end{aligned} \tag{5.2}$$

with the assumption that $\dot{d}(t) = 0$. The matrices A_j, B_j, and C_j are defined

as follows:

$$A_j \triangleq \begin{bmatrix} A_j^c & O_{n\times p} \\ C_j^c & O_{p\times p} \end{bmatrix} \; B_j \triangleq \begin{bmatrix} B_j^c \\ O_{p\times m} \end{bmatrix} \; C_j \triangleq \begin{bmatrix} O_{p\times n} & I_{p\times p} \end{bmatrix}$$

The MPC cost function using the jth linear model is given by:

$$J_j = \int_0^{T_p} ([r_s(t) - y_j(t+\tau|t)]^T [r_s(t) - y_j(t+\tau|t)] + \dot{u}_j(\tau)^T R \dot{u}_j(\tau)) d\tau$$

Following the steps in the previous chapters, the optimal control law $u_j(t)$ is given as;

$$u_j(t) = \int_0^t \dot{u}_j(\tau) d\tau \tag{5.3}$$

where in the unconstrained case, $\dot{u}_j(t)$ is

$$\dot{u}_j(t) = - \begin{bmatrix} L_1(0)^T & 0 & \dots & 0 \\ 0 & L_2(0)^T & \dots & 0 \\ \vdots & \vdots & \ddots & \vdots \\ 0 & \dots & 0 & L_m(0)^T \end{bmatrix} \Pi_j^{-1} \Lambda_j x(t)$$

Π_j and Λ_j are defined as:

$$\Pi_j = \int_0^{T_p} \Psi_j(\tau) Q_j \Psi_j(\tau)^T d\tau + R_y \quad \text{and} \quad \Lambda_j = \int_0^{T_p} \Psi_j(\tau) Q_j e^{A_j \tau} d\tau \tag{5.4}$$

Also,

$$\begin{aligned} \Psi_j(\tau)^T &= \int_0^{\tau} e^{A_j(\tau-\gamma)} [B_{j,1} L_1(\tau)^T \ \ldots \ B_{j,m} L_m(\tau)^T] d\tau \\ \text{and} \ \ \eta_j^T &= [\eta_{j,1}^T \ \eta_{j,2}^T \ \ldots \ \eta_{j,m}^T] \end{aligned}$$

and in the constrained case, $u_j(t)$ is bounded by

$$\dot{u}_{min} \leq \dot{u}_j(t) \leq \dot{u}_{max} \tag{5.5}$$

Since $\dot{u}_j(\tau) = L(\tau)^T \eta_j$ then, the constraints can be written in the form $M\eta_j \leq N$ as

$$\begin{bmatrix} -L(\tau) \\ L(\tau) \end{bmatrix} \eta_j \leq \begin{bmatrix} -\dot{u}_{min} \\ \dot{u}_{max} \end{bmatrix} \tag{5.6}$$

Using a sampling interval of Δt, the control signal $u_j(t)$ within the optimization window can be written as:

$$u_j(t) = u_j(t - \Delta t) + L(0)^T \eta_j \Delta t \tag{5.7}$$

where $L(0)^T \eta_j$ represent the derivative of the control signal at the beginning of the optimization window [17]. The constraints on the control signal is thus written as:

$$u_{min} - u_j(t - \Delta t) \leq L(0)^T \eta_j \Delta t \leq u_{max} - u_j(t - \Delta t) \tag{5.8}$$

The control action $\dot{u}_j(t)$ is then obtained in terms of the variable η_j by optimizing (3.13) with respect to (4.14) and (4.16) using quadratic programming.

The control input $u(t)$ to the system 2.12, is a weighted sum of the control input obtained from the jth linear system $u_j(t)$.

$$u(t) = \sum_{j}^{N_m} w_j(t) u_j(t) \tag{5.9}$$

$w_j(t)$ is a time-varying weight based on the error between the output of the non-linear system $y(t)$ and the output at the operating point j denoted $\bar{y}_j$

$$w_j(t) = \begin{cases} \dfrac{p_j(t)}{\sum_{i=1}^{N_m} p_i(t)} & p_j(t) > \delta \\ 0 & \text{otherwise} \end{cases} \tag{5.10}$$

δ ia a predefined tolerance limit and $p_j(t)$ is a Bayesian probability function defined by the following dynamics.

$$\dot{p}_j(t) = \frac{exp(-0.5\epsilon_j(t)^T \Xi_j \epsilon_j(t)) p_i(t)}{\sum_{i=1}^{N_m} exp(-0.5\epsilon_i(t)^T \Xi_i \epsilon_i(t)) p_i(t)} - p_j(t) \tag{5.11}$$

$\epsilon_i(t)$ is defined as:

$$\epsilon_j(t) = y(t) - \bar{y}_j \tag{5.12}$$

and Ξ_i is a covariance matrix. $\bar{y}_j$ is the output at the j_{th} operating point.

5.3 Simulation Studies

Simulation studies were conducted using step changes in wind speed and turbulent wind speeds. Four controllers were designed around operating wind speeds of $4ms^{-1}$, $8ms^{-1}$, $11ms^{-1}$ and $18ms^{-1}$ representing low, mid, top and high operating regimes respectively. The generator torque $T_{g,ref}$ is the main control input in the

low, mid and high region while the pitch angle β_{ref} should be kept at its optimal value $\beta_{opt} = 0$.

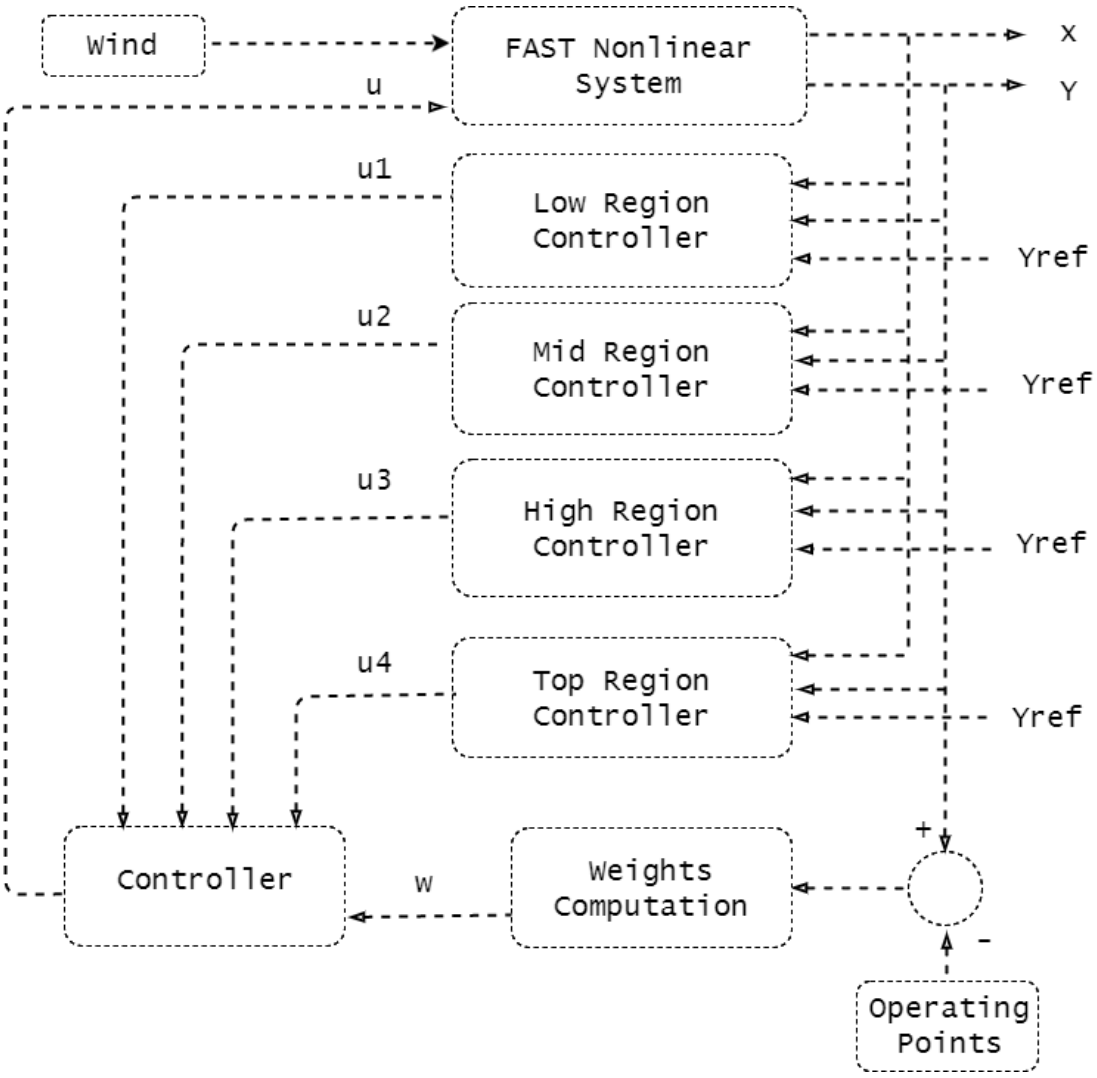

Figure 5.1: Schematic diagram showing components of the proposed multi-model predictive controller

In these regions, the generator power P_g is below its nominal value P_{norm} and the control objectives are both tracking of the optimum power curve and regulating the rotor speed. However, in the low region, rotor speed regulation is more important than reference tracking because Ω_r should not fall below $\Omega_{r,min} = 6.9\ rev/min$. Therefore, the diagonal entries of the weighting matrix Q were

tuned to give more priority to regulating Ω_r over P_g. In the mid/high region, Ω_r is now above $\Omega_{r,min}$ but below $\Omega_{r,max}$, therefore the output weighting matrix Q was tuned to balance the magnitude difference between Ω_r and P_g.

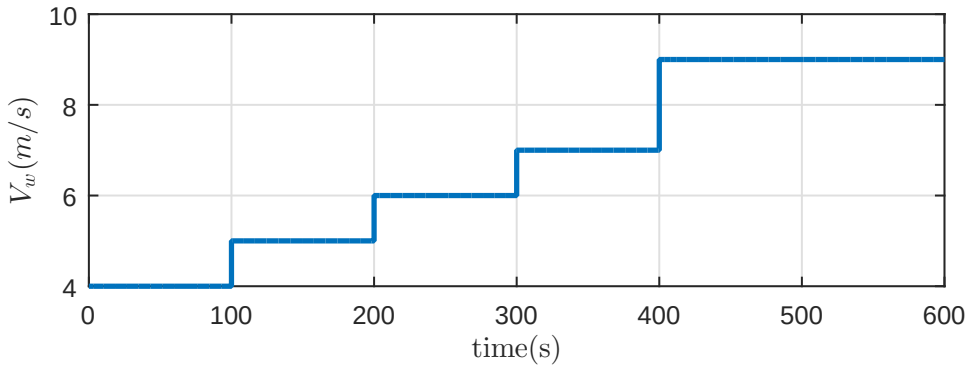

Figure 5.2: Step changes in wind speed from $4ms^{-1}$ to $9ms^{-1}$

In the top region, Ω_r and P_g are at their rated values $\Omega_{r,max}$ and P_{norm}, and should remain at these values as the wind speed changes, more priority is given to P_g over Ω_r with respect to tuning of Q. The main control action in the top region is pitch control thus, β_{ref} is allowed to vary but should not exceed its limits β_{min} and β_{max}, while $T_{g,ref}$ is should be held below its rated value $T_{g,rated}$. As indicated in Figure 5.4, the main control action in the low region is the generator torque while the pitch angle was held at $\beta_{opt} = 0$.

The reference inputs, $P_{g,ref}$ and $\Omega_{r,ref}$ were computed using (3.25) and (3.26) respectively. Step changes in wind velocity from $4ms^{-1}$ to $9ms^{-1}$ were applied to the WTS to evaluate the performance of the proposed controller in the low to mid wind speed regime. Figure 5.3 shows the output response of the system to the wind profile in Figure 5.2. As shown in Figure 5.3, both Ω_r and P_g were

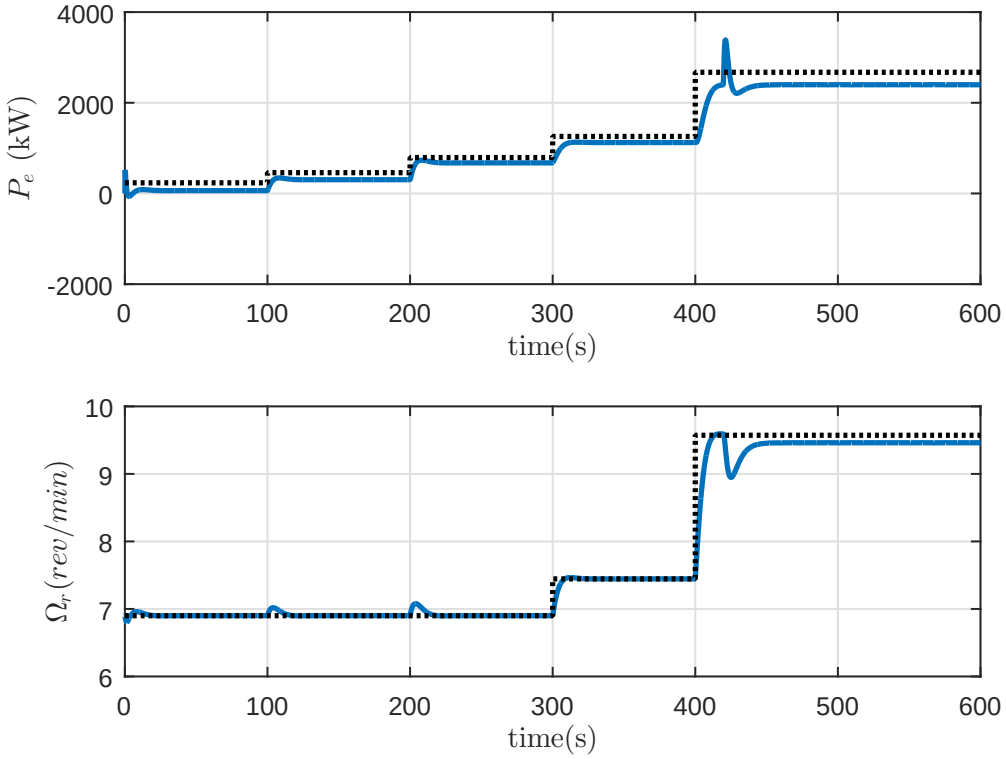

Figure 5.3: Simulation with step changes in wind speed from $4ms^{-1}$ to $9ms^{-1}$: generator power (top) and rotor speed (bottom)

able to track their reference values. In Figure 5.5, p_1, p_2, p_3, p_4 are transition probabilities related to the sub-controllers in the low, mid, high and top regions respectively. Also, w_1, w_2, w_3, w_4 are control weights on each of the sub-controllers calculated using (5.10) based on the transition probabilities. It is expected that the control inputs should be switched amongst the sub-controllers using the transition probabilities and weights based on the current operating condition. It can be observed from Figure 5.5 that the main control contribution was given by the low region controller, although when the wind speed approached $9ms^{-1}$, a transition can be observed from the low to the mid region controller indicating a change in operating points. Simulations were also conducted with turbulent winds generated

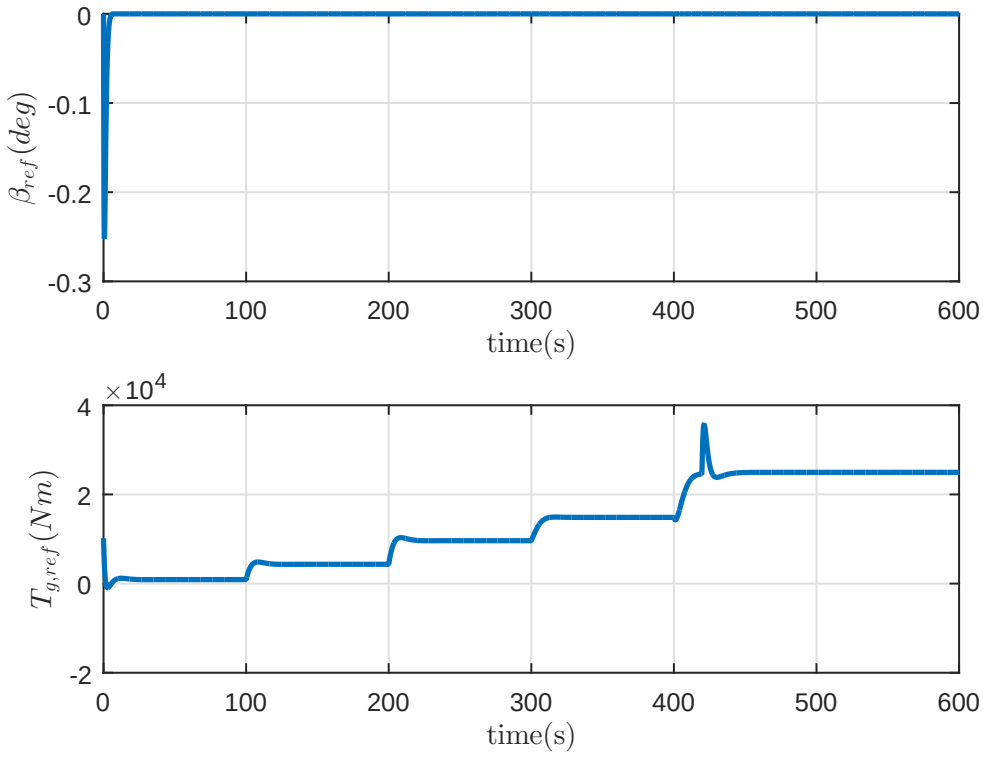

Figure 5.4: Simulation with step changes in wind speed from $4ms^{-1}$ to $9ms^{-1}$: generator torque (top) and blade pitch angle (bottom) command

using TurbSim Software by NREL with mean speeds of $8ms^{-1}$ and $18ms^{-1}$ as given in Figures 5.6 and 5.10 respectively. Both P_g and Ω_r followed their fast changing references as shown in Figure 5.7. The main control input in this region is also T_g as reflected in Figure 5.8. Since the mean wind speed of $8ms^{-1}$ lie in the mid region, then the main controller in this region is the mid-region controller, this preference can be observed in the transition probability and control weight response in Figure 5.9. With the wind speed profile in Figure 5.10, both P_g and Ω_r, should be maintained at their rated values as shown in Figure 5.11. The main control input in the top region is the pitch angle as shown in Figure 5.12. The turbine is operating in the top region, therefore the main control contribution

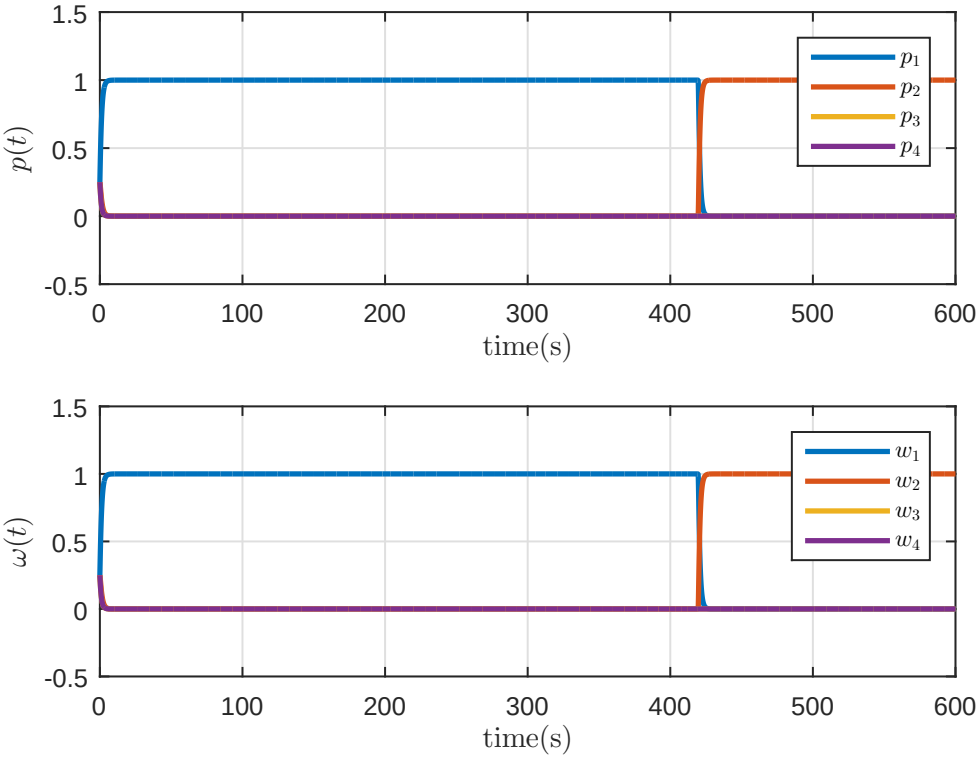

Figure 5.5: Simulation with step changes in wind speed from $4ms^{-1}$ to $9ms^{-1}$: transition probabilities (top) and control weights (bottom)

should be from the top region controller as demonstrated by the probabilities in Figure 5.13.

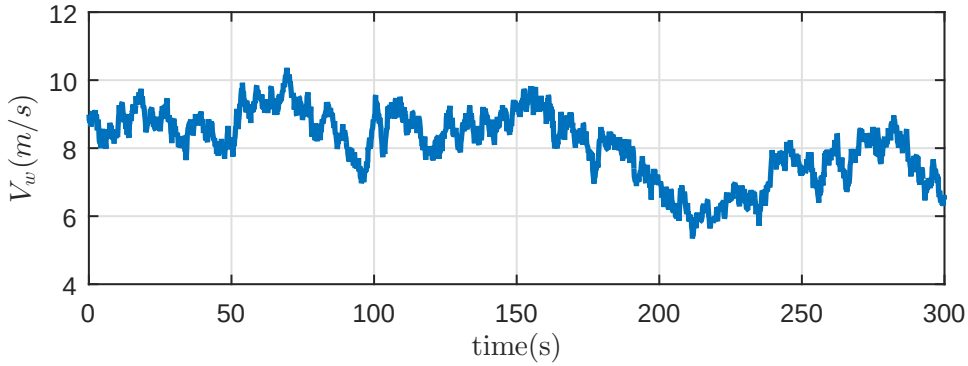

Figure 5.6: Turbulent wind with mean speed of $8ms^{-1}$

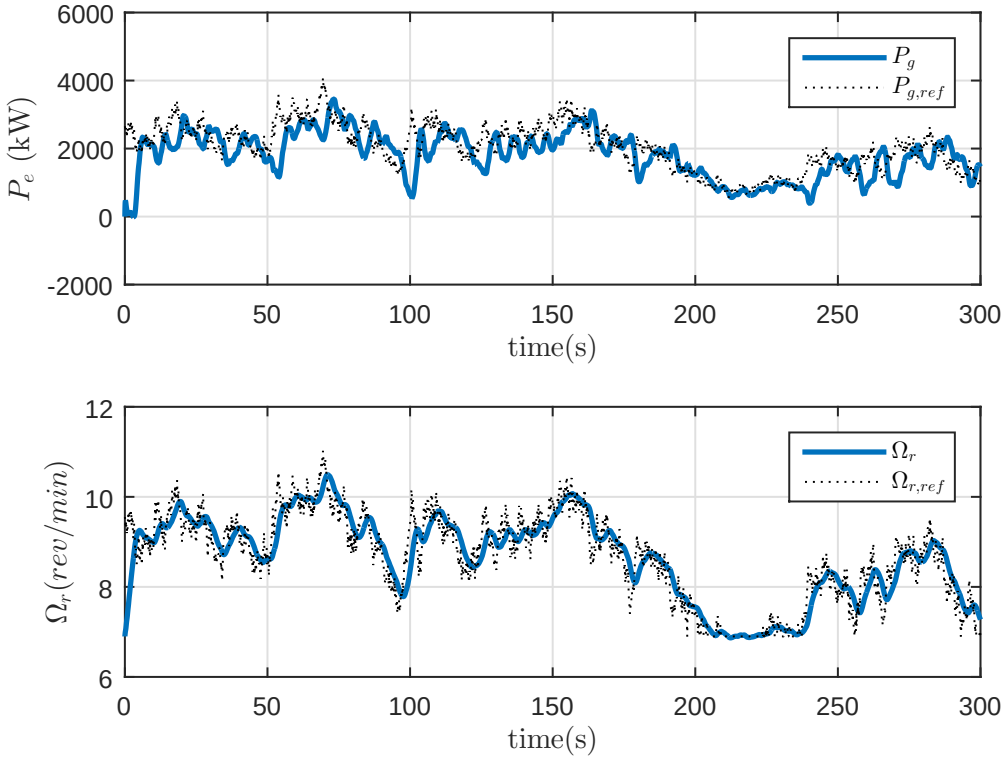

Figure 5.7: Simulation with turbulent wind with mean speed of $8ms^{-1}$; generator power (top) and rotor speed(bottom) response

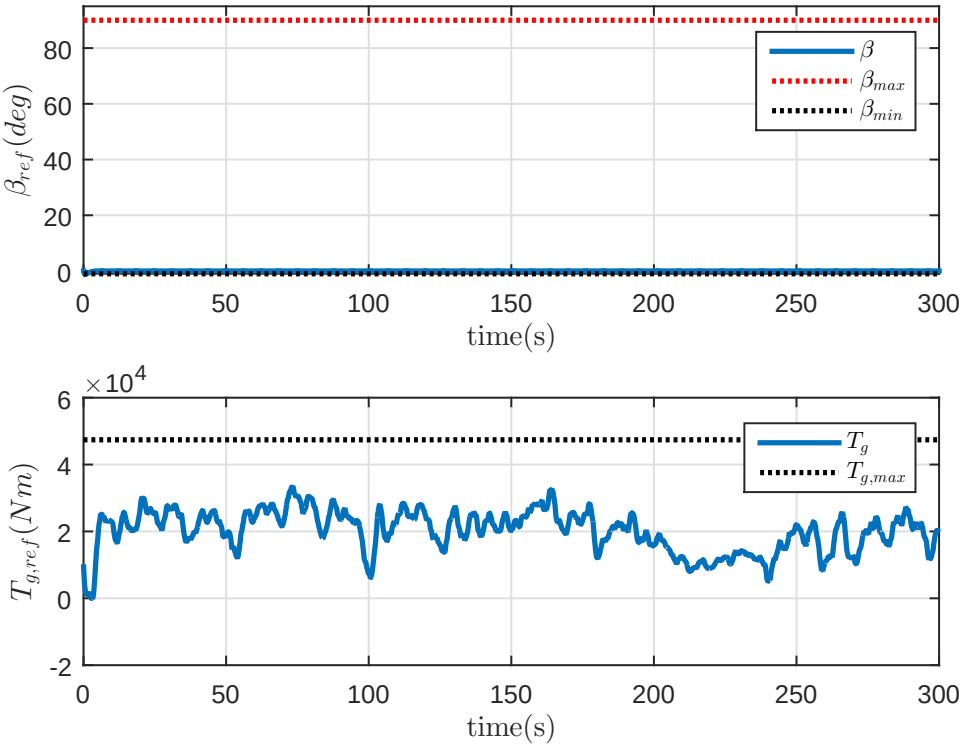

Figure 5.8: Simulation with turbulent wind with mean speed of $8ms^{-1}$; generator torque (top) and blade pitch(bottom) command

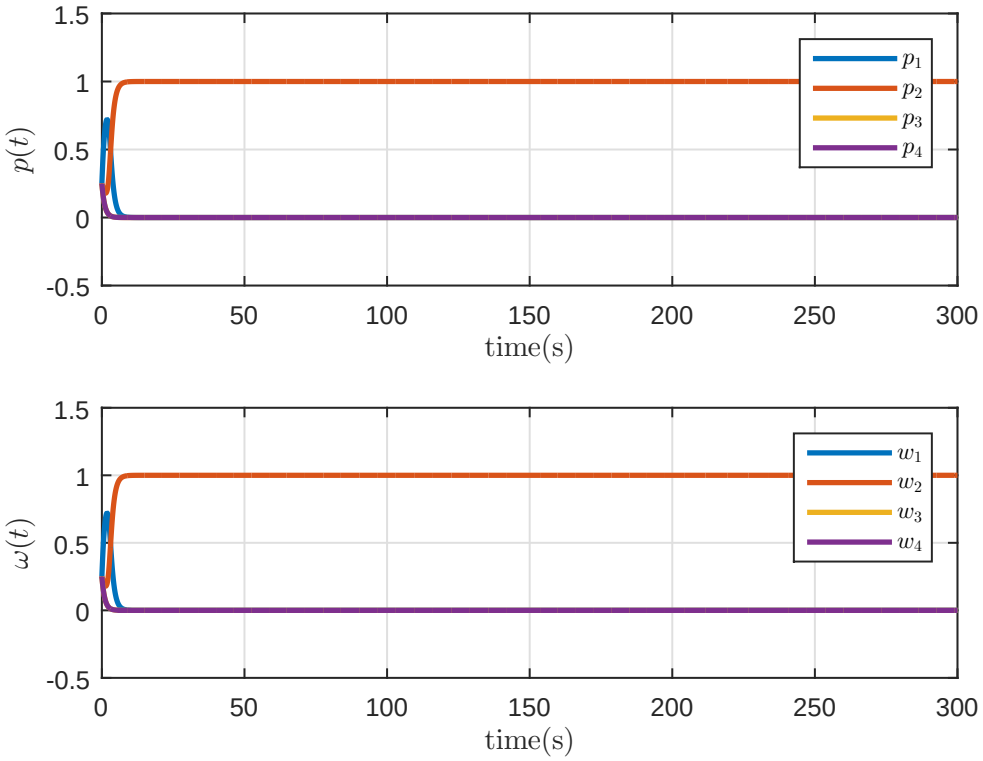

Figure 5.9: Simulation with turbulent wind with mean speed of $8ms^{-1}$; transition probabilities (top) and control weights(bottom)

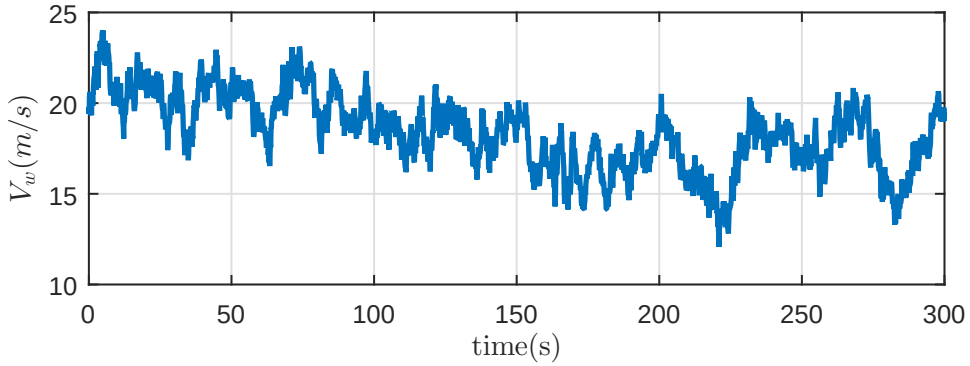

Figure 5.10: Turbulent wind with mean speed of $18ms^{-1}$

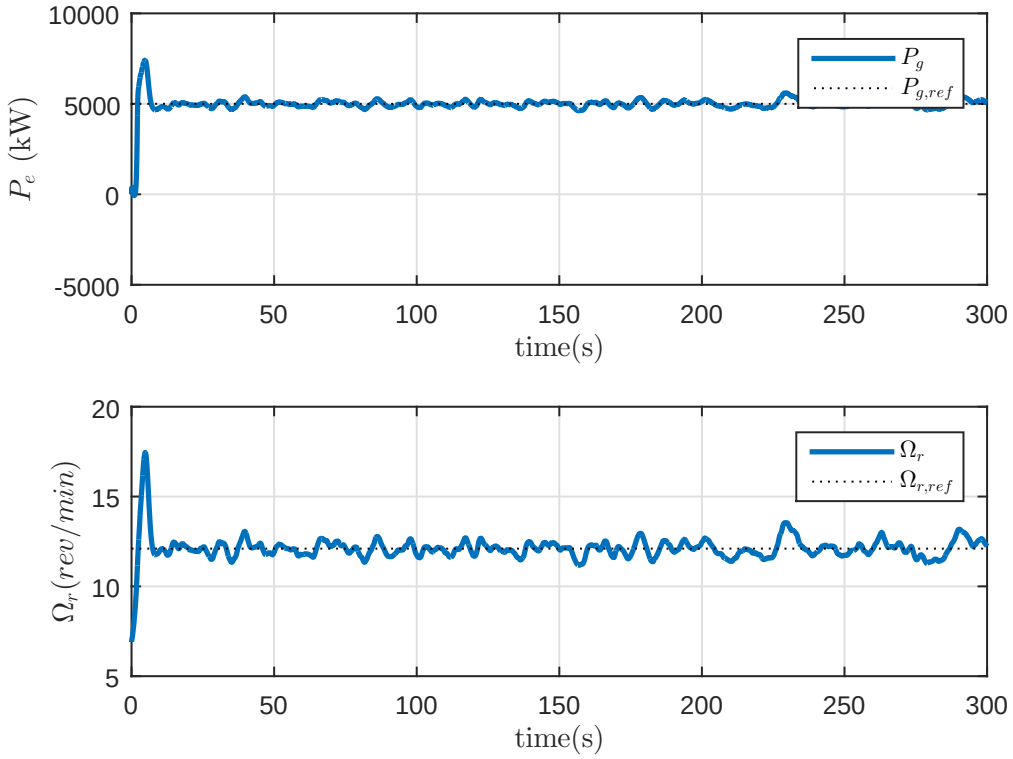

Figure 5.11: Simulation with turbulent wind with mean speed of $18ms^{-1}$; generator power (top) and rotor speed(bottom)

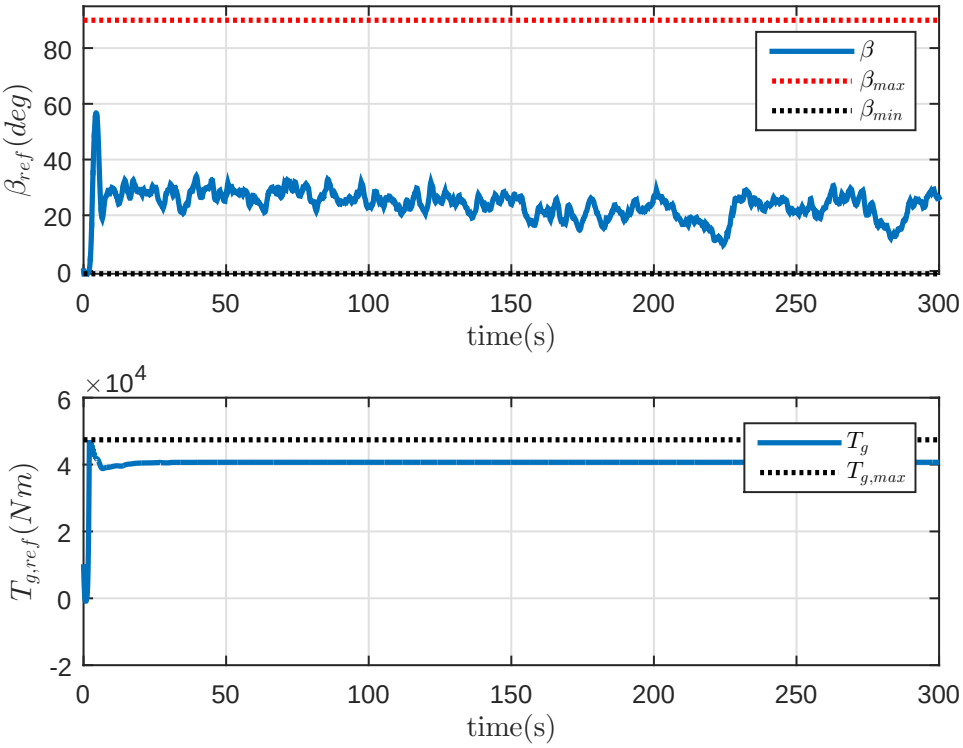

Figure 5.12: Simulation with turbulent wind with mean speed of $18ms^{-1}$; generator torque (top) and blade pitch angle (bottom) command

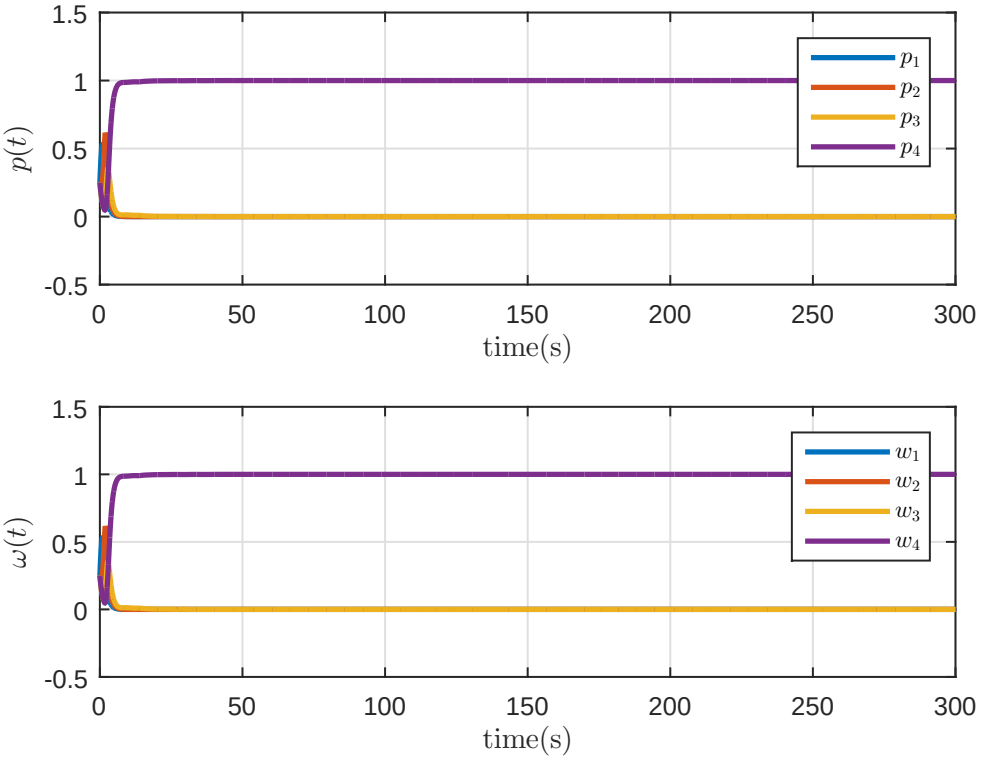

Figure 5.13: Simulation with turbulent wind with mean speed of $18ms^{-1}$; transition probabilities (top) and control weights(bottom)

5.4 Summary

In this chapter, a continuous-time multi-model predictive controller was designed for a wind turbine system. Four operating regions of the turbine were considered namely; low, mid, high and top regions. Linear controllers were designed at each of these regions using linearized models obtained around these regions. A continuous-time bayesian inference function was used to transition between these controllers using the error between the system output and each operating point. From simulation studies, it was observed that the closed loop system demonstrated excellent reference tracking performance.

CHAPTER 6

CONCLUSION AND RECOMMENDATION

The design of model predictive controllers using continuous-time orthonormal functions for variable-speed variable-pitch wind turbines have been discussed in this thesis. Both adaptive and multi-model control schemes have been considered. In the adaptive case, a linear model predictive controller was designed using a linearized model of the turbine which was parameterized as a function of measured wind speed. In the implementation of the multi-model scheme, linearized models of the turbine were obtained at four operating wind speeds representing different operating regions of the turbine.

Simulation studies were conducted using a 5MW baseline wind turbine and FAST, an aero-elastic computer-aided engineering software. Apart from guaranteeing stability and fulfilling the control objectives across all operating regions, due to the continuous-time design approach, the controllers gave smoother re-

sponse, eliminated sampling-time constraints and eliminated drawbacks resulting from discretization using fast-sampling approaches.

In comparison with the multi-model controller, the adaptive controller requires accurate measurements of the control inputs to compute the appropriate control action at each time instant. Also, in the multi-model case, the controller gains for each sub-controller can be obtained offline, thereby reducing the computational time. However, the adaptive controller offers a better transition between all the operating regions of the turbine compared with the multi-model controller.

Some recommendations for future work are as follows;

1. In the application of orthonormal (Laguerre) functions for controller design, the control inputs are represented using orthonormal functions. The exponential decay rate and order of the functions are parameters that need to be specified in the design. In this thesis, these parameters were chosen arbitrarily as mere trade-off between speed of response and computational-time. More investigations need to be carried out to determine the optimal selection of these parameters.

2. Although, some investigations have been conducted in application of fuzzy inference systems to multi-model predictive controller design. These controllers were designed using discrete-time models. Based on the approach presented in these study, an investigation can be conducted into the application of fuzzy inference systems to continuous-time multi-model predictive controller design.

REFERENCES

[1] A. Tummala, R. Kishore, D. Kumar, V. Indraja, and V. H. Krishna, "A review on small scale wind turbines," *Renewable and Sustainable Energy Reviews*, vol. 56, pp. 1351–1371, 2016.

[2] M. J. Mercado-Vargas, D. Gómez-Lorente, O. Rabaza, and E. Alameda-Hernandez, "Aggregated models of permanent magnet synchronous generators wind farms," *Renewable Energy*, vol. 83, pp. 1287–1298, 2015.

[3] I. M.-B. Hassine, M. W. Naouar, and N. Mrabet-Bellaaj, "Predictive control strategies for wind turbine system based on permanent magnet synchronous generator," *ISA Transactions*, vol. 62, pp. 73–80, 2015.

[4] F. Y. Yan, J. Lin and Z. Zhu, "Control of a Grid-Connected Direct-Drive Wind Energy Conversion," *Renewable Energy*, vol. 66, pp. 371–380, 2014.

[5] H. Li, S. K.L., and M. P.G., "Neural-network-based sensorless maximum wind energy capture with compensated power coefficient," *IEEE Transactions on Industrial Applications*, vol. 41, no. 6, pp. 1548–1556, 2005.

[6] M. G. Simoes, B. K. Bose, and R. J. Spiegal, "Fuzzy logic-based intelligent control of a variable speed cage machine wind generation system," *IEEE Transactions on Power Electronics*, vol. 12, no. 1, pp. 87–95, 1997.

[7] A. G. Abo-Khalil, D. C. Lee, and J. K. Seok, "Variable speed wind power generation system based on fuzzy logic control for maximum power output tracking," in *Proc. 35th Annual IEEE Power Electronics Specialists Conference*, vol. 3, pp. 2039–2043, 2004.

[8] C. Shao, X. Chen, and Z. Liang, "Application research of maximum wind-energy tracing controller based adaptive control Strategy in WECS," in *Proc. International Power Electronics and Motion Control Conference*, pp. 1–6, 2006.

[9] A. Raju, B. Fernandes, and K. Chatterjee, "A UPF power conditioner with maximum power point tracker for grid connected variable speed wind energy conversion system," in *Proc. 1st International Conference on Power Electronics Systems and Applications*, pp. 107–112, 2004.

[10] R. Hilloowala and A. M. Sharaf, "A rule-based fuzzy logic controller for a PWM inverter in a stand alone wind energy conversion scheme," *IEEE Transactions on Industry Applications*, vol. 32, no. 1, pp. 57–65, 2004.

[11] G. Hua and Y. Geng, "A novel control strategy of MPPT taking dynamics of the wind turbine into account," in *Proc. 37th IEEE Power Electronics specialist Conference*, pp. 18–22, 2002.

[12] V. Galdi, A. Piccolo, and P. Siano, "Designing an adaptive fuzzy controller for maximum wind energy extraction," *IEEE Transactions on Energy Conversion*, vol. 23, no. 2, pp. 559–569, 2008.

[13] Q. Wang and L.Chang, "An intelligent maximum power extraction algorithm for inverter-based variable speed wind turbine systems," *IEEE Transactions on Power Electronics*, vol. 19, no. 5, pp. 1242–1249, 2004.

[14] E. Koutroulis and K. Kalaitzakis, "Design of a maximum power tracking system for wind energy conversion applications," *IEEE Transactions on Industrial Electronics*, vol. 53, no. 2, pp. 486–494, 2006.

[15] M. Matsui, D. Xu, L. Kang, and Z. Yang, "Limit Cycle Based Simple MPPT Control Scheme for a Small Sized Wind Turbine Generator System," in *Proc. 4th International Power Electronics and Motion Control Conference*, pp. 1746–1750, , 2004.

[16] Y. Higuchi, N. Yamamura, and M. Ishida, "An improvement of performance for small-scaled wind power generating system with permanent magnet type synchronous generator," in *Proc. IEEE International Conference on Industrial Electronics, Control and Instrumentation*, pp. 1–6, 2000.

[17] S. Wang, Z. Qi, and T. Undeland, "State space averaging modeling and analysis of disturbance injection method of MPPT for small wind turbine generating systems," in *Proc. Asia-Pacific Power and Energy Engineering Conference*, pp. 1–6, 2009.

[18] R. J. Wai, C. Lin, and Y. Chang, "Novel maximum-power extraction algorithm for PMSG wind generation system," *IET Electric Power Applications*, vol. 1, no. 2, pp. 275–283, 2007.

[19] J. Yaoqin, Y. Zhongqing, and C. Binggang, "A new maximum power point tracking control scheme for wind generation," in *Proc. International Conference on Power System Technology*, pp. 144–148, 2002.

[20] J. Hui and A. Bakhshai, "A new adaptive control algorithm for maximum power point tracking for wind energy conversion systems," in *Proc. IEEE Power Electronics Specialists Conference*, pp. 4003–4007, 2008.

[21] J. Hui and A. Bakhshai, "Adaptive algorithm for fast maximum power point tracking in wind energy systems," in *Proc. IEEE Annual Conference of the IEEE Industrial Electronics Society*, pp. 2119 – 2124, 2008.

[22] M. G. Molina and P. E. Mercado, "A new control strategy of variable speed wind turbine generator for three-phase grid-connected applications," in *Proc. IEEE Power Electronics Society Transmission and Distribution Conference and Exposition: Latin America*, pp. 1–8, 2008.

[23] T. Tafticht, K. Agbossou, and A. Chériti, "DC Bus Control of Variable Speed Wind Turbine Using a Buck-Boost Converter," in *Proc. IEEE Power Engineering Society General Meeting*, pp.1–6, 2006.

[24] J. M. Kwon, J. H. Kim, S. H. Kwak, and H. H. Lee, "Optimal power extraction algorithm for DTC in wind power generation systems," in *Proc. IEEE*

International Conference on Sustainable Energy Technology, pp. 639–643, 2008.

[25] C. Patsios, A. Chaniotis, and A. Kladas, "A Hybrid Maximum Power Point Tracking System for Grid-Connected Variable Speed Wind-Generators," in *Proc. IEEE Power Electronics Specialists Conference*, pp. 1749–1754, 2008.

[26] J. S. Thongam, P. Bouchard, H. Ezzaidi, and M. Ouhrouche, "ANN-Based Maximum Power Point Tracking Control of Variable Speed Wind Energy Conversion Systems," in *Proc. 18th IEEE International Conference on Control Applications*, pp 1–6, 2009.

[27] B. Fernando, D. B. Hernan, and R. J. Mantz, *Wind Turbine Control System: Principles, Modelling, and Gain Scheduling Design.* London, UK:Springer-Verlag, 2007.

[28] S. Bououden, M. Chadli, S. Filali, and A. El Hajjaji, "Fuzzy model based multivariable predictive control of a variable speed wind turbine: LMI approach," *Renewable Energy*, vol. 37, pp. 434–439, 2012.

[29] A. Evans, C. Mark, and K. Basil, "Robust MPC Tower Damping for Variable Speed Wind Turbines," *IEEE Transactions on Control Systems Technology*, vol. 23, no. 1, pp. 290–296, 2014.

[30] D. Castaignet, I. Couchman, N. K. Poulsen, T. Buhl, and J. J. Wedel-heinen, "Frequency-Weighted Model Predictive Control of Trailing Edge Flaps on a

Wind Turbine Blade," *IEEE Transactions on Control Systems Technology*, vol. 21, no. 4, pp. 1105–1116, 2013.

[31] C. Bottasso, P. Pizzinelli, C. Riboldi, and L.Tasca, "LiDAR-enabled model predictive control of wind turbines with real-time capabilities," *Renewable Energy*, vol. 71, pp. 442–452, 2014.

[32] L. Henriksen, M. Hansen, and N. Poulsen, "Wind turbine control with constraint handling," *IET Control Theory and Applications*, vol. 6, no. 11, pp. 1722–1734, 2013.

[33] R. Galeazzi, K. T. Borup, H. Niemann, N. K. Poulsen, and F. Caponetti, "Adaptive Backstepping Control of Lightweight Tower Wind Turbine," in *Proc. American Control Conference*, pp. 3058–3065, 2015.

[34] B. Vedran and V. Mario, "Adaptive H-infinity Control of Large Wind Turbines," in *Proc. IEEE International Conference on Industrial Technology*, pp. 85–92, 2015.

[35] C. Vivas, F. Casta, and F. R. Rubio, "Adaptive H-infinity control of variable-speed Wind Turbines with wind speed estimator," in *Proc. European Control Conference*, pp. 4217–4222, 2009.

[36] X. Yao, Y. Liu, and C. Guo, "Adaptive Fuzzy Sliding-mode Control in Variable Speed Adjustable Pitch Wind Turbine," in *Proc. IEEE International Conference on Automation and Logistics*, pp. 313–318, 2007.

[37] H. Jafarnejadsani, J. Pieper, and J. Ehlers, "Adaptive Control of a Variable-Speed Variable-Pitch Wind Turbine Using Radial-Basis Function Neural Network," *IEEE Transactions on Control Systems Technology*, vol. 21, no. 6, pp. 2264–2272, 2013.

[38] D. Xiang, J. C. Turu, and T. Wang, "On-Site LVRT Testing Method for Full-Power Converter Wind Turbines," *IEEE Transactions on Sustainable Energy*, vol. 8, no. 1, pp. 395–403, 2017.

[39] M. Nasiri and R. Mohammadi, "Peak Current Limitation for Grid Side Inverter by Limited Active Power in PMSG-Based Wind Turbines During Different Grid Faults," *IEEE Transactions on Sustainable Energy*, vol. 8, no. 1, pp. 3–12, 2017.

[40] J. Mohammadi, S. Afsharnia, S. Vaez-zadeh, and S. Farhangi, "Improved fault ride through strategy for doubly fed induction generator based wind turbines under both symmetrical and asymmetrical grid faults," *IET Renewable Power Generation*, vol. 10, no. 8, pp. 1114–1122, 2016.

[41] H. M. Yassin, H. H. Hanafy, and M. M. Hallouda, "Enhancement low-voltage ride through capability of permanent magnet synchronous generator-based wind turbines using interval type-2 fuzzy control," *IET Renewable Power Generation*, vol. 10, no. 3, pp. 339–348, 2016.

[42] J. N. Sakamuri, Z. H. Rather, and J. Rimez, "Coordinated Voltage Control in Offshore HVDC Connected Cluster of Wind Power Plants," *IEEE*

Transactions on Sustainable Energy, vol. 7, no. 4, pp. 1592–1601, 2016.

[43] A. Kirakosyan, M. S. E. Moursi, P. Kanjiya, and V. Khadkikar, "A Nine Switch Converter-Based Fault Ride Through Topology for Wind Turbine Applications," *IEEE Transactions on Power Delivery*, vol. 31, no. 4, pp. 1757–1766, 2016.

[44] J. Hu, Q. Hu, B. Wang, H. Tang, and Y. Chi, "Small Signal Instability of PLL-Synchronized Type-4 Wind Turbines Connected to High-Impedance AC Grid During LVRT," *IEEE Transactions on Energy Conversion*, vol. 31, no. 4, pp. 1676–1687, 2016.

[45] A. Egea-àlvarez, M. Aragüés-peñalba, O. Gomis-bellmunt, J. Rull-duran, and A. Sudrià-andreu, "Sensorless control of a power converter for a cluster of small wind turbines," *IET Renewable Power Generation*, vol. 10, no. 5, pp. 721–728, 2016.

[46] S. Nanou and S. A. Papathanassiou, "Grid Code Compatibility of VSC-HVDC Connected Offshore Wind Turbines Employing Power Synchronization Control," *IEEE Transactions on Power Systems*, vol. 31, no. 6, pp. 5042–5050, 2016.

[47] B. V. Yaramasu, B. Wu, P. C. Sen, S. Kouro, and M. Narimani, "High-Power Wind Energy Conversion Systems : State-of-the-Art and Emerging Technologies," *Proceedings of the IEEE*, vol. 103, no. 5, pp. 740 – 788, 2015.

[48] F. Valenciaga and R. D. Fernandez, "Multiple-input multiple-output high-order sliding mode control for a permanent magnet synchronous generator wind-based system with grid support capabilities," *IET Renewable Power Generation*, vol. 9, no. 8, pp. 925–934, 2015.

[49] K. Musasa, M. N. Gitau, and R. C. Bansal, "Dynamic analysis of DC – DC converter internal to an offshore wind farm," *IET Renewable Power Generation*, vol. 9, no. 6, pp. 542–548, 2015.

[50] H. Mohammadpour, S. G. Zadeh, and S. Tohidi, "Symmetrical and asymmetrical low-voltage ride through of doubly-fed induction generator wind turbines using gate controlled series capacitor," *IET Renewable Power Generation*, vol. 9, no. 7, pp. 840–846, 2015.

[51] W. Chen, D. Xu, N. Zhu, M. Chen, and F. Blaabjerg, "Control of Doubly-Fed Induction Generator to Ride-Through Recurring Grid Faults," *IEEE Transactions on Power Electronics*, vol. 31, no. 7, pp. 4831–4846, 2016.

[52] R. Zhu, Z. Chen, X. Wu, and F. Deng, "Virtual Damping Flux-Based LVRT Control for DFIG-Based Wind Turbine," *IEEE Transactions on Energy Conversion*, vol. 30, no. 2, pp. 714–725, 2015.

[53] L. Zhou, J. Liu, and S. Zhou, "Improved Demagnetization Control of a Doubly-Fed Induction Generator Under-Balanced Grid Fault," *IEEE Transactions on Power Electronics*, vol. 30, no. 12, pp. 6695–6705, 2015.

[54] Q. Huang, X. Zou, D. Zhu, and Y. Kang, "Scaled Current Tracking Control for Doubly Fed Induction Generator to Ride-Through Serious," *IEEE Transactions on Power Electronics*, vol. 31, no. 3, pp. 2150–2165, 2016.

[55] T. Karaipoom and I. Ngamroo, "Optimal Superconducting Coil Integrated Into DFIG Wind Turbine for Fault Ride Through Capability Enhancement and Output Power Fluctuation Suppression," *IEEE Transactions on Sustainable Energy*, vol. 6, no. 1, pp. 28–42, 2015.

[56] L. Huchel, M. S. El-Moursi, and H. H. Zeineldin, "A Parallel Capacitor Control Strategy for Enhanced FRT Capability of DFIG," *IEEE Transactions on Sustainable Energy*, vol. 6, no. 2, pp. 303–312, 2015.

[57] P.-H. Huang, S. M. El-Moursi, and S. A. Hasen, "Novel Fault Ride-Through Scheme and Control Strategy for Doubly Fed Induction Generator-Based Wind Turbine," *IEEE Transactions on Energy Conversion*, vol. 30, no. 2, pp. 635–645, 2015.

[58] I. A. Gowaid, A. A. Elserougi, and A. S. Abdel-khalik, "A series flywheel architecture for power levelling and mitigation of DC voltage transients in multi-terminal HVDC grids," *IET Generation, Transmission and Distribution*, vol. 8, no. 12, pp. 1951–1959, 2014.

[59] B. B. Ambati, P. Kanjiya, and V. Khadkikar, "A Low Component Count Series Voltage Compensation Scheme for DFIG WTs to Enhance Fault Ride-

Through Capability," *IEEE Transactions on Energy Conversion*, vol. 30, no. 1, pp. 208–217, 2015.

[60] I. Ngamroo and T. Karaipoom, "Improving Low-Voltage Ride-Through Performance and Alleviating Power Fluctuation of DFIG Wind Turbine in DC Microgrid by Optimal SMES With Fault Current Limiting Function," *IEEE Transactions on Applied Superconductivity*, vol. 24, no. 5, pp. 1–8, 2014.

[61] P. Monica Argagues, G.-B. Oriol, and M. Marcia, "Coordinated Control for an Offshore Wind Power Plant to Provide Fault Ride Through Capability," *IEEE Transactions on Sustainable Energy*, vol. 5, no. 4, pp. 1253–1261, 2014.

[62] N. Jelani and M. Molinas, "Asymmetrical Fault Ride Through as Ancillary Service by Constant Power Loads in Grid-Connected Wind Farm," *IEEE Transactions on Power Electronics*, vol. 30, no. 3, pp. 1704–1713, 2015.

[63] B. Silva, C. L. Moreira, and H. Leite, "Multiterminal HVDC Grids," *IEEE Transactions on Power Delivery*, vol. 29, no. 1, pp. 395–405, 2014.

[64] M. S. El-Moursi, H. H. Zeineldin, J. L. Kirtley, and K. Alobeidli, "A Dynamic Master / Slave Reactive Power- Management Scheme for Smart Grids With Distributed Generation," *IEEE Transactions on Power Delivery*, vol. 29, no. 3, pp. 1157–1167, 2014.

[65] H. Po-hsu, S. M. El-Moursi, X. Weidong, and J. L. Kirtley, "Fault Ride-Through Configuration and Transient Management Scheme for Self-Excited

Induction Generator-Based Wind Turbine," *IEEE Transactions on Sustainable Energy*, vol. 5, no. 1, pp. 148–159, 2014.

[66] G. Xu, L. Xu, and J. Morrow, "Power oscillation damping using wind turbines with energy storage systems," *IET Renewable Power Generation*, vol. 7, no. 5, pp. 449–457, 2013.

[67] S. M. El-Moursi, X. Weidong, and J. L. Kirtley, "Fault ride through capability for grid interfacing large scale PV power plants," *IET Generation, Transmission and Distribution*, vol. 7, no. 9, pp. 1027–1036, 2013.

[68] A. Surour, M. Ahmed, S. M. El-Moursi, and K. Vinod, "Voltage Booster Schemes for Fault Ride-Through Enhancement of Variable Speed Wind Turbines," *IEEE Transactions on Sustainable Energy*, vol. 4, no. 4, pp. 1071–1081, 2013.

[69] M. Ke, M. Liserre, and F. Blaabjerg, "Operating and Loading Conditions of a Three-Level Neutral-Point-Clamped Wind Power Converter Under Various Grid Faults," *IEEE Transactions on Industry Applications*, vol. 50, no. 1, pp. 520–530, 2014.

[70] T. Lei, M. Barnes, and M. Ozakturk, "Doubly-fed induction generator wind turbine modelling for detailed electromagnetic system studies," *IET Renewable Power Generation*, vol. 7, no. 2, pp. 180–189, 2013.

[71] G. Pannell, B. Zahawi, D. J. Atkinson, and P. Missailidis, "Evaluation of the Performance of a DC-Link Brake Chopper as a DFIG Low-Voltage Fault-

Ride-Through Device," *IEEE Transactions on Energy Conversion*, vol. 28, no. 3, pp. 535–542, 2013.

[72] S. Q. Bu, W. Du, H. F. Wang, and S. Gao, "Power angle control of grid-connected doubly fed induction generator wind turbines for fault ride-through," *IET Renewable Power Generation*, vol. 7, no. 1, pp. 18–27, 2013.

[73] M. Firouzi, G. B. Gharehpetian, and S. Member, "Improving Fault Ride-Through Capability of Fixed-Speed Wind Turbine by Using Bridge-Type Fault Current Limiter," *IEEE Transactions on Energy Conversion*, vol. 28, no. 2, pp. 361–369, 2013.

[74] X. Dongliang, X. Zhao, Y. Lihui, O. Jacob, X. Yusheng, and W. Kit Po, "A Comprehensive LVRT Control Strategy for DFIG Wind Turbines With Enhanced Reactive Power Support," *IEEE Transactions on Power Systems*, vol. 28, no. 3, pp. 3302–3310, 2013.

[75] H.-N. Wessels, Christian, M. Molinas, and F. W. Fuchs, "StatCom Control at Wind Farms With Fixed-Speed Induction Generators Under Asymmetrical Grid Faults," *IEEE Transactions on Industrial Electronics*, vol. 60, no. 7, pp. 2864–2873, 2013.

[76] T. H. Nguyen and D.-C. Lee, "Advanced Fault Ride-Through Technique for PMSG Wind Turbine Systems Using Line-Side Converter as STATCOM," *IEEE Transactions on Industrial Electronics*, vol. 60, no. 7, pp. 2842–2850, 2013.

[77] M. Geev, S. Pierluigi, P. Antonio, and C. Zhe, "Improving Fault Ride-Through Capability of Variable Speed Wind Turbines in Distribution Networks," *IEEE Systems Journal*, vol. 7, no. 4, pp. 713–722, 2013.

[78] J. Hu, H. Xu, and Y. He, "Coordinated Control of DFIG ' s RSC and GSC Under Generalized Unbalanced and Distorted Grid Voltage Conditions," *IEEE Transactions on Industrial Electronics*, vol. 60, no. 7, pp. 2808–2819, 2013.

[79] L. Yang, Z. Xu, and J. Østergaard, "Advanced Control Strategy of DFIG Wind Turbines for Power System Fault Ride Through," *IEEE Transactions on Power Systems*, vol. 27, no. 2, pp. 713–722, 2012.

[80] C. H. Ng, L. Ran, and J. Bumby, "Unbalanced-Grid-Fault Ride-Through Control for a Wind Turbine Inverter," *IEEE Transactions on Industry Applications*, vol. 44, no. 3, pp. 845–856, 2008.

[81] D. Xiang, L. Ran, P. J. Tavner, and S. Yang, "Control of a Doubly Fed Induction Generator in a Wind Turbine During Grid Fault Ride-Through," *IEEE Transactions on Energy Conversion*, vol. 21, no. 3, pp. 652–662, 2006.

[82] T. D. Vrionis, X. I. Koutiva, and N. A. Vovos, "A Genetic Algorithm-Based Low Voltage Ride-Through Control Strategy for Grid Connected Doubly Fed Induction Wind Generators," *IEEE Transactions on Power Systems*, vol. 29, no. 3, pp. 1325–1334, 2014.

[83] H. Zhao, Q. Wu, C. N. Rasmussen, and M. Blanke, "L1 Adaptive Speed Control of a Small Wind Energy Conversion System for Maximum Power Point Tracking," *IEEE Transactions on Energy Conversion*, vol. 29, no. 3, pp. 576–584, 2014.

[84] H. Jafarnejadsani and J. Pieper, "Gain-Scheduled 1 -Optimal Control of Variable-Speed–Variable-Pitch Wind Turbines," *IEEE Transactions on Control Systems Technology*, vol. 23, pp. 372–379, 2015.

[85] E. Iyasere, M. Salah, D. Dawson, and J. Wagner, "Nonlinear Robust Control to Maximize Energy Capture in a Variable Speed Wind Turbine," in *Proc. American Control Conference*, pp. 1824–1829, 2008.

[86] C. Sloth, T. Esbensen, M. Niss, J. Stoustrup, and P. F. Odgaard, "Robust LMI-Based Control of Wind Turbines with Parametric Uncertainties," in *Proc. IEEE Control Applications, (CCA) and Intelligent Control, (ISIC)*, pp. 776–781, 2009.

[87] B. M. Endusa, S. Tomonobu, U. Naomitsu, Y. Atsushi, and F. Toshihisa, "Robust Predictive Control of Variable-Speed Wind Turbine Generator by Self-Tuning Regulator," in *Proc. 2007 IEEE Power Engineering Society General Meeting*, pp. 1–8, 2007.

[88] H. Aschemann and J. Kersten, "Control and Robust Tower Oscillation Damping for a Wind Turbine Equipped With a Hydrostatic Drive Train and a Synchronous Generator," in *Proc. 21st International Conference on*

Methods and Models in Automation and Robotics (MMAR), pp. 1051–1056, 2016.

[89] K. B. Alaoui, E. Boufounas, and I. Boumhidi, "Integral Sliding Mode Control without Reaching Phase for a variable Speed Wind Turbine," in *Proc. 2016 International Conference on Electrical and Information Technologies (ICEIT)*, pp. 78 – 83, 2016.

[90] M. Doumbia, M. Bouhamida, and M. Benghanem, "Control of Wind Turbine Based on DFIG Using Fuzzy-PI and Sliding Mode Controllers," in *Proc. Ninth International Conference on Ecological Vehicles and Renewable Energies (EVER)*, pp. 1 – 8, 2014.

[91] X. Zhu, S. Liu, and Y. Wang, "Second-order Sliding-mode Control of DFIG-based Wind Turbines," in *3rd Renewable Power Generation Conference*, pp. 1–6,2016.

[92] S. Rajendran and D. Jena, "Backstepping Sliding Mode Control for Variable Speed Wind turbine," in *Proc. Annual IEEE India Conference (INDICON)*, pp. 1 – 6, 2014.

[93] X.-X. Yin, Y.-G. Lin, W. Li, H.-W. Liu, and Y.-J. Gu, "Adaptive sliding mode back-stepping pitch angle control of a variable-displacement pump controlled pitch system for wind turbines," *ISA Transactions*, vol. 58, pp. 629–634, 2015.

[94] G. Jianying and X. I. E. Rong, "Adaptive Control of PMSG-based Small Wind Turbines in Region II," *Proceedings of the 35th Chinese Control Conference*, pp. 8518–8522, 2016.

[95] O. Barambones and J. M. G. De-Durana, "Adaptive sliding mode control strategy for a wind turbine systems using a HOSM wind torque observer," in *Proc. IEEE International Energy Conference (ENERGYCON)*, pp. 1 – 6, 2016.

[96] S. Kai, C.-k. Zhang, X. Zhou, and L. Jiang, "Nonlinear Adaptive Power Control for DFIG-based Wind Turbine Under Unbalanced Network Conditions," in *Proc. IEEE 8th International Power Electronics and Motion Control Conference (IPEMC-ECCE Asia)*, pp. 1 – 6, 2016.

[97] M. Koumir, A. E. Bakri, and I. Boumhidi, "Optimal Control for a Variable Speed Wind Turbine Based on Extreme Learning Machine and Adaptive Particle Swarm Optimization," in *Proc. 5th International Conference on Systems and Control, Cadi Ayyad University, Marrakesh, Morocco*, pp. 151–156, 2016.

[98] S. M. Muyeen and A. Al-Durra, "Application of an Adaptive Neuro-Fuzzy Controller for Speed Control of Switched Reluctance Generator Driven by Variable Speed Wind Turbine," *Modern Electric Power Systems (MEPS)*, pp. 1–6, 2015.

[99] C. A. Evangelista, A. Pisano, P. Puleston, and E. Usai, "Receding Horizon Adaptive Second-Order Sliding Mode Control for Doubly-Fed Wind Turbine," *IEEE Transactions on Control Systems Technology*, vol. 25, no. 1, pp. 73–84, 2016.

[100] S. Abulanwar, W. Hu, A. Chen, and F. Iov, "Adaptive voltage control strategy for variable speed wind turbine connected to a weak network," *IET Renewable Power Generation*, vol. 10, no. 2, pp. 238–249, 2015.

[101] A. Tohidi, H. Hajieghrary, and M. A. Hsieh, "Adaptive Disturbance Rejection Control Scheme for DFIG-Based Wind Turbine : Theory and Experiments," *IEEE Transaction on Industry Applications*, vol. 52, no. 3, pp. 2006–2015, 2016.

[102] O. Barambones, J. Maria, and G. De-Durana, "Wind Turbine Control Scheme based on Adaptive Sliding Mode Controller and Observer," in *Proc. IEEE 20th Conference on Emerging Technologies and Factory Automation (ETFA)*, pp. 1–7,2015.

[103] Q. Luo, Q. Yang, C. Han, and P. Cheng, "Pitch Angle Controller of Variable-Speed Wind Turbine Based on L1 Adaptive Control Theory," in *Proc. International Conference on Mechatronics and Control (ICMC)*, pp. 955–960,2014.

[104] S. Rajendran and D. Jena, "Adaptive Nonsingular Terminal Sliding Mode Control for Variable Speed Wind Turbine," in *Proc. IEEE 28th Canadian*

Conference on Electrical and Computer Engineering, pp. 1–8, 2015.

[105] J. Chen, L. Jiang, W. Yao, and Q. H. Wu, "Perturbation Estimation Based Nonlinear Adaptive Control of a Full-Rated Converter Wind Turbine for Fault Ride-Through Capability Enhancement," *IEEE Transactions on Power Systems*, vol. 29, no. 6, pp. 2733–2743, 2014.

[106] V. Azimi, M. B. Menhaj, and A. Fakharian, "Adaptive Control of a Wind Turbine Based on Neural Networks," in *Proc. 13th Iranian Conference on Fuzzy Systems (IFSC)*, pp. 1–8,, 2013.

[107] P. Bagheri and Q. Sun, "Adaptive robust control of a class of non-affine variable-speed variable-pitch wind turbines with unmodeled dynamics," *ISA Transactions*, vol. 63, pp. 233–241, 2016. [Online]. Available: http://www.sciencedirect.com/science/article/pii/S0019057816300532

[108] D.-C. Phan and S. Yamamoto, "Rotor speed control of doubly fed induction generator wind turbines using adaptive maximum power point tracking," *Energy*, vol. 111, pp. 377–388, 2016.

[109] A. Hatami and B. Moetakef-imani, "Innovative adaptive pitch control for small wind turbine fatigue load reduction," *Mechatronics*, vol. 40, pp. 137–145, 2016.

[110] E. Assareh and M. Biglari, "A novel approach to capture the maximum power from variable speed wind turbines using PI controller , RBF neu-

ral network and GSA evolutionary algorithm," *Renewable and Sustainable Energy Reviews*, vol. 51, pp. 1023–1037, 2015.

[111] R. Aissou, T. Rekioua, and D. Rekioua, "Robust nonlinear predictive control of permanent magnet synchronous generator turbine using Dspace hardware," *International Journal of Hydrogen Energy*, vol. 41, no. 1, 2016.

[112] P. Fogh, L. F. S. Larsen, R. Wisniewski, and T. Gybel, "On using Pareto optimality to tune a linear model predictive controller for wind turbines," *Renewable Energy*, vol. 87, pp. 884–891, 2016.

[113] J. Hu, J. Zhu, and D. G. Dorrell, "Model-predictive direct power control of doubly-fed induction generators under unbalanced grid voltage conditions in wind energy applications," *IET Renewable Power Generation*, vol. 8, no. 6, pp. 687–695, 2014.

[114] Z. Jin, F. Li, M. Xiao, and S. M. Djouadi, "Semi-Definite Programming for Power Output Control in a Wind Energy Conversion System," *IEEE Transactions on Sustainable Energy*, vol. 5, no. 2, pp. 466–475, 2014.

[115] L. Xiangjie and K. Xiaobing, "Nonlinear Model Predictive Control for DFIG-Based Wind Power Generation," *IEEE Transactions on Sustainable Energy*, vol. 11, no. 2, pp. 1046–1055, 2014.

[116] A. Koerber and R. King, "Combined Feedback Feedforward Control of Wind Turbines Using State-Constrained Model Predictive Control," *IEEE Trans-*

actions on Control Systems Technology, vol. 21, no. 4, pp. 1117 – 1128, 2013.

[117] H. M. Nguyen, "Advanced Control Strategies for Wind Energy Conversion Systems," Ph.D. dissertation, Idaho State University, 2012.

[118] J.G. SlootWeg H. Polinder and W. L. Kling, "Dynamic Modeling of a wind turbine with doubly fed induction generator," in *Proc. IEEE Power Engineering Society Summer Meeting*, pp. 644–649, 2001.

[119] N. P. W. Strachan and D. Jovcic, "Dynamic Modeling, simulation and analysis of an offshore variable-speed directly driven permanent magnet wind energy conversion and storage system," in *Proc. Europe OCEANS*, pp. 1–6, 2007.

[120] A. M. Marinelli A.Morini and F.Silvestro, "Modelling of doubly fed induction generator (DFIG) equipped wind turbine for dynamic studies," in *Proc. International Universities Power Engineering Conference*, pp. 1–6, 2008.

[121] E. S. Abdin and W. Xu, "Control design and dynamic performance analysis of a wind-turbine-induction generator unit," *IEEE Transaction on Energy Conversion*, vol. 15, no. 1, pp. 91–96, 2000.

[122] S. Aimani, "Modeling and Control Structures for variable speed wind turbine," in *Proc. International Conference on Multimedia Computing and Systems*, pp. 1–5, 2010.

[123] N. A. C. I. Muntaeanu A.I. Bratcu and E. Ceanga, *Optimal Control of Wind Energy Systems: Towards a Global Approach.* Springer, 2008.

Vitae

Personal Details

Name	Mojeed Opeyemi Oyedeji
Nationality:	Nigerian
Date of Birth	November 8, 1991
Email:	mojeed.oyedeji@gmail.com
Permenant Address:	21A, Osun State University Road,
	Oke-Baale, Osogbo, Osun State, Nigeria.
Phone:	+966534128071, +2347065363100

Education

2007-2012	B.Sc Electrical and Electronic Engineering
	Osun State University, Osogbo, Osun State, Nigeria
2015-present	M.Sc Systems and Control Engineering
	King Fahd University of Petroleum and Minerals, Saudi Arabia.

Publications

Published

Mahmoud, M.S. and Oyedeji, M.O. (2017) Optimal Control of Wind Turbines under Islanded Operation. Intelligent Control and Automation, vol. 8, 1-14.

Alawode, K.O. and Oyedeji, M.O. (2013), A Comparison of Neural Network Models for Load Forecasting in Nigerian Power System, International Journal of Research in Engineering and Technology (IJRET), vol.2, no.5, pp. 218-222

Under Review

Mahmoud, M.S. and Oyedeji, M.O. (2017), Adaptive and Predictive Control Strategies for Wind Turbine Systems: A Survey, *submitted to: Power Systems Journal of Modern and Clean Energy*

Mahmoud, M.S. and Oyedeji, M.O. (2017), LMI-based Pitch Controller Design for Tower Vibrations and Output Power Regulation in Wind Turbines Systems, *submitted to: IET Renewable Power Generation*

Mahmoud, M.S. and Oyedeji, M.O. (2017), Continuous-time Gain-Scheduled Predictive Control of Variable-Speed Variable-Pitch Wind Turbines, *submitted to: IET Generation, Transmission and Distribution*

Mahmoud, M.S. and Oyedeji, M.O. (2017),Continuous-time Multi-Model Predictive Control of Variable-Speed Variable-Pitch Wind Turbines, *submitted to: International of Journal of Systems Science*